SPATIAL IDENTIFICATION OF
PASSIVE RADIO FREQUENCY IDENTIFICATION TAGS
USING SOFTWARE DEFINED RADIOS

THESIS

Paul A. Cornn, Captain, USAF

AFIT/GCE/ENG/12-04

DEPARTMENT OF THE AIR FORCE
AIR UNIVERSITY

AIR FORCE INSTITUTE OF TECHNOLOGY

Wright-Patterson Air Force Base, Ohio

AFIT/GCE/ENG/12-04

SPATIAL IDENTIFICATION OF
PASSIVE RADIO FREQUENCY IDENTIFICATION TAGS
USING SOFTWARE DEFINED RADIOS

THESIS

Presented to the Faculty

Department of Electical and Computer Engineering

Graduate School of Engineering and Management

Air Force Institute of Technology

Air University

Air Education and Training Command

In Partial Fulfillment of the Requirements for the

Degree of Master of Science in Computer Engineering

Paul A. Cornn, B.S.E.E.

Captain, USAF

March 2012

AFIT/GCE/ENG/12-04

SPATIAL IDENTIFICATION OF PASSIVE RADIO FREQUENCY IDENTIFICATION TAGS USING SOFTWARE DEFINED RADIOS

Paul A. Cornn, B.S.E.E.

Captain, USAF

Approved:

/signed/	5 Mar 2012
Maj Mark D. Silvius, PhD (Chairman)	date
/signed/	5 Mar 2012
Dr. Richard K. Martin, (Member)	date
/signed/	5 Mar 2012
Maj Todd R. Andel, PhD (Member)	date

AFIT/GCE/ENG/12-04

Abstract

This research seeks to utilize a software defined radio for the detection and spatial identification of radio frequency identification tags. A software defined radio (SDR) is a hardware platform that provides the ability to broadcast and receive across multiple bands of the radio frequency (RF) spectrum, depending on the RF front end and software profile loaded on it. The focus of this research is on the spatial identification (SID) of passive radio frequency identification tags (RFID). It should be noted that this is closely related to the more common term of geo-location, but differs in a fundamental way. Geo-location focuses on obtaining the precise location of the target object, while SID aims to not only locate the object in three dimensional space, but also provide information on its velocity and bearing. This research is applicable to many areas of day-to-day operation both within the DoD and industry. Flight line safety tracking of equipment and personnel, as well as perimeter defense, are two areas that may benefit from this technology. One dual-purpose, civilian and military, application would be the tracking and locating of inventory within a warehouse. This research developed and implemented a SID process, and proved its suitability to quickly identify and locate target tags within range. A profile of the system's capabilities and limitations in the lab environment was developed including the range, sensitivity and accuracy.

Acknowledgements

I would like to thank my beautiful wife for her support during this process. Her patient ear and technical insight helped me to K.I.S.S. She also knew just when to kick me and the dog out of the house for a long walk. It is amazing what fresh air and a little distance will do for your ability to think about a problem. I would also like to thank my wonderful lab assitant. What other daughter would jump at the chance to spend a weekend in the lab collecting radio captures of a tag moving on a rope.

I would also like to thank my fellow VLSI lab trolls. The light hearted mood of the lab prevented a very trying program from becoming overwelming. Contrary to popular belief, this group never cut corners.

Most of all, I owe a sincere debt of gratitude to my advisor, Maj. Mark Silvius, USAF. His willingness to re-teach signal processing and patience as I worked through it allowed me to cross the finishline. In addition his calm under fire attitude excused repeated salvos of water from his students at the combat dining in. Thank you.

Paul A. Cornn

Table of Contents

List of Figures

x

xi

List of Tables

SPATIAL IDENTIFICATION OF
PASSIVE RADIO FREQUENCY IDENTIFICATION TAGS
USING SOFTWARE DEFINED RADIOS

I. Introduction

1.1 Introduction

While many technological devices are currently employed to detect intruders at the perimeter of secured areas, they are not always able to discern between a human intruder and natural occurrences. Animals, blowing grass, or heavy rain and snow can cause motion sensors and ground based radar to provide false alarms. In order to eliminate these false alarms, a perimeter security system would need to detect a truly human characteristic. One such characteristic is the array of electronic devices that we carry every day. Items such as cell phones, two-way radios, and radio frequency identification (RFID) tags can be found on just about every person. This research focuses on the development of a software defined radio solution to identify and provide the spatial identification of passive RFID tags. To this end, a spatial identification algorithm and hardware implementation is developed and validated using a demonstration platform. The ability to identify and track these devices from a distance would allow security personnel to focus their attention on viable threats – and spend less time chasing coyotes across missile fields.

1.2 Goals and Hypothesis

It is possible to locate and track a signal if one knows some information about it such as its center frequency and transmission power. The challenge comes when you want to identify and track a signal without prior knowledge of its transmission characteristics. Techniques such as RSSI would be able to tell you if the signal was moving towards you or away and at what bearing it is but not specifics like the range to target. Therefore, if the signal is analyzed in a different manor using Phase Difference Of Arrival (PDOA), a vector can be generated on a map showing the direction of travel, velocity, and range to target of the unknown transmitter. The goal of this research is to show, that it is possible to generate a vector for a captured signal based on analysis of its PDOA. The hypothesis of this research is that it is possible to take a transmitter that has not be previously characterized can be spatially identified using PDOA. For this research, the spatial identification method is measured against a simulation of the same transmitter modeled in three dimensional space with reflection and additive white Gaussian noise. An effective spatial identification will produce a location vector to with no more than a order of magnitude margin of error.

1.3 Motivation

The United States (U.S.) Department of Defense (DoD) spends millions of dollars each year securing the perimeters of its military installations and the high-valued assets within those bases. Fiber optic fence sensors, which detect vibrations, and ground based radars, which detect anomalies at the perimeter, are often put into

an alarm state by natural phenomena. High winds can cause a fence to vibrate, and wildlife or even blowing grass can cause either of these sensors to enter an alarm state. In order to tune out these false alarms, the sensitivity would have to be reduced to a level that could allow an intruder to bypass them. In addition to the false alarm problem, ground based radar has no way to uniquely identify a target once it has been spotted. Two targets can approach each other and their image will merge. Upon separation, there is no way to identify each target. An effective way to protect these areas is through the use of infrared cameras, but they cost tens of thousands of dollars each and require line-of-sight which limits their range. In addition to perimeter security, this technology could be adapted for safety and logistics applications. It stands to reason, that if we can identify and track an unknown transmitter entering the base, we could track known transmitters within areas of the base. In this way, we could tag vehicles, workers, and even tools along the flight line. This would allow a clear picture of where personnel are, if they are where they are supposed to be, and even detect possible accidents before they happen. Now, in addition to a painted "red line" that has to be physically watched by Security Forces, a virtual line would also exist. Some tags would be permitted to cross it at given times, while other tags would never be allowed into this exclusion zone. I propose a new way of looking at both the security and safety problems, by expanding the way that we locate and track spurious emitters. In particular, I look at Radio Frequency Identification (RFID) tags. These tags are appealing, because many people carry them every day without realizing it. They are included in some Department of Defense (DoD) Common Access Cards (CAC),

Enhanced ID Driver's Licenses, US and European Passports, tags sewn into clothing to prevent theft, and even casino poker chips. While we cannot count on a potential intruder to carry a pocketful of tagged poker chips while sneaking onto the flight line, these tracking techniques will be applicable to a large range of emitters from RFID tags to cell phones, Bluetooth, WiFi, and walkie-talkies. The flexibility of this approach comes from two areas: the spatial identification (SID) technique chosen, and the hardware on which it is implemented.

1.4   Materials and Equipment

For this research, I have chosen to use a software defined radio (SDR). A SDR incorporates many of the traditional hardware parts of a radio such as mixers, filters, modulators, and demodulators, and implements them in software on a PC, a modular daughtercard, or an embedded field programable gate array (FPGA). An SDR radio that is an RFID tag reader, can easily be reprogrammed, even from a distance, into a walkie-talkie repeater or some other use. In this way, one SDR could be used to track many of the devices listed above, allowing our security posture to rapidly adapt to the environment in which they are operating. Standard EPC Generation 2 RFID tags, for example, operate at 915 MHz in North America and 850 MHz in the European Union [1]. If we used commercial readers, the system built for stateside deployment would have to be redesigned for the European hardware. However, a SDR would simply need a quick code change or possibly even a menu choice by the operator.

This flexibility also provides a level of cost savings. A SDR can be bought for under a thousand dollars, while consumer level RFID readers start at two thousand dollars.

1.5 Methodology

To complete the characterization of the RFID tag transaction, we configured the SDR as a listener that captures the transaction between the commercial reader and the tag. In this way we can use the commercial reader to read the tag and use the SDR to record the electronic conversation from different angles and distances to both the reader and the tag. Our initial setup of this configuration seperates the reader antennas and the tag by one meter, with the SDR antenna positioned directly between them to capture the transaction. In this way, we are able to examine the Alien 9800 commercial reader's output and the log file from the SDR listener, as seen in Figure 1.1, to find the query, query repeat (QREP), and acknowledgements (ACK) of the tag. The times listed in the left column are in seconds and taken from the system time. For the first query at 0.627 seconds, I had removed all tags from within range by obstructing the stationary tag with an anti-static bag. As a result, the reader sends all six Qrep slot advertisements, explained in further detail in Chapter 3, before starting a new query. At the 0.725 seconds query, the tag was visible to the reader and you can see its response at 0.806 seconds. The low latency evident in this response further illustrates the issue with using TDOA to calculate a RFID tags SID. This system also has the benefit of reporting tag errors in a separate tag log file. In this file, we record read/response errors of the tag reads. The most common error

```
56493.432   POWER UP
56493.624   POWER UP
56493.627   QUERY
56493.628   QREP
56493.629   QREP

...
56493.720   QREP
56493.721   QREP
56493.722   QREP
56493.723   QREP
56493.725   QUERY
56493.726   QREP
56493.727   QREP
56493.728   QREP

...
56493.803   QREP
56493.804   QREP
56493.806 _ ACK
```

Figure 1.1:   SDR Listener Log

is a cyclic redundancy check (CRC) error in which only a portion of the tag ID is received. The next step is to modify the flow graph of the listener above to not only listen for the interaction, but to pipe the I and Q data from the interaction to a file for analysis in MATLAB. From that pointa system can map the phase interaction of the read and response of the tag at different known locations and apply the phase based SID models that are discussed in Chapter 2.

1.6   Scope

There are three portions of the phase based SID model: Time Domain Phase Difference of Arrival (TD-PDOA), Frequency Domain Phase Difference of Arrival (FD-PDOA), and Spatial Domain Phase Difference of Arrival (SD-PDOA) [7]. Each of these three domains provides us with a different portion of the SID puzzle. TD-PDOA provides us with an angular velocity of the tag relative to the reader, or how

fast it is moving towards or away from the reader. FD-PDOA, much like traditional radar or sonar, provides a distance of the tag to the reader but due to the stationary antenna used in our experiments it does not provide a direction. This direction, or bearing, to the tag can be provided by the SD-PDOA. For this research effort I focus on TD-PDOA and FD-PDOA.

II. Background

2.1 Introduction

The commercial use of the DoD Global Positioning System (GPS) has brought awareness of geolocation to all corners of the population. The desire by commanders to have real time data on both friendly and opposing forces is ever growing. The tracking of friendly forces can be achieved in many ways, but is simplified by having them carry a tracking device. RFID tags provide a unique challenge for geo-location. The tags work by modulating the signal they receive and reflecting back to a reader. Passive tags, the focus of this research, does this without the aid of an internal power source. They provide a relatively short range communication channel of only about 30 feet in commercial applications when implemented in the 902-928 MHz band [1]. The use of passive tags is further complicated by the fact that this band is unlicensed in the United States, so noise floor can vary greatly based on the location [8]. This chapter provides a background on the geo-location techniques available today, an overview of RFID tags, and the SDR radios that can be used to track them. Finally, a survey of related research is presented.

2.2 Geo-Location Techniques

There are three primary geo-location techniques in use today. The two most popular are Time Difference of Arrival (TDOA) and Receive Signal Strength Indication (RSSI). The third method, Phase Difference of Arrival (PDOA), is not as widely used but, is well suited for the spatial identification of uncooperative targets.
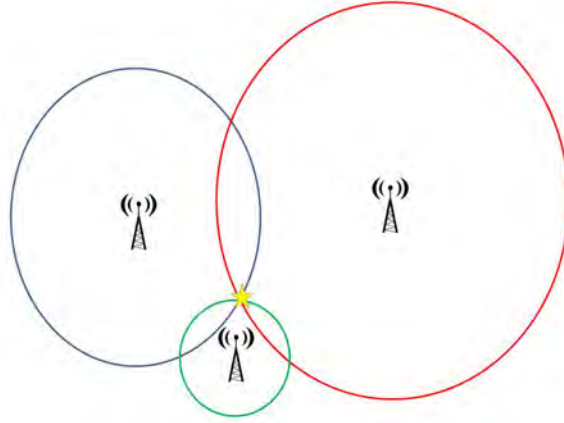
Figure 2.1:   Time Domain Of Arrival Illustration

2.2.1 Time Difference of Arrival.   TDOA is the most commonly used method of geo-location. It is the basis for the GPS system and receivers are embedded in everything from mobile phones to dog collars [9]. TDOA uses the difference in arrival times from multiple, at least three, transmitters to triangulate a target's position. In order to achieve this, several pieces of information must be known. First is the exact location of each transmitter. In the case of GPS, your receiver knows where each satellite is in geostationary orbit over a specific latitude and longitude. Second is the propagation delay of the signal in the transmission medium. GPS uses a radio signal through the atmosphere, but this could just as easily be a sound wave through water such as SONAR interaction with transponders. Given these two data points, the receiver then calculates the distance from each of the transmitters. When plotted, these distance will intersect at a point, or the location of the receiver, as illustrated in Figure 2.1 by the star. Accuracy of TDOA is increased by the availability of additional transmitters and the modeling of propagation delay for the system. As we all know by the success of GPS, this technique can rapidly provide the location of

9

a receiver to within a couple of feet. The problem with using TDOA for the perimeter defense senerio is that an intruder is not going to be carrying a GPS receiver and will not be willingly transmiting their location to Security Forces.

Passive RFID tag geo-location based on TDOA is not feasible due to the limited range of RFID tags. A GPS signal travels, at a minimum, thirty five thousand kilometers to the receiver. The signal from tag to receiver can travel, at most, 20 meters. At this distance, the receiver would have to be able to detect a nanosecond difference in the arrival of the signals, to calculate the target's location within a meter. Which is why TDOA is not suitable for passive RFID tracking.

2.2.2 Receive Signal Strength Indicator. RSSI uses the known propagation properties of a signal in the transmission medium to determine the distance from the sensor. There are two ways that RSSI can be used. The first is tracking a target with a transmitter. Multiple sensors receive the signal from the target transmitter and determine the distance to the target. The point where those distances intersect is the location of the target, much like TDOA. The shortcoming of this approach is that you need to know, or be able to calculate, the transmission power of the target transmitter. For the identification and tracking of a friendly target this is just a matter of procedure. For an unknown target multiple sensors would have to work together to model the decay of the received signal strength. The second RSSI technique is more applicable for such a target. In this technique a grid of transmitter and receiver pairs is set up and the signal strength is baselined. When an object moves in between one

of the pairs, the signal will be degraded. Based on experimental data from [10], one can then identify the size and rough shape of the object. The downside of this method is the extensive setup and calibration of the system. Even an active transmitter from the first method will be affected by environmental changes as demonstrated in the LANDMARC system [11].

2.2.3 Phase Difference of Arrival.   Given the difficulties stated above with more traditional geo-location techniques, the research has shifted to using the phase of the modulated signal as a means to find the SID of a tag [7]. The phase of the signal is a preferred method for spatial identification of passive RFID tags, because it is not dependant on the power incident to the tag. In this way, we are able to isolate one of the variables in the spatial identification problem, and focus on those items that allow us to place the tag in three-dimensional space. Nikitin Et al. look at three different techniques; each one calculates part of the puzzle [7].

2.2.3.1 Time Domain PDOA.   Time Domain PDOA (TD-PDOA) allows for the estimation of a velocity vector with respect to the reader. This method calculates this vector as the derivative of the phase with respect to time, as seen in Equation 2.1. Where c is the speed of light, f is the carrier frequency and π is the phase of the signal. The heart of this method is to compare the phase of a received signal at two points in time. If we know, or can calculate, the center frequency of a signal, we can predict the phase of the second sample to be relative to the first. When the target, an RFID tag in this case, is moving, the phase shifts slightly from

11

the expected value. This shift then allows us to calculate a velocity vector. This vector is relative to the receive antenna of the sensor and represents the velocity of the target when it is moving away from the antenna.

$$V = \frac{-c}{4\pi f} \cdot \frac{\delta \phi}{\delta t} \tag{2.1}$$

2.2.4 TD-PDOA Derivation.   Inspection of the signal phase on arrival in the time domain allows us to calculate the velocity of the target relative to the sensor, i.e. how fast it is moving towards or away from it. For a signal in free space, this is represented by the phaser formula in Equation 2.2 where k is the wave-vector defined as $k = \frac{2\pi f}{c}$. In this way, $d1$ and $d2$, can be used to calculate the phase change due to the distance traveled, for each moment in time. This is shown in Figure 2.2. If the distance is constant between two separate points in time, then the velocity is zero. However, if there is a change in the distance, then the target has moved some distance between the two samples.

$$\phi_{prop} = -2kd \tag{2.2}$$

To derive Equation 2.1, it is best to start with the definition of velocity as seen in Equation 2.3. The term $\frac{\Delta d}{\Delta t}$ can be expanded into the difference in the distance, divided by the difference in the time of each sample, as seen in Equation 2.4. In the next step, both sides of the equation are multiplied by $-\frac{4\pi f}{-c}$, as seen in Equation 2.5.
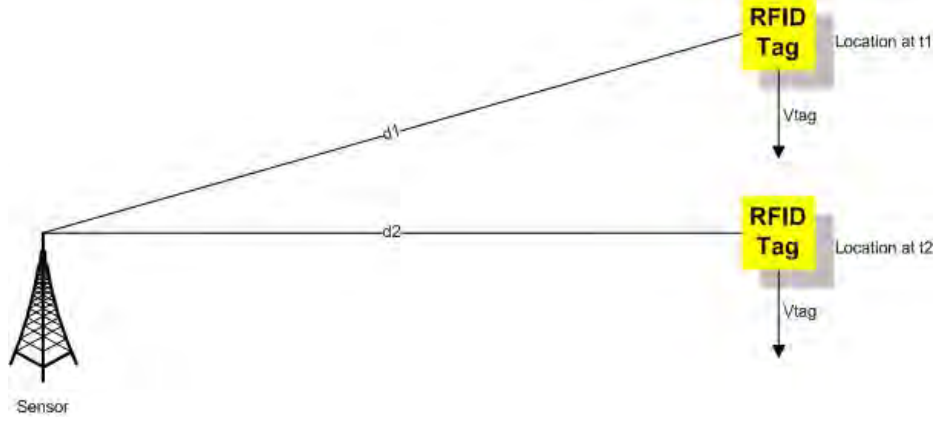
Figure 2.2:   Time Domain PDOA Illustration

Equation 2.6 substitutes the wave-vector, k, for a portion of the multiplicand from the previous step. The distributive property is applied and the result, Equation 2.7, contains two terms that equal the right side of the phasor formula. The angles ϕ_1 and ϕ_2 can then be substituted for these terms as seen in Equation 2.8. After solving for V_r and a substitution for $\frac{\phi_1-\phi_2}{t_1-t_2}$, we arrive at Equation 2.10. If the target is moving sufficiently fast and we can sample such that $\Delta t \to 0$, we arrive at Equation 2.1.

$$V_r = \frac{\Delta d}{\Delta t} \tag{2.3}$$

$$V_r = \frac{d_1 - d_2}{t_1 - t_2} \tag{2.4}$$

$$V_r \cdot -\frac{4\pi f}{-c} = -\frac{4\pi f}{-c} \cdot \frac{d_1 - d_2}{t_1 - t_2} \tag{2.5}$$

$$V_r \cdot -\frac{4\pi f}{-c} = -2k\frac{d_1 - d_2}{t_1 - t_2} \tag{2.6}$$

$$V_r \cdot -\frac{4\pi f}{-c} = \frac{-2kd_1 - -2kd_2}{t_1 - t_2} \tag{2.7}$$

$$V_r \cdot -\frac{4\pi f}{-c} = \frac{\phi_1 - \phi_2}{t_1 - t_2} \tag{2.8}$$

$$V_r = \frac{-c}{4\pi f} \cdot \frac{\phi_1 - \phi_2}{t_1 - t_2} \tag{2.9}$$

$$V_r = \frac{-c}{4\pi f} \cdot \frac{\Delta\phi}{\Delta t} \tag{2.10}$$

Equation 2.10 makes the assumption that the TX (Reader) and RX (Sensor) are co-located. In this way the distance to and from the tag are equal. If the TX/RX antennas are not co-located a correction for the difference in the transmission path will have to be added to the formula. Figure 2.3 illustrates this case. To correct for this we will need to find the angle of arrival for each sample. This value, θ, can be found using Spatial Domain PDOA (SD-PDOA) as seen in Section 3.1.5 for the sample taken at $t1$ and the sample at $t2$. With the assumption that the distance to the reader is greater than one wavelength the phase change due to the different propagation paths is $\frac{2\pi}{\lambda}(\sin\theta_2 - \sin\theta_1)$. Including this term in Equation 2.10 gives us an updated formula seen in Equation 2.11.
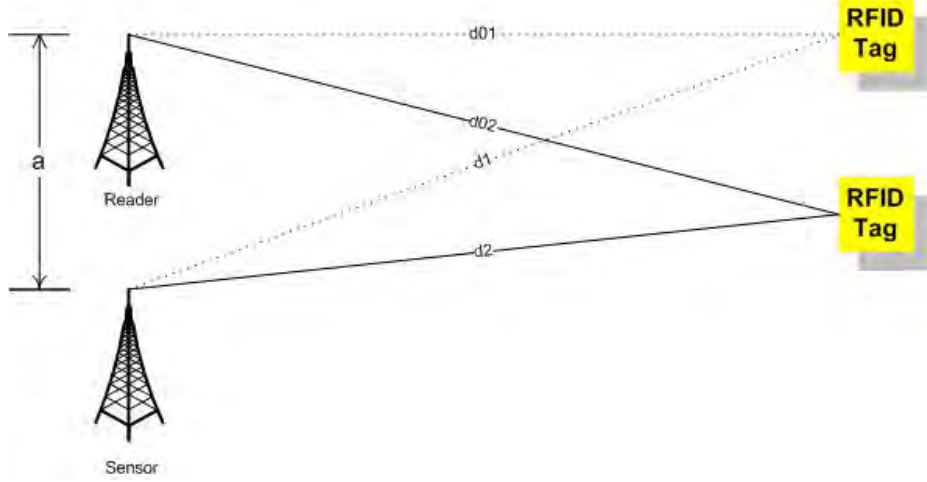
Figure 2.3:   Time Domain PDOA Illustration

$$V_r = \frac{-c}{4\pi f} \cdot \frac{\Delta\phi - \left(\frac{2\pi f}{c}\left(\sin\theta_2 - \sin\theta_1\right)\right)}{\Delta t} \tag{2.11}$$

2.2.4.1 Frequency Domain PDOA.   Frequency Domain PDOA (FD-PDOA) allows one to measure the distance to the tag by measuring the phase shift in different frequencies. This is calculated by taking the derivative of the phase with respect to frequency as seen in Equation 2.12.

$$d = \frac{-c}{4\pi} \cdot \frac{\delta\phi}{\delta f} \tag{2.12}$$

In order to do this, we sample the received signal at its center frequency, 915 MHz in the case of RFID tags, and a frequency just off center, say 914 MHz. A good analogy for how this works is to compare two tires of different sizes. Tire one has a circumference of one meter while tire two meters has a circumference of 0.75 meters,
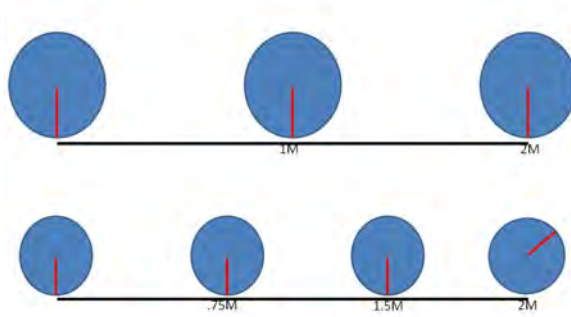
Figure 2.4:   Frequency Domain PDOA Illustration

each starting with a line painted on them pointed at the ground. If we roll both of them two linear meters, tire one will stop with its mark pointed at the ground, while tire two's mark will be about sixty degrees from top dead center, as seen in Figure 2.4. By comparing where the mark, symbolic of the tire's phase is when the wheels arrive, we can calculate the distance traveled. Due to the fact that these samples are taken at the same moment in time, this technique is available even if the target is not moving, unlike TD-PDOA.

2.2.5 *FD-PDOA Derivation.*   FD-PDOA, like TD-PDOA, uses the physical principle that the propagation of sinusoids of different frequencies, and hence different wavelengths, propagate at different rates through space. To compare the relative phase difference in the received signals to calculate a distance to the transmission source. If two frequencies start at the same point, and at the same phase, as the response from the tag would they will arrive at the sensor with aphase difference, $\Delta\phi$. This effect is illustrated in Figure 2.5. In this research, the phase difference is found

16
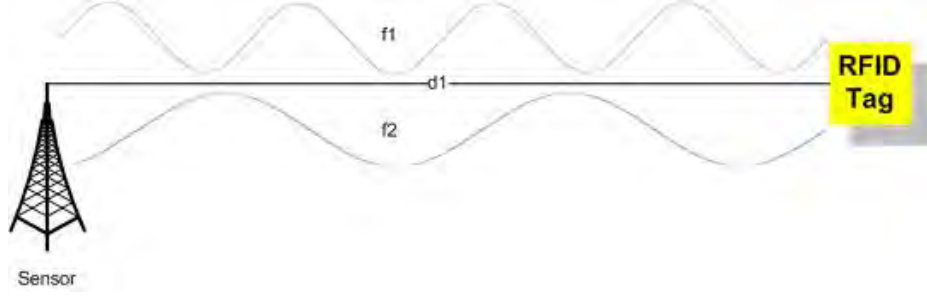
Figure 2.5:   Frequency Domain PDOA Illustration

using the center carrier frequency and one of the side lobes of the FFT discussed in Section 2.3 with the phase of this lobe calculated in the same manner as the phase of the center frequency.

To derive the FD-PDOA formula, Equation 2.12, we first define the expected phase in terms of the two frequencies, f_1 and f_2, and the distance to the tag, d_{tag}. This process can be seen in Equations 2.13 – 2.20. Subtracting Equation 2.20 from Equation 2.19 results in Equation 2.21 which combines the two phase terms into a single equation. As was done in the derivation of the TD-PDOA formula, the term $\phi_2 - \phi_1$ and $f_2 - f_1$ can now be represented as a delta of the phase and frequency, respectively, as seen in Equation 2.22. Solving for d_{tag} results in Equation 2.23. Once again, if we were able to get Δf to approach zero, we would end in our given FD-PDOA seen in Equation 2.12.

$$\phi_1 = -2k_1 d_{tag} \tag{2.13}$$

$$\phi_2 = -2k_2 d_{tag} \tag{2.14}$$

$$k_1 = \frac{2\pi f_1}{c} \tag{2.15}$$

$$k_2 = \frac{2\pi f_2}{c} \tag{2.16}$$

$$\phi_1 = -2\left(\frac{2\pi f_1}{c}\right) d_{tag} \tag{2.17}$$

$$\phi_2 = -2\left(\frac{2\pi f_2}{c}\right) d_{tag} \tag{2.18}$$

$$\phi_1 = \frac{-4\pi f_1}{c} d_{tag} \tag{2.19}$$

$$\phi_2 = \frac{-4\pi f_2}{c} d_{tag} \tag{2.20}$$

$$\phi_2 - \phi_1 = -\frac{4\pi d_{tag}}{c}(f_2 - f_1) \tag{2.21}$$

$$\Delta\phi = -\frac{4\pi d_{tag}}{c}\Delta f \tag{2.22}$$

$$d_{tag} = -\frac{c}{4\pi}\frac{\Delta\phi}{\Delta f} \tag{2.23}$$

2.2.5.1 Spatial Domain PDOA. Spatial Domain PDOA (SD-PDOA) allows for the estimation of the bearing, or the angle of arrival. This technique differs from the other two in that it requires at least two antennas to calculate the desired result. By spacing the two antennas apart the signal received will have to travel two different distances. Much like the tire metophor above, the signal will arrive at the two locations at a different phase. Dividing by the distance between the two antennas, a, the difference in phase will provide theta, or the bearing from antenna one to the

target tag. Several considerationsmust be calculated in when this measurement is performed. The phase progression within the transmission lines of the two antennas will have to be accounted for very carefully.

$$\theta = arcsin\left(\frac{-c}{2\pi f} \cdot \frac{\phi_2 - \phi_1}{a}\right) \tag{2.24}$$

Analysis of the phase in the spatial domain differs from the other two in that a second receive antenna is required. In this way the phase of the arriving signal is measured at two points in space, separated by some distance, a. In is important that these receivers be coherent or in-phase with each other. In this research, this requirement is accomplished by using two daughter cards on the same USRP1 main board. By using coherent receivers, we only have to account for the additional phase delay due to propagation through the antennas' transmission lines of segment a from Figure 2.6, because segment b's delay cancels out. If coherent receivers are not possible a correction for the propagation across b and a must be accounted for. The setup for this metric can be seen in Figure 2.6. Much like the inspection of the TD-PDOA, the signal travels two distinct paths. Unlike TD-PDOA, the signal departs the tag at a single point in time and travels the the receive antennas, transversing some distance d_1 or d_2. Since the length of these paths differ, the signal will arrive at RX1 and RX2 with two different phase values due to the length of the propagation channel. Through application of right triangle geometry, we can then calculate the angle of arrival of the signal to the primary sensor, RX1.
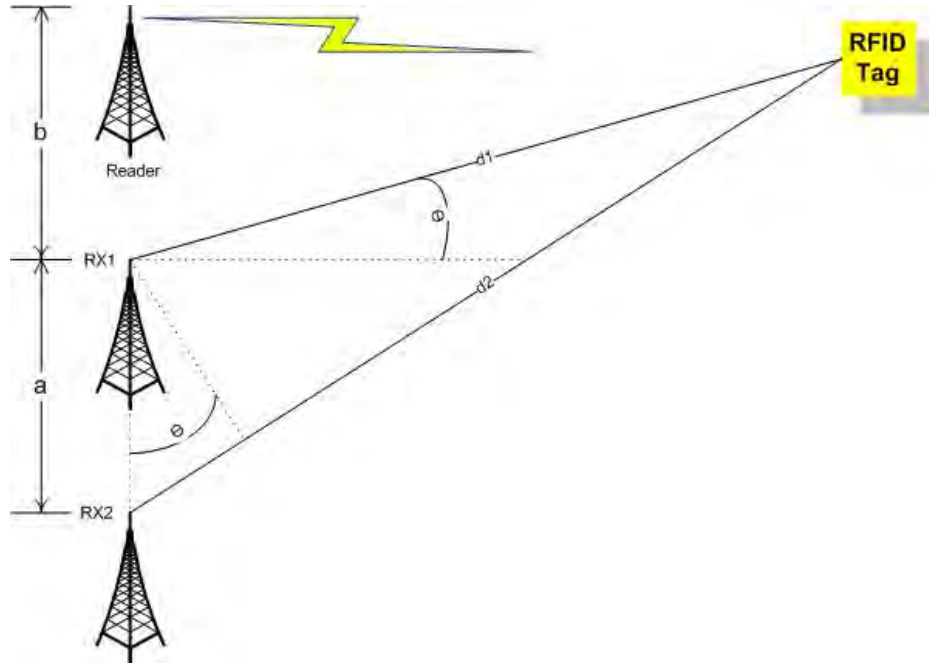
Figure 2.6:   Spatial Domain PDOA Illustration

To derive the formula for the we start with the phasor formula for each of the two receive antennas and solve for d_1 and d_2. These steps can be seen in Equations 2.25 – 2.30. The term $d_2 - d_1$ provides us with the length of one of the legs of the right triangle created by extending a line from RX1 to a point on d_2. In this case, it is the opposite side from the angle we want to calculate, giving Equation 2.32, In the case of Figure 2.6 the result of $d_2 - d_1$ is positive and will result in a positive value for θ. If the difference was negative, the resulting θ would also be negative. What this means in terms of an (x, y) coordinate is discussed in Section 2.3

$$\phi_1 = -kd_1 \tag{2.25}$$

$$\phi_2 = -kd_2 \tag{2.26}$$

$$\phi_1 = -\frac{2\pi f}{c}d_1 \tag{2.27}$$

$$\phi_2 = -\frac{2\pi f}{c}d_2 \tag{2.28}$$

$$\phi_1\left(-\frac{c}{2\pi f}\right) = d_1 \tag{2.29}$$

$$\phi_2\left(-\frac{c}{2\pi f}\right) = d_2 \tag{2.30}$$

$$-\frac{c}{2\pi f}\left(\phi_2 - \phi_1\right) = d_2 - d_1 \tag{2.31}$$

$$\sin\theta = \frac{d_2 - d_1}{a} \tag{2.32}$$

$$\sin\theta = \frac{-\frac{c}{2\pi f}\left(\phi_2 - \phi_1\right)}{a} \tag{2.33}$$

$$\sin\theta = -\frac{c}{2\pi f}\frac{\phi_2 - \phi_1}{a} \tag{2.34}$$

$$\theta = \arcsin -\frac{c}{2\pi f}\frac{\phi_2 - \phi_1}{a} \tag{2.35}$$

2.3   Spatial Identification (SID) Solution

Sections 3.1.3 – 3.1.5 provide us with a method to extract three different metrics

by analyzing the received phase of the target signal. These metrics, however, are not

useful to an operator as they stand, nor do they truly spatially identify a target. This

section illustrates how the metrics calculated can be translated into (x, y) coordinates

and an actual velocity of the target. As it stands, this system would only function

21
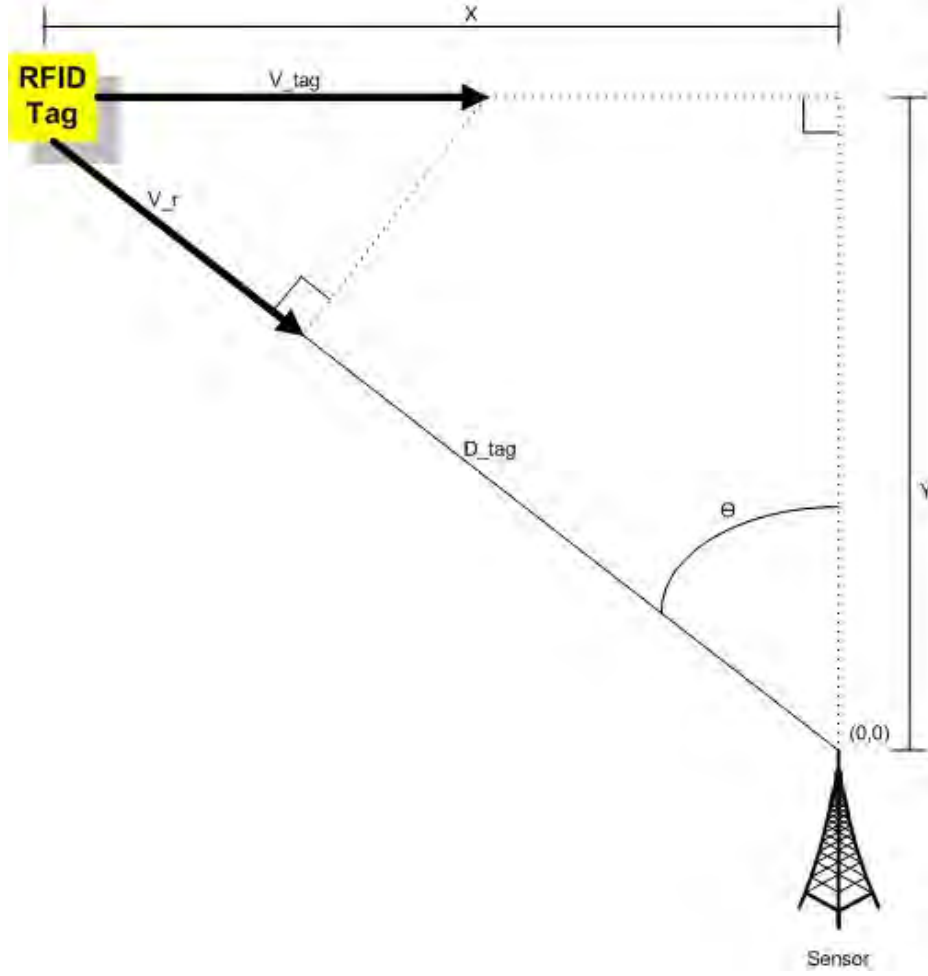
Figure 2.7:   SID Solution

in a two dimensional field with the SD-PDOA being the limiting factor. The two receiver model described in Section 3.1.5 provides an angle of arrival on the (x,y) plane. It would be possible to add the third dimension if another receive antenna was positioned directly above RX1 at some height a_z. Using this new receiver, a second angle of arrival, θ_z, could be calculated using SD-PDOA with Equation 2.35. Figure 2.7 illustrates the metrics we have all ready found. The velocity relative to the sensor, V_r, is found using Equation 2.1. The distance to target, D_{tag} is found using Equation 2.12, and θ is found using Equation 2.24.

22

In order to translate these metrics into something that could be ploted on a map and be useful to an operator, we look at the geometry of Figure 2.7. By defining the sensor location as the origin, we can calculate an (x, y) position pair that could later be overlayed to a map given a latitude, longitude for the sensor. This also lets us form a right triangle with the x and y offsets from the sensor as the legs and the metric D_{tag} as the hypotenuse. Since we already know one of the angles, θ, finding the lengths of the legs becomes an exercise in trigonometry. The x value shown in Equation 2.36 is based on the fact that it is opposite the known angle, θ. In a similar fashion, the y value is calculated using Equation 2.37 and its relationship to θ . While the V_r metric provides us with an instantaneous value for the velocity relative to the sensor, a single value of V_r is not sufficient to calculate an estimate of the velocity components in the x and y directions, $(\dot{x}, \dot{y})$. The value V_r does provide the operator with a closing rate of the target to the sensor, and can be used to provide a sanity check on the velocities $(\dot{x}, \dot{y})$. In order to calculate this value, we would have to have at least two samples that provide both d_{tag} and θ, as well as the time difference between the two samples, Δt. By applying Equations 2.36 and 2.37 to these two samples we can arrive at x_1, x_2, y_1 and y_2. Going back to the definition of velocity as discussed in section 2.2.4we arrive at Equations 2.38 and 2.39. As when calculating V_r, the smaller we are able to make Δt, the more accurate our velocity vector estimation and the sooner we detect a change in direction.

$$x = d_{tag} \sin \theta \qquad (2.36)$$

23

$$y = d_{tag} \cos \theta \qquad (2.37)$$

$$\dot{x} = \frac{d_{tag1} \sin \theta_1 - d_{tag2} \sin \theta_2}{\Delta t} \qquad (2.38)$$

$$\dot{y} = \frac{d_{tag1} \cos \theta_1 - d_{tag2} \cos \theta_2}{\Delta t} \qquad (2.39)$$

2.4   Radio Frequency Identification Tags

Radio Frequency Identification (RFID) Tags are an emerging technology whose adoption has grown immensely over the past ten years. There are two broad categories of RFID tags: active and passive. Active tags have a power source within them and when they are queried by a reader, they draw power from their internal source to respond. Examples of active tags include those used to track cargo containers within a shipyard and the automatic toll readers such as iPass of Illinois and EZPass of New York. The higher signal strength of active tags have made them more favorable to geo-location and are the basis for earlier research [11]. Passive tags harvest the power from the read signal, apply internal logic, and reflect the signal back to the reader. Due to their lower cost, passive tags are much more common in commercial applications. They can be found in the new electronic passports, enhanced driver's licenses and even retail anti-theft devices. The rest of this section describes the physical, link, and session layer communications of the passive RFID tags used in this research.

2.4.1   Symbol Encoding - Physical Layer.   This section goes into greater detail of the physical layer of the EPC Gen 2 RFID tags used in this research. The encoding method, backscatter coupling, and pulse shaping is described.

2.4.1.1 On Off Keying (OOK).   The EPC Gen 2 RFID reader and tags used in this research encode the query and response using On-Off Keying (OOK) [12]. OOK is a digital modulation technique that uses the absence of a carrier wave to encode data. It is a simple scheme for of Amplitude Shift Keying (ASK) and as such is sensitive to atmospheric noise and distortion in the transmission path. The biggest advantage of OOK over other forms of ASK is that it does not require phase lock between radios, which means it can be non-coherently demodulated. The implementation of RFID OOK in the UHF band is defined in ISO-IEC 1800 part 6 [1]]. One of the key characteristics of OOK is the length of a symbol. If you equate a zero and one in OOK to a dot and dash on an old telegraph line the issue becomes apparent: "was that a dot or dash that just came in." In Morse code the standard became the length of a dot, a dash being equal to three dots. ISO 1800-6 defines the standard time unit for RFID communications as a Tari. A *Tari* is defined as 20 microseconds with a tolerance of plus or minus 100 pulses per minute [1]. This means that a Tari must last between 19 and 21 microseconds to remain within specification. While all data is encoded in binary as either a one or zero, there are actually four symbols used in RFID communication. Aside from the before mentioned one and zero, there is a Start of Frame (SOF), and End of Frame (EOF) symbol. These symbols and their encoding can be seen in Figure 2.8. As can be seen, the four symbols are not the same duration, ranging from one to four Taris. The biggest impact of this encoding method is that the data rate is defined by the content of the frame. If we

Symbol	Number of Tari
'0'	1
'1'	2
SOF	4
EOF	4
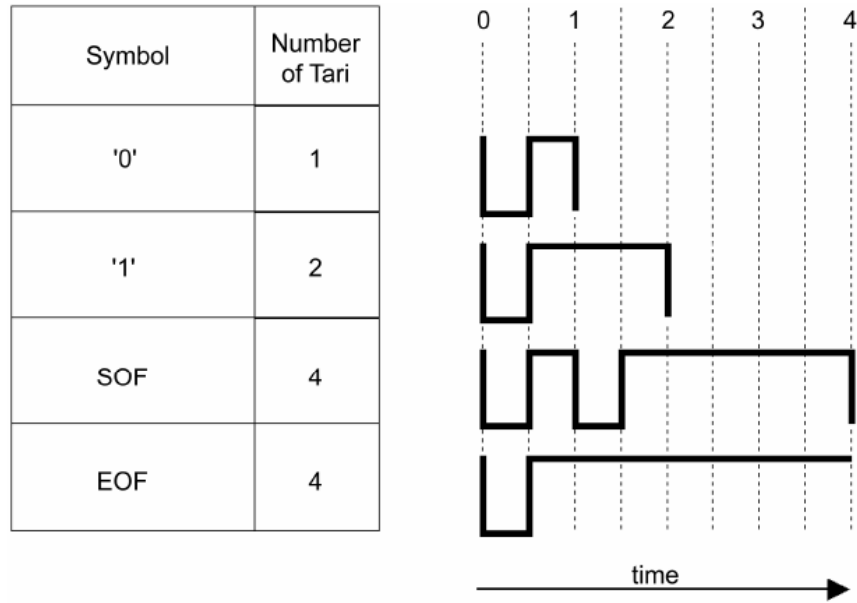
Figure 2.8:   RFID OOK Symbols [1].

look at Morse code again, six dashes would take three times longer to transmit that six dots. In RFID OOK, 16 bits of ones would take twice as long as 16 bits of zeros.

2.4.1.2 Backscatter Coupling.   The on/off pulses for the encoding process in the tag are generated using backscatter coupling. The power from the reader is incident on the tag's antenna. In a normal surface, the antenna would backscatter a portion of the signal directly to the reader. In RFID tags this power provides the power up current for the logic on the tag. RFID tags also have a resistor connected in parallel to the antenna and logic circuits. Using this resistor, the load connected to the antenna can be controlled by the logic circuit. By tuning this load from high to low, the amount of power that is reflected back is varied from high to
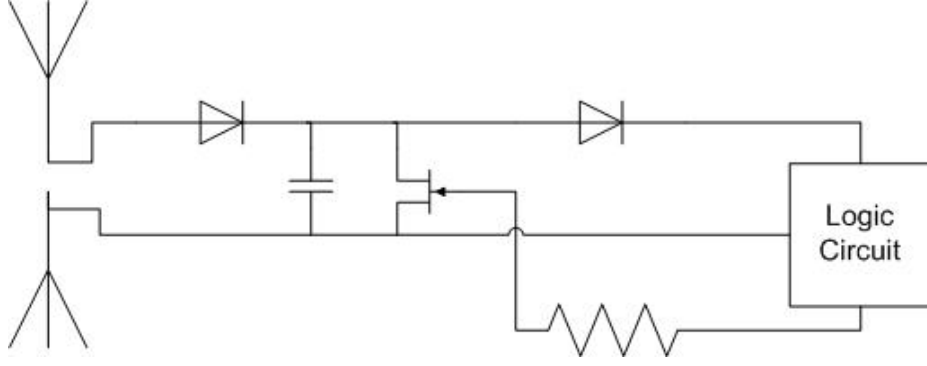
Figure 2.9:   Simple Tag Schematic [2]

low generating the OOK response. A simplified circuit diagram of this resistor layout
is shown in Figure 2.9 [2].

2.4.1.3   Pulse-Interval Encoding.   Given the binary nature of OOK
and the data being encoded, one might expect a zero to be represented by a lack of
carrier and a one to have the carrier present. While this would standardize the data
rate it would cause problems in passive RFID tags. A frame with a lot of zeros would
not provide sufficient power to the tag in order for it to provide a response. In light
of this the symbols were designed using pulse-interval encoding (PIE). The encoding
of the symbols using this PIE scheme ensures that a query from the reader, even if
all zeros, will transmit at full power at least fifty percent of the time. There is now
sufficient energy, given the tag is in range with a clear path, for the tag to power up
and provide a response if needed. This requirement for power from the reader also
adds complications in the session layer, as discussed in a later section.

2.4.1.4   Pulse Shaping.   One other consideration of the encoding
method is the bandwidth of the spectrum occupied by the communications. As UHF

RFID communications occurs in the unlicensed portion of the UHF spectrum, it must limit the amount of power that is evident at frequencies other than the designated carrier frequency. These frequencies are 840 MHz in Europe and 915 MHz in the United States [1]. A sharp cut off of the signal as represented in Figure 2.8, would cause a significant amount of power bleed into other frequencies, as shown in Figure 2.10. A purely digital OOK generates a rectangular pulse function as seen in the left side of Equation 2.40. The Fourier Transform of a rectangular pulse is the sinc function as seen on the right side of Equation 2.40. If the time domain pulse is first convolved with the impulse response of a pulse shaping low pass filter, the side lobes in the frequency domain will be significantly attenuated. This shaping of the symbol, as seen on the right side of Figure 2.10, attenuates the power signature in frequencies far from the carrier [3]. An example of a portion of a tag response is shown in Figure 2.11 with the digital symbols overlayed on the actual transmission. If the FFT is taken of the symbols from Figure 2.11, the power attenuation discussed earlier is evident as seen in Figure 2.12. The central spike shows the frequency that this interaction took place at, 925 MHz. This frequency is not the before mentioned 915MHz operating frequency of the tags. This frequency is a result of a frequency hopping implementation in the reader; the tag just reflects the frequency it receives. Readers can be configured to hop frequencies within the unlicensed 900 MHz band in order to minimize interference. During the data capture portion of this research, the reader was observed to operate on frequencies ranging from 908 MHz up to 925 MHz.
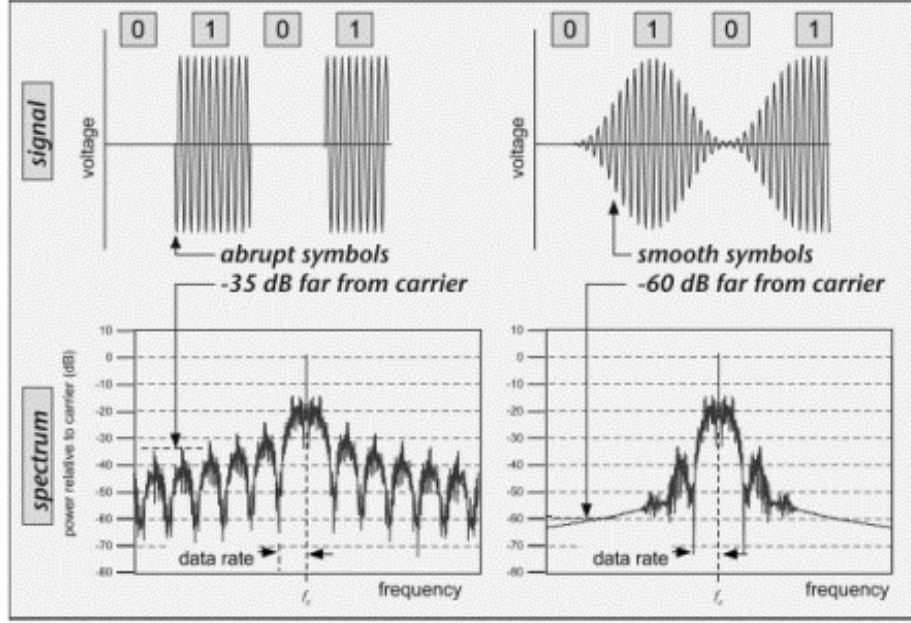
Figure 2.10:   RFID Symbol Shaping [3]

Figure 2.13 shows the phase of each index of the FFT. At the peak power level, 925 MHz, the phase is -0.69 radians.

$$f[x] = \begin{cases} 1 & \text{if On} \\ 0 & \text{if Off} \end{cases} \iff F(\omega) = sinc\frac{\omega}{2} = \frac{sin(\pi\omega)}{\pi\omega} \qquad (2.40)$$

2.4.2   RFID Standard Frame - Link Layer.

2.4.2.1   Reader Frame Types.   Frames from the reader come in two formats, long and short. The short format command frame is 16 bits long and its structure can be seen in Table 2.1. The short format command is limited in that it can not reference an individual tag as there is no allocation for the unique identified (UID) or sub unique identifier (SUID). The UID is similar to a Media Access Control (MAC)

29
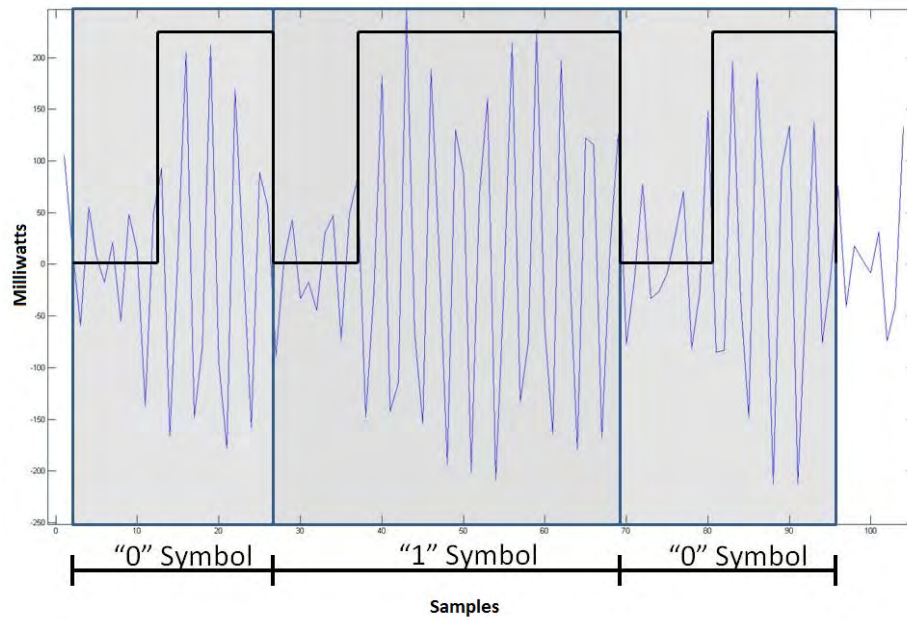
Figure 2.11:   OOK Symbols Overlayed on Capture
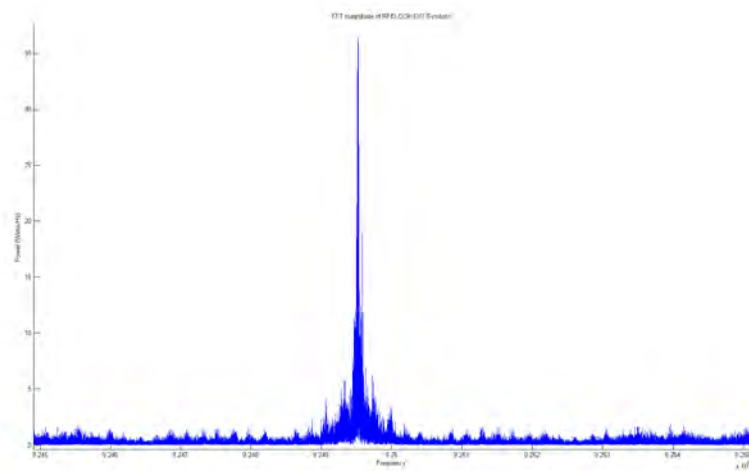
Figure 2.12:   Magnitude of OOK '010' Symbols
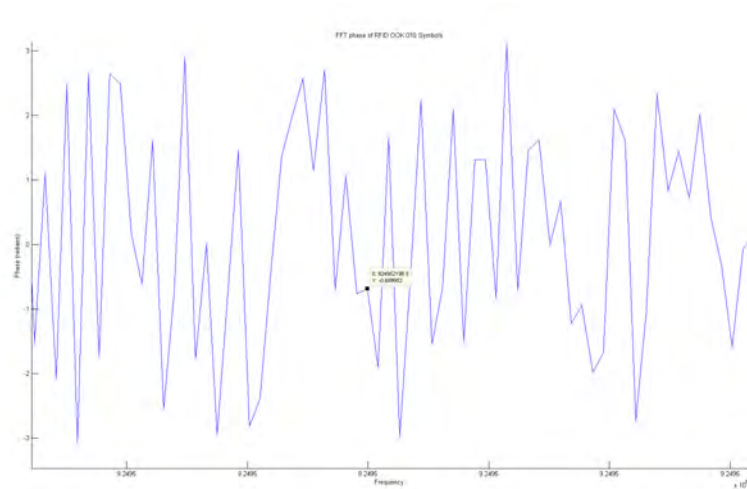
Figure 2.13:   Phase of OOK '010' Symbols

SOF	RFU	Command Code	Parameters/Flags	CRC-5	EOF
	1 bit	6 bits	4 bits	5 bits	

Table 2.1:   Short Command Format

number on a network device. It begins with the manufacturer code and is followed

by the individual tag's identifier. The SUID consists of only the tag's individual

identifier. Due to this limitation the most common use of the short format is the

QueryRep command. This command will be explained further in the next section as

it relates to the communication protocol used in RFID tags. The format of the long

command format is shown in Table 2.2. The longer formats SUID field enables it to

issue commands to a single tag even if several are within range.

SOF	RFU	Command Code	Parameters or Flags	CRC-5	SUID	Data	Data-optional	CRC-16	EOF
	1 bit	6 bits	4 bits	5 bits	40 bits	8bits	8 to n	16 bits	

Table 2.2:   Long Command Format

Preamble	Flags	Parameters	Data	CRC-16

Table 2.3:   Tag Response Format

2.4.2.2   Tag Frame Types.   The general format of the tag response frame can be seen in Table 2.3. In obvious contrast to the reader frame formats, the tag response lacks sizes for each of the fields. The lengths for each of these fields is driven by the command the tag is responding to and the state of the tag. All responses will include the SUID in the data field so the reader knows what tag it is talking to.

2.4.3   RFID Tag-Reader Interaction - Session Layer.   Most commercial RFID readers work in one of two modes, Global Scroll and Inventory. The benefits and mechanisms of each mode are described in the following subsections.

2.4.3.1   Global Scroll.   The first, more primitive, method is called global scroll. In this method the reader sends a single request out and all tags that receive it respond. This mode allows for more rapid reads of a single tag, but if multiple tags are in the area, only the strongest response signal is read. The trade space created by the rapid read times of a single tag make this ideal for high speed applications, where only a single tag will be within view of the reader at a time, like assembly lines. An illustration of the reader to single tag interaction is shown in Figure 2.14. In the single tag example the reader sends the query and the tag responds. All future interactions from the reader to the tag will include the tag's SUID. This prevents a new tag from entering the area and interfering in the ongoing
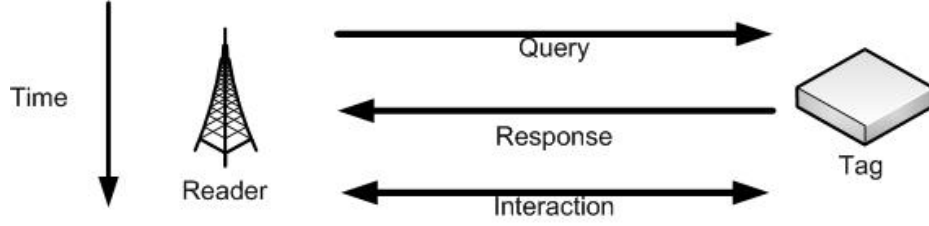
Figure 2.14:   Global Scroll Single Tag Interaction
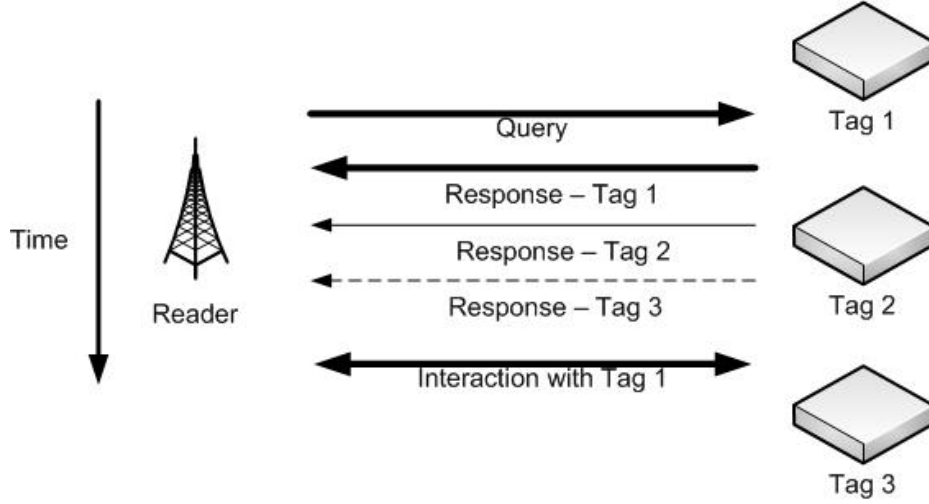
Figure 2.15:   Global Scroll Multiple Tag Interaction

exchange. In the case of multiple tags, as shown in Figure 2.15, we can see all three

tags respond. Tags two and three's responses are represented as a weaker signal by the

thinner and dashed lines. In this case, the reader responds only to tag one's stronger

signal, once again including tag one's SUID to let the tags know who it is talking to.

2.4.3.2 Inventory.   The second read method is called inventory and

is based on the Time Slotted ALOHA protocol. The original ALOHA protocol was

developed at the University of Hawaii Manoa campus as a computer network topology

[13]. It had no collision prevention technique. If a computer had data to send,

it tried to send it. If a collision occurred, it would wait and try again at a later

33

point in time. Time slotted ALOHA was an improvement on this as it introduced time slots. A node could only begin transmission at the beginning of a slot, and the message had to fit inside the time slot. This improved throughput and did not require central coordination. It did require a common time reference between the nodes. This common time reference is not available in RFID tags, particularly passive tags. The solution for this was to modify the slotted ALOHA protocol to be centrally coordinated, or polled in this case. The reader serves as the central coordinator and will start an inventory round by advertising the number of slots it is using. This is an integer and can range from 1 to 1024, determination of the optimal number of slots depends on the number of tags expected to be in range. This advertisement of the number of slots occurs in the Query command message, 2.16 (a). The tags each then pick a random number between 0 and the number of slots minus 1. This slot choice is shown in Figure 2.16 in parasynthesis after each tag. Each time the reader sends out a QueryRep short command, 2.16 (b-d), the tag increments its internal counter. When the counter and the selected slot number match the tag sends an ACK response including the tag's SUID. In Figure 2.16 (e,f) two tags had chosen slot 2 and responded to the reader in this same slot. Upon seeing the multiple backscatter responses the reader can either try to filter the stronger one out and respond to it or ignore both. Our example ignores both and sends the next QueryRep (g). Tags one and two, having not been acknowledged now await the beginning of a new inventory round where they will pick new random slots. In step (g), Tag 3 sees the new QueryRep and increments its counter to match the random slot it choose earlier and responds, (h).
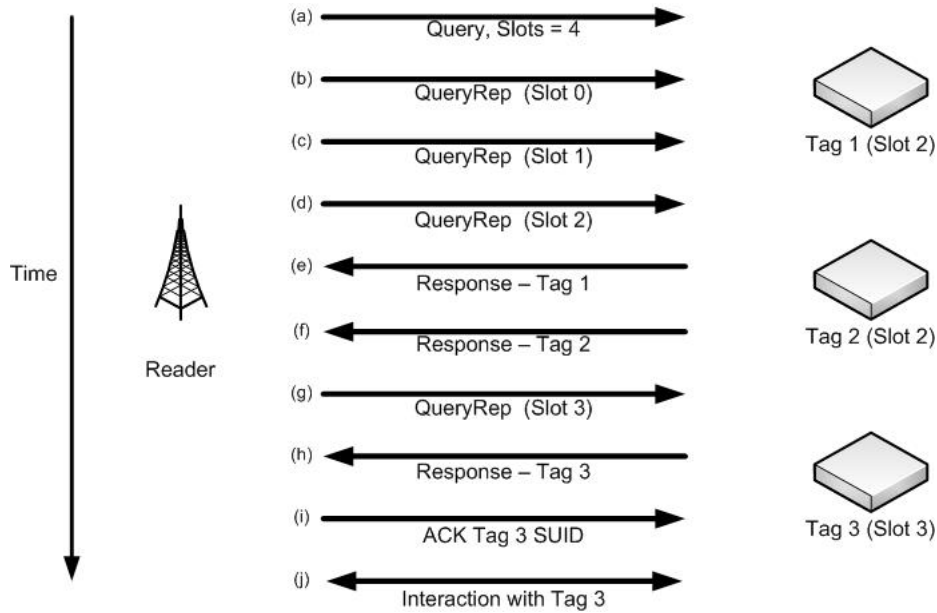
Figure 2.16:   Inventory Query Round

Since it is the only tag to respond in this slot the reader sends an ACK including the

tag's SUID,(i), similar to the way a teacher would call on a student in a classroom.

Further commands are then executed depending on the reader's configuration, (j).

Once the interaction is complete and since the reader has checked all slots it will start

a new inventory round, allowing tag one and two to try and report again.

2.5 Software Defined Radios

Software defined radios have been utilized as experimental platforms for RFID

research at the University of Washington. Michael Buettner is the author of the Gen2

RFID reader and listener [14]. This software package is widely used in SDR circles as

the building block for any RFID related system. Chris Paget used it when he set his

RFID tag read distance record of 217 feet [15]. Mr. Buettner also used the software

as a basis for several papers on RFID technology [16–18]. Of particular interest

to this research is his paper titled"A Software Radio-based UHF RFID Reader for PHY/MAC Experimentation." Buettner provides a solid background on the actual interaction of the reader and tag, as well as a software platform that can be easily modified to capture data not readily available on commercial RFID readers. The rest of this section provides an overview of the USRP1 main board and Flex 900 daughtercard used in this research.

2.5.1 *USRP 1 Mainboard.*   The USRP 1 main board is manufactured by Ettus Research LLC as a reference design and experiment platforms for engineers and students. When paired with a daughter card it is capable of sending and receiving a wide range of signal types. The USRP 1 used in this research has been discontinued and replaced with the USRP E100 series of boards. Figure 2.17 show the internals of the USRP. In general terms it consists of: 1. FPGA; 2. Analog to Digital / Digital to Analog Converters; 3. USB Controller; and 4. Clock. Each of these subsystems is discussed at more length in the following subsections.

2.5.1.1 *FPGA.*   The FPGA in the USRP 1 is from Altera's Cyclone family, the EP1C12 to be precise. This FPGA operates at 1.5V and uses a 0.13 μm manufacturing process. The EP1C12 is the second most powerful member of the Cyclone family and has 12,060 logic elements (LE) and 239,616 total RAM bits [19]. While Ettus does not make mention of the FPGA utilization of the standard USRP1 firmware in any of its documentation, a installation guide generated by UCLA students shows 92% utilization. According to the Ettus web site FAQs, the newer
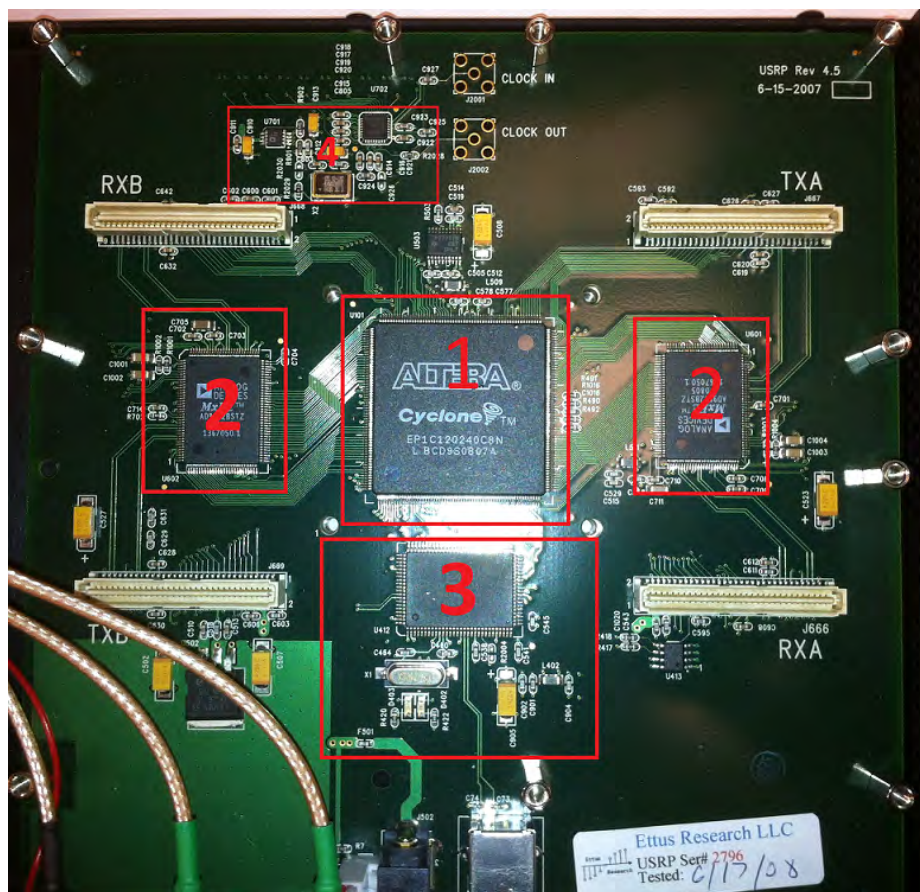
Figure 2.17:   USRP 1

USRP, which utilize the Spartan 3, have up to 63% of their logic elements free for user functions.

2.5.1.2 *Analog to Digitial (ADC) / Digitial to Analog (DAC) Converter.*

The ADC/DAC subsystem of the USRP 1 is implemented in Analog Devices' Mixed-Signal Front-End Processor for Broadband Communications, AD9862 chip. As can be seen in Figure 2.18, each of the two chips on the main board consist of dual ADC and DAC pipelines. The ADC are 12-bit converters and are capable of processing up to 64 megasamples per second (MSPS). The DAC, while not used in this research, are 14-bit and can handle up to 128 megasamples per second. The chip integrates a programable gain amplifier (PGA) to boost a weaker signal and maximizes the resolution of the digitized sample. The PGA can provide from 0 to 20 dB of gain in 1 dB steps. The AD9862 provides good channel isolation of greater than 80 dB between the two receive channels and greater than 90 dB between transmission and receive channels [4].

2.5.1.3 *USB Controller.* The heart of the USB controller is the CY7C68103A integrated circuit. This chip is manufactured by Cypress and marketed as the EZ-USB FX2 USB Microcontroller. It supports the USB 2.0 standard and supports the standard's maximum data rate of 56 MBytes per second [20]. All communications between the main board and GNU Radio on the host PC take place through this controller. More recent USRP models have moved some (E100) or all (N210) of this communication to a Gigabit Ethernet port which would allow the host
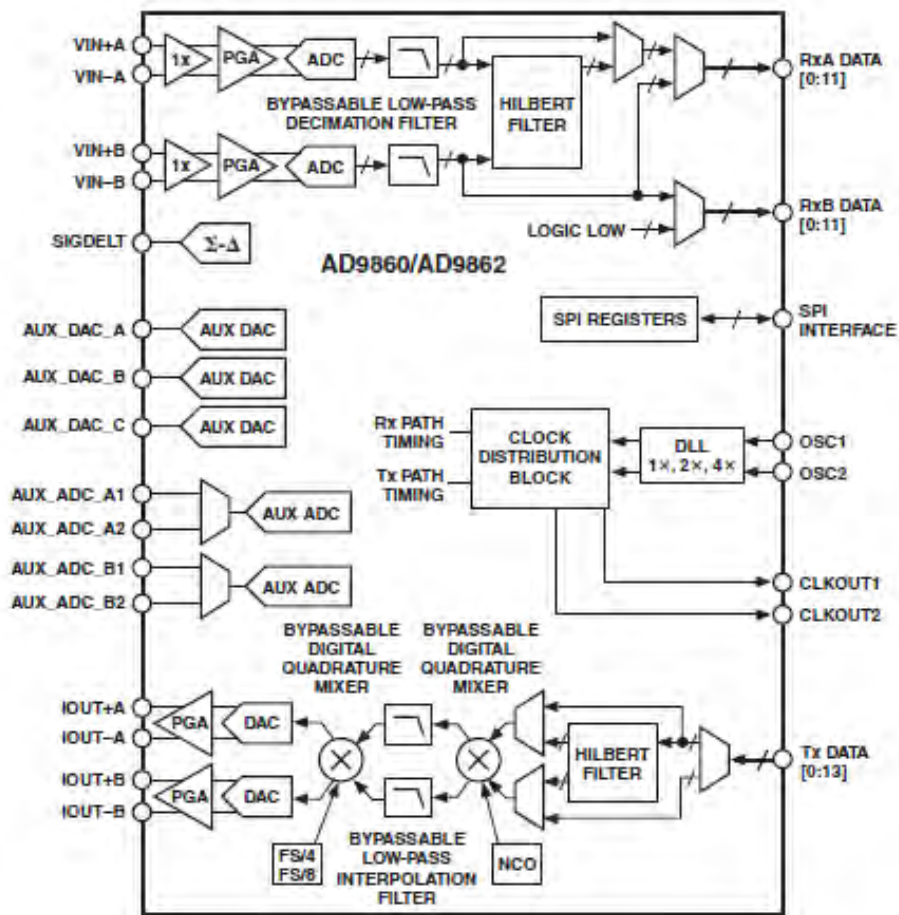
Figure 2.18:   ADC/DAC Functional Block Diagram [4]

computer to be located in a different location. While most of this communication is directed towards the Cyclone FPGA, direct communications with the daughter cards is possible using standard SPI and I2C bus protocols. The controller is able to run at either 48 MHz, 24 MHz or 12 MHz. In the USRP 1, it runs at 24 MHz and has its own oscillator, the ECSR240EX.

2.5.2 Flex 900 Daughter Card.   The Flex 900 daughter card used in this research contains both a receive (Rx) and transmission (Tx) path and is shown in Figure 2.19. The Tx capabilities of the card were not used and are omitted from this description. The key elements of the Rx path are: 1. Analog Mixer, 2. Frequency Synthesizer, 3. and Band-Pass Filters. The main function of this Rx path is to down convert the received RF signal to an intermediate frequency (IF). The band-pass filters are hard-wired LRC networks on the daughter card, and they are specifically tuned for the frequency range of the Flex 900. Similar networks would exist on other daughter cards and would be tuned for the frequency of the card. The demodulator and local oscillator are described in the following subsections.

2.5.2.1 Analog Mixer.   The first stage mixer on the Flex 900 is implemented by Analog Devices' 0.8 GHz to 2.7 GHz Direct Conversion Quadrature Demodulator (AD8347). The functional block diagram for this self contained, surface mount, IC is shown in Figure 2.20. As is evident from the AS8347's long name the chip can process signals from 800 MHz to 2.7 GHz. The AD8347 takes the signal from the antenna and mixes it with a sinusoid from the local oscillator to provide I and
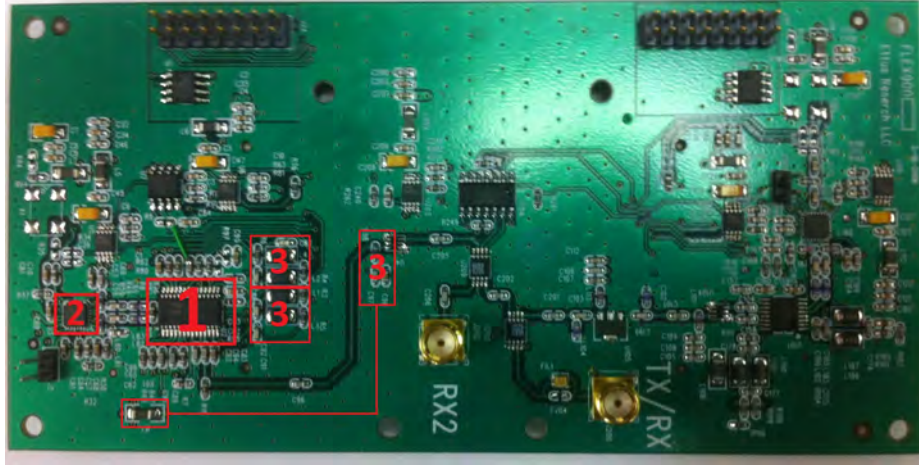
Figure 2.19:   Flex 900 Daughter Card
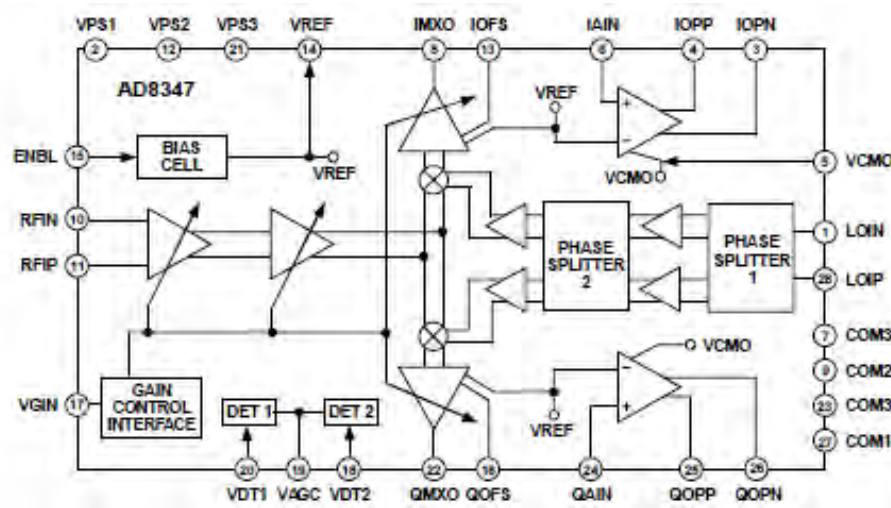
Figure 2.20:   Analog Mixer Functional Block Diagram [5]

Q channels for A-to-D conversion on the main board. The Flex 900 also utilizes the chip's integrated separate I and Q amplifiers after processing the channels through hard-wired band-pass filters. Total possible gain from the variable amplifiers and final amplifiers is 69.5 dB. The external band pass filters prior to final amplification allow the Flex 900 to remove high level out of channel noise [5].
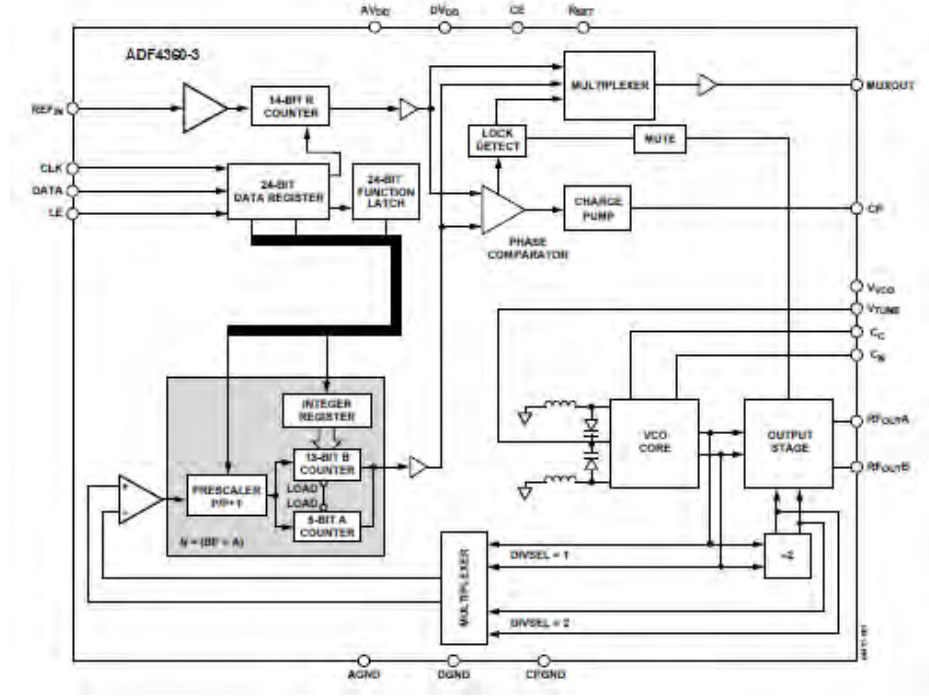
Figure 2.21:   Frequency Synthesizer Functional Block Diagram [6]

2.5.2.2   Frequency Synthesizer.   The frequency synthesizer used in the first stage down conversion stage on the Flex 900 is implemented on Analog Devices' Integrated Synthesizer and VCO (ADF4360-3). The ADF4360 operates on a center frequency of 1750 MHz. It uses a divide by 2 operation to generate sinusoids with frequencies from 800 to 975 MHz. A functional block diagram can be seen in Figure 2.21 [6].

2.6   System Overview

The USRP 1 system is capable of transmitting and receiving on a wide range of frequencies from 1 MHz to 5 GHz depending on the daughter card installed. This research used the Flex 900 daughter card which has a frequency range of 840 to 975

MHz. The IF is limited by the 64 MSPS rate of the ADC. To meet Nyquist and frequency translation requirements the centering of the RF signal an IF range of 16 - 84 MHz is possible.

2.7 System Logical Block Diagrams

This section provides a logical view of a received signal's transition from a real RF signal to the I and Q baseband information transmitted over USB to the host PC.

2.7.1 Flex 900 Logical Block Diagram. The target signal is received from the user selected antenna and goes to the MGA82563 amplifier. After amplification the signal travels through a hard wired band-pass filter to remove out of band noise from the signal. The band for this filter is the entire range of the daughter card, in this case 840-975 MHz. From the filter the signal enters the AD8347 mixer and proceeds through the internal two-stage variable amplifiers. The gain for these amplifiers is controlled by the Digital AGC signal from the main board. The other external signal to the AD8347 is from the ADF 4360. The ADF 4360 synthesizes the local oscillator based on the *Clk* and *Data* information it receives from the main board over the SPI bus. The gain for the Digital AGC and Data signal from the main board are both determined by the Python code generated by GNU Radio on the host PC. This local oscillator signal from the ADF 4360 then goes through a phase splitter in the AD 3847 to generate the *sin* and *cos* signals used to mix the signal. Once the RF signal is mixed with the two local oscillator signals the two portions, the I-Analog and Q-Analog, are again amplified by internal variable gain amplifiers before entering

43
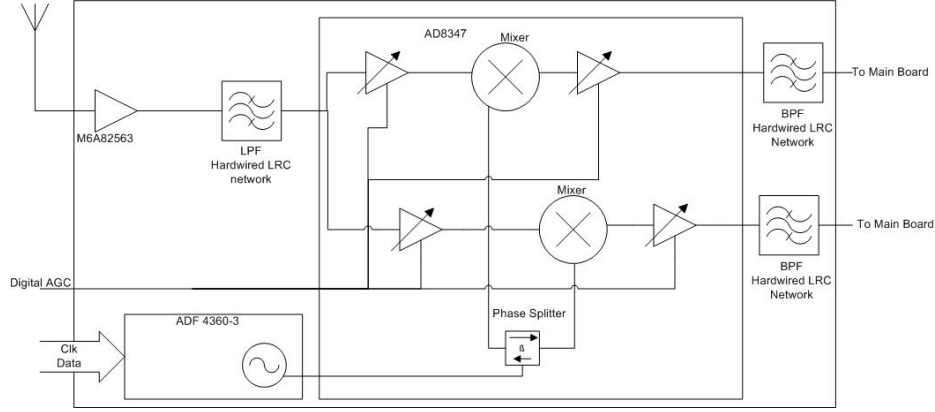
Figure 2.22:   Flex 900 Rx Functional Block Diagram

into external hard-wired band-pass filters. The last stop on the daughter card for the
two signals is to go back through the output amplifier in the AD8347. This output
amplifier uses active feedback to boost the output to a level useable by most A-to-
D converters while minimizing distortion. For this research, this entire process is
happening in parallel on the second Flex 900 daughter card as well. Each Flex 900
receives the same *Clk* and *Data* signal from the mainboard, so the local oscillators
can be considered coherent.

2.7.2 Mainboard Logical Block Diagram.   For this research, the mainboard
receives and processes two signals from separate daughter cards at the same time. This
section describes the transition of one signal, the second signal transitions through
the same process in parallel. The mainboard receives the two analog IF channels of
the target signal from the daughter card in analog. Each channel enters into one of
the ADC in the AD9862 chip. The signals are first amplified by the internal PGA,
the gain controlled by a function of user settings and an effort to maximize resolution.
The ADC then converts each to a 12-bit digital signal that transitions into the FPGA.

44

Once in the FPGA, each signal channel enters the second stage down-converter. The purpose of this second stage is to convert the digital IF signal to digital baseband. To accomplish this, task each IF channel is mixed with a cosine or sine signal provided by a CORDIC algorithm running in the FPGA. While the block diagram shows two mixers, they are implemented on the FPGA as a single complex multiplier. The signals now pass to a digital low pass filter before entering into the 4 stage CIC Decimator. Normally the decimator would be preceded by its own low-pass filter, but since the mixer would have one also the FPGA implements both as a single low-pass filter. The purpose of the decimator is to remove samples so that the signal sent to the USB controller can transmit it to the host computer without being overloaded. In this research, with the USB only responsible for sending a receive signal to the PC and no transmit signal from the PC, the minimum decimation rate we were able to achieve was four. Equation 2.41 illustrates the considerations that go into the minimum decimation rate. The max sample rate is determined by the ADC and is 64 megasamples a second, each sample being 16 bits longs. This research used two daughtercards. Without decimation this would result in 128 MBytes per second of data. With the additional data required for the USB frames a minimum decimation rate of four is necessary. Now the two A-Side channels and the two B-Side channels arrive at a multiplexer. The baseband I and Q signals are interleaved by the MUX and its control logic before moving to the USB controller. The USB controller then
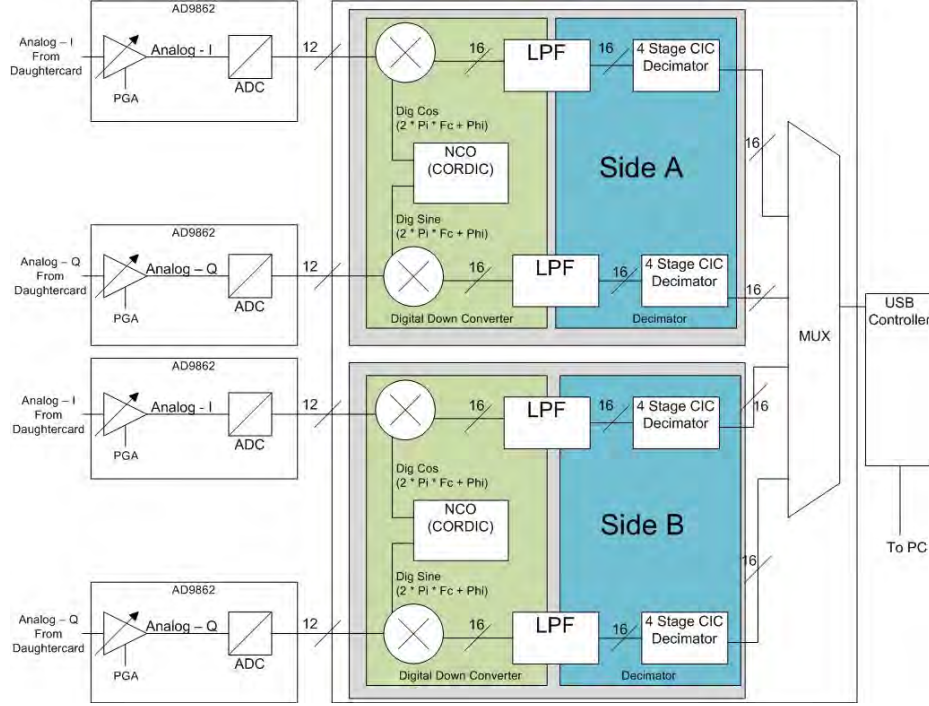
Figure 2.23:   Main Board Functional Block Diagram

puts them into USB frames for transmission to the host PC.

$$(\frac{(\text{ Max Sample Rate})(\frac{16\,bits}{1\,sample})(\frac{1\,byte}{8\,bits})}{\text{Decimation rate}})*\text{Daughter cards}+\text{USB Overhead} \leq \text{USB bandwidth}$$

(2.41)

2.8   Signal processing in SDR

2.8.1   Antenna.   When the USRP receives the signal at the antenna, in the case of shaped OOK RFID encoding, it is a chain of high and low pulses shaped by a low-pass filter. The time domain formula for such a signal can be seen in Equation 2.42. The $s(t)$ term represents the shaping function and $h(t)$ is the data to be encoded. The carrier frequency is present in the cosine function. When transformed into the frequency domain, the signal takes the form seen in Equation 2.43. In the frequency

46
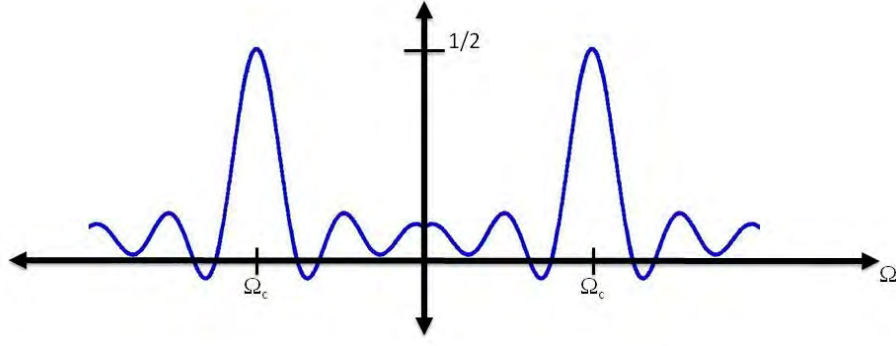
Figure 2.24:   Antenna signal in frequency domain.

domain, the signal forms a SINC function centered on the carrier frequency, Ω_c as seen in Figure 2.24

$$x_1(t) = [s(t) \star h(t)]cos(\Omega_c t) + h(t) \tag{2.42}$$

$$X_1(\Omega) = 1/2S(\Omega - \Omega_c)H(\Omega - \Omega_c) + 1/2S(\Omega + \Omega_c)H(\Omega + \Omega_c) \tag{2.43}$$

2.8.2   Entering First Stage Mixer.   Prior to entering the mixer chip for first stage mixing, the signal is amplified and goes through a band-pass filter, as shown by Figure 2.25. This increases the amplitude of the signal by a gain factor of A and attenuates the out of band noise levels. A graphical representation of this effect in the frequency domain can be seen in Figure 2.26

2.8.3   Frequency Synthesized Local Oscillator.   In the first mixing stage the signal is down-mixed with a synthesized local oscillator to the IF. The mathematical representation of this synthesized frequency can be seen in Equation 2.44. When plotted in the frequency domain it can be seen in Figure 2.27.

47
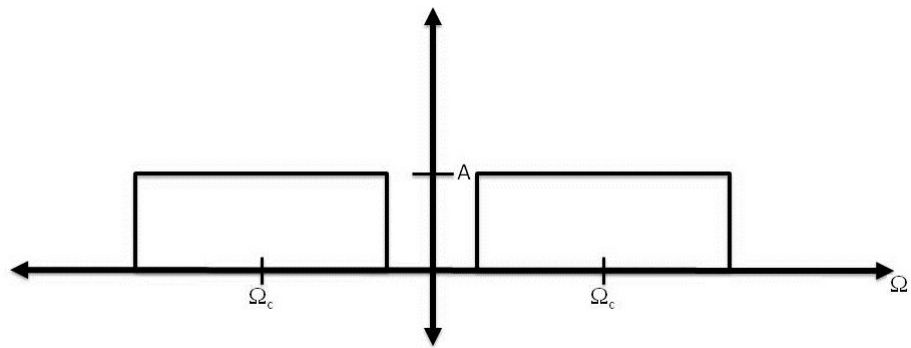
Figure 2.25:   Band pass filter in frequency domain.
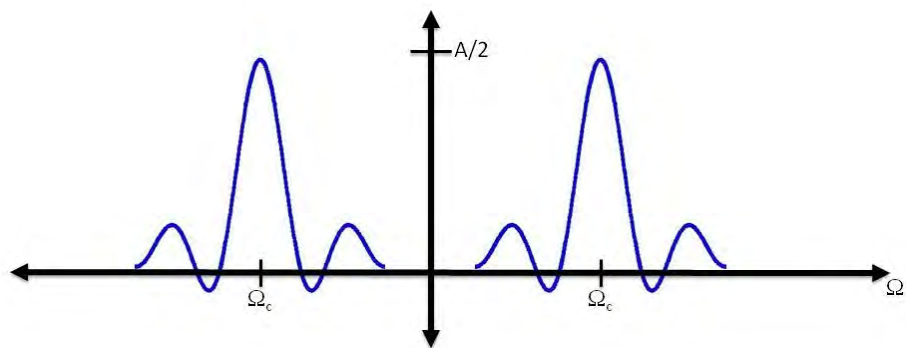
Figure 2.26:   Filtered signal in frequency domain.

48
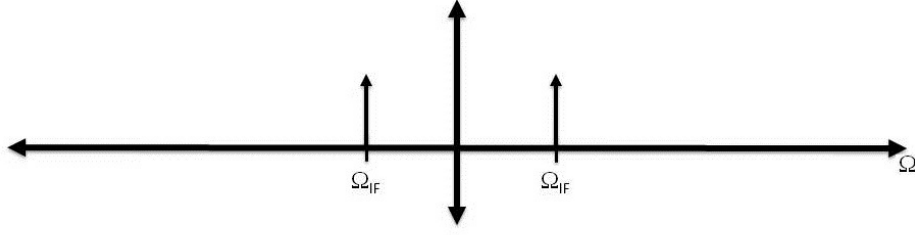
Figure 2.27:   Synthesized local oscillatorl in frequency domain.

$$F_{IF} = \Im\{cos(\Omega_{IF}t)\} = 1/2\delta(\Omega - \Omega_{IF}) + 1/2\delta(\Omega + \Omega_{IF}) \tag{2.44}$$

2.8.4   After First Stage Mixer.   The signal is now convolved with the synthe-sized local oscillator from the previous section down to the IF and is represented by $x_2(t)$. The equation for the in-phase portion of the signal in the time domain is shown in equation 2.45 and the frequency domain is shown in Equation 2.46. To generate the quadrature signal, the inbound signal is mixed with the sine function of the local oscillator, as seen in Equation 2.47 and Equation 2.48. This mixing action attenuates the power signature and creates duplicate sincs in the frequency domain as seen in Figure 2.28.

$$x_2(t) = x_1cos(\Omega_{IF}t) \tag{2.45}$$

$$X_2 = \frac{1}{2}X_1(\Omega - \Omega_{IF}) + \frac{1}{2}X_1(\Omega + \Omega_{IF}) \tag{2.46}$$

$$x_2(t) = x_1sin(\Omega_{IF}t) \tag{2.47}$$

49
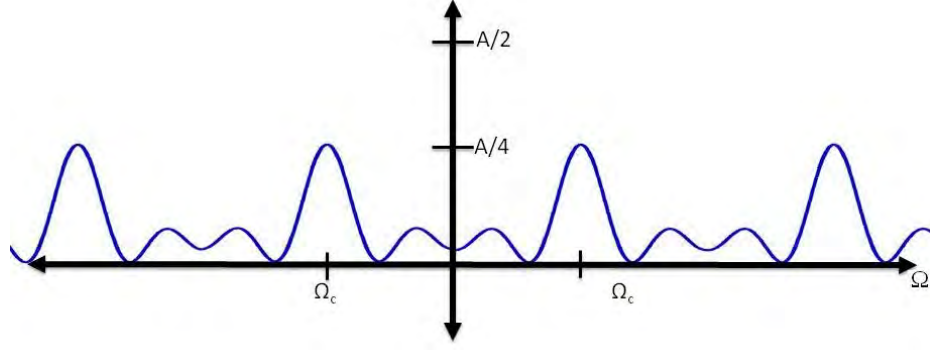
Figure 2.28:   First stage mixed signal in frequency domain.

$$X_2 = j(\frac{1}{2}X_1(\Omega - \Omega_{IF}) + \frac{1}{2}X_1(\Omega + \Omega_{IF})) \tag{2.48}$$

2.8.5   Final Analog Band Pass Filter.   Just prior to leaving the daughter card the signal travels through one more band pass filter. This filter is designed so that it removes the duplicate SINCs in the frequency filter that result from the first stage mixing. The result of Figure 2.28 is convolved with this band pass function as seen in Figure 2.29. This final analog signal is then passed from the daughter card to the ADC on the main board.

2.8.6   ADC Sampling Pulse.   Within the ADC a sampling pulse is generated. The frequency of this pulse, f_s, is determined by the sampling rate of the hardware. In the USRP 1 this is 64 MHz. A representation of this pulse in the time domain is seen in first line of Figure 2.30. Each pulse in that figure is spaced T_s, which is the sampling period, or $\frac{1}{f_s}$. Based on the sampling frequency of 64 MHz this is $1.67 * 10^{-7}$ seconds. In the frequency domain, this appears as a series of impulses space at integer multiples of the sampling frequency, as shown on second line of Figure 2.30.

50
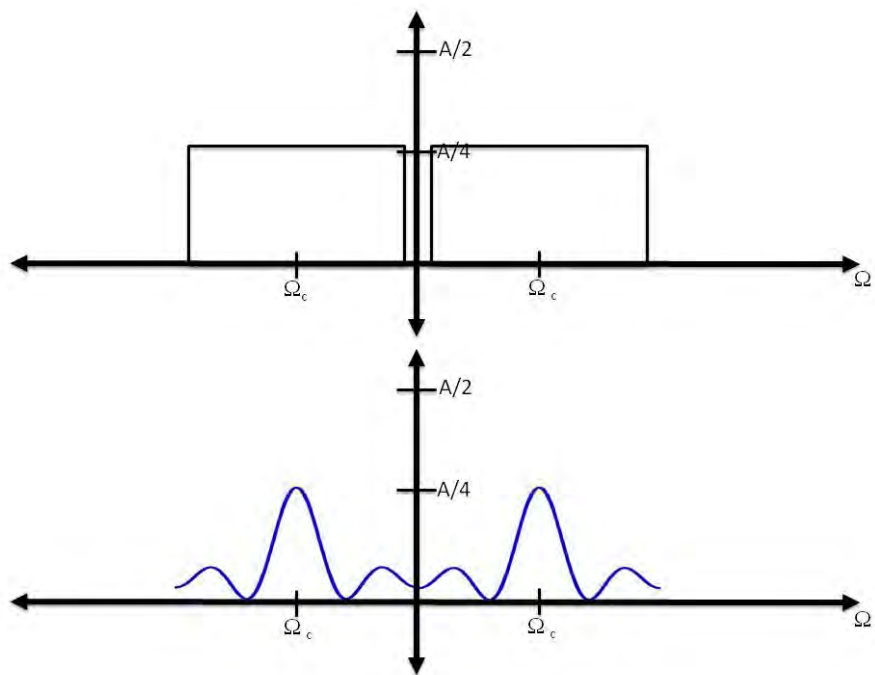
Figure 2.29:   Final analog signal in frequency domain.
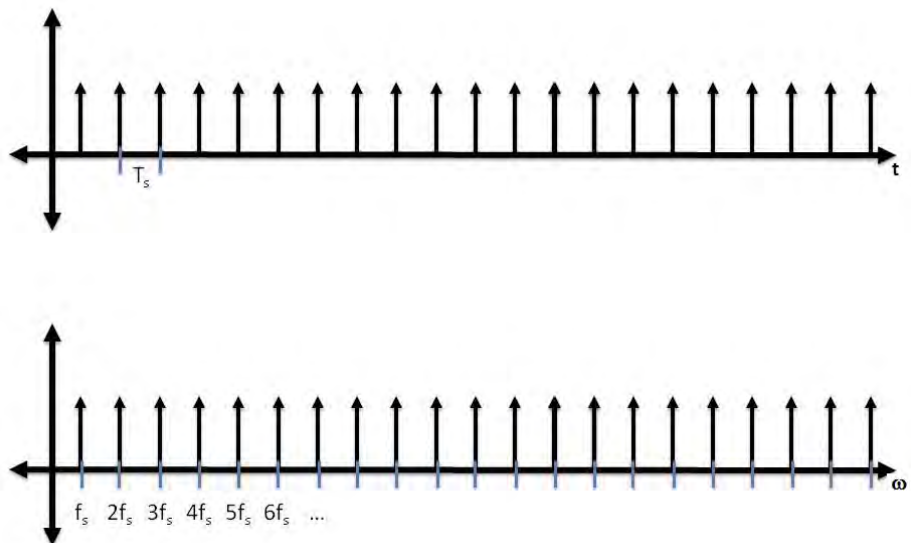
Figure 2.30:   Digital sampling signal.
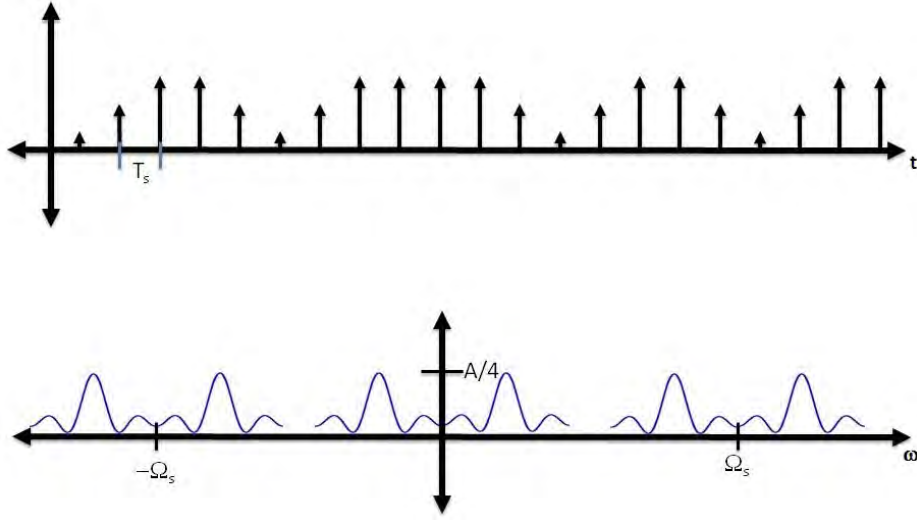
Figure 2.31:   Digitaly sampled signal.

2.8.7   Analog-to-Digital Converter.   The ADC converts the continuous time

signal, X, to discrete time by multiplying it by the sampling pulse as shown in Equa-

tion 2.49. In this way, the signal transform from a continuous wave to a series of

impulses spaced T_s apart. The results of this function is shown in Figure 2.31 (a). It

appears in the frequency domain as shown in Figure 2.31 (b.)

$$x_5[n] = x_3(nT_s) \tag{2.49}$$

2.8.8   Frequency Synthesized Digital Local Oscillator.   As with the first stage

mixer, the second down converter generates a cosine function but this one is digital.

The digital cosine is generated by equation 2.50. Equation 2.51 is the frequency

domain equivalent.

52
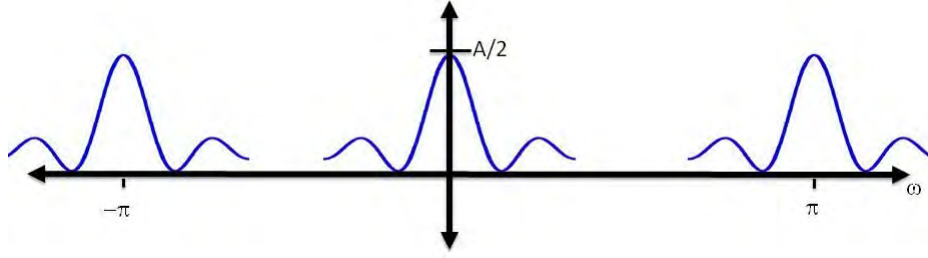
Figure 2.32:   Digital baseband signal.

$$f[n] = cos(\Omega_{IF} n T_s) \tag{2.50}$$

$$\omega = \frac{\omega}{\omega_s} 2\pi \tag{2.51}$$

2.8.9   Digital Mixing from IF to Baseband.   The system then mixes the digital IF signal with the synthesized local oscillator to generate the digital baseband signal. This mixing causes constructive interference and raises the magnitude of the signal back to A/2. It also moves the signal to the discrete time domain. The discrete time frequency domain representation of the digital baseband signal can be seen in Figure 2.32.

2.8.10   Digital Decimation.   The four stage decimator removes a set number of samples dependant on the decimation rate set by the user. As discussed earlier the minimum decimation rate is four. Figure 2.33 shows the effect of the reduced number of samples in the frequency domain.

53
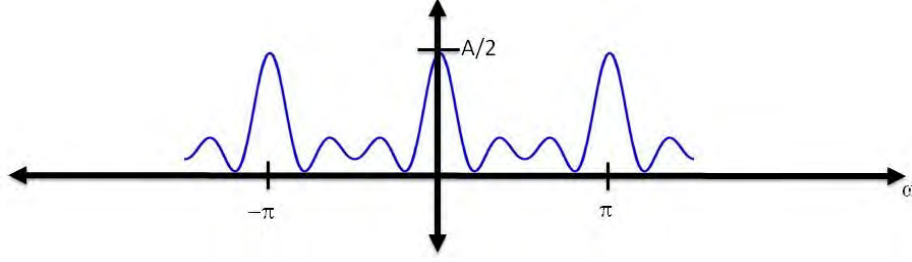
Figure 2.33:   Decimated digital baseband signal.

2.9   Related Research

2.9.1   LANDMARC.   Due to the inability to use TDOA, many of the earlier localization methods for RFID tags, such as LANDMARC [11], use a read/no-read of the subject marker, known tags, and known readers to calculate a location based on Received Signal Strength Indicator (RSSI). This localization technique querys a array of readers, whose positions are known, to see which tags they can see and at what power level they can see them. A sample array is shown in Figure 2.34. When a target tag is identified, it compares its received power levels it was read at to the power levels that known tags are read at. By comparing the distances of the known tags and their power levels to the power levels of the target tag a location can be surmised [11]. The subject paper recognized that this procedure works but we identified several issues for real world implementation. RSSI can be severely affected by the propagation environment. If a new object enters the area, be it an emitter or absorber of RF, the system must recalibrate the power levels of the known tags. It was also found that the power incident on a tag can cause its calculated location to vary greatly.
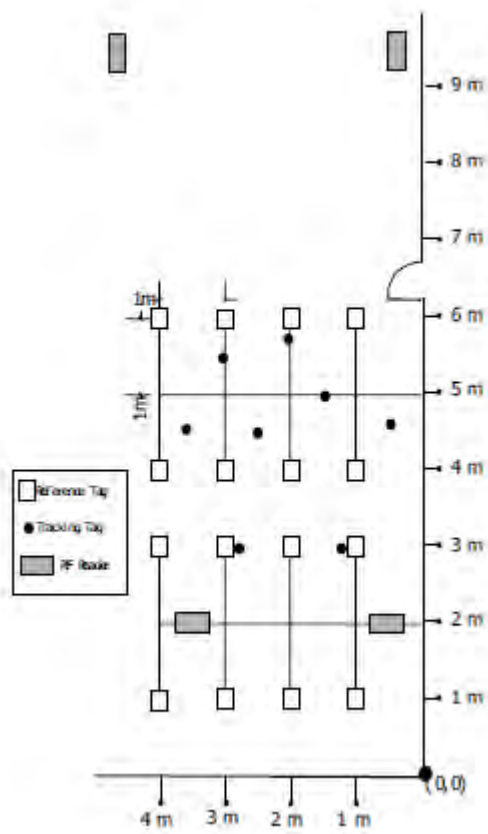
Figure 2.34:   LANDMARC Identification Layout

III. Methodology for SID of Passive RFID Tags

3.1   Approach

This research develops and analyzes the effectiveness of the three-part PDOA spatial identification algorithm. The first part of PDOA is time domain analysisto provide a relative velocity towards the receive antenna. The second part is frequency domain analysis which provides a range to the target signal. The final portion of the PDOA algorithm is the spatial domain analysis, in which two receive antennas provide a bearing to the target signal. The locations provided by all three parts are compared to the same portion of the algorithm from a simulation of the same target signal.

3.1.1   Create Simulation.   In order to determine the effectiveness of the spatial identification method, a simulation of the test bed is created to provide a baseline for comparison. These simulations provide verification that, given a good extraction of the phase of a signal, the PDOA metrics can be calculated from captured data. The velocity of the target signal, reflection from the table surface, and the path traveled are modeled in MATLAB. Additive Gaussian White Noise is also added to the simulated signal based on the observed noise floor of the laboratory in use. Multiple simulations are run for each configuration and the results are averaged to establish the baseline performance expected out of the real world system.

3.1.2   Phase of Received Signal.   The phase of the captured signal is calculated using a Fast Fourier Transform in MATLAB. Once the I and Q data is imported

```
X1_freq = fft(x1);
phase_x1_fc = angle(X1_freq(kc));
```

Figure 3.1:   Code to Extract Phase of Received Signal

```
v_r(sample) = (3e10/(4*pi*fc))*((phase_x1_fc(sample)- phase_x1_fc(sample-1))/step);
```

Figure 3.2:   Code for TD-PDOA

and the start of the tag response is located in the capture, the FFT is found using the

code snippet in Figure 3.1, where kc is the center frequency of the captured signal.

Since an EPC Gen 2 tag is used in all tests, the center frequency remains constant at

915 MHz. This step is repeated for every sample captured in each test.

3.1.3 Time Domain PDOA.   When the PDOA is analyzed in the time

domain it yields the velocity of the target transmitter with respect to the receive

sensor. This is done with the code snippet contained in Figure 3.2 in MATLAB based

on the phase found in 3.1.2.

This code snippet implements Equation 2.1 described in Chapter 2. The cen-

ter frequency, fc, is found for each signal sample piece using FFT. In all cases the

distances are in centimeters. The speed of light required in all calculations, c, is also

represented in cm/s or 3e10. $\delta\phi$ is calculated by taking the angle of the FFT bin

that represents the center frequency of each signal sample. The time delta is simply

the time between the two samples stored in the variable named step. If the tag is

stationary the phase of sample and sample-1 will be the same resulting in an angular

velocity of zero. The function will also report an angular velocity of zero at the center

crossing of the tag, when the target is directly in front of the sensor antenna. This

```
d_found(sample) = -(3e10/(4*pi))*((phase_x1_fc(sample)-phase_x1_fc2(sample))/(fc-fc2));
```

Figure 3.3:   Code for FD-PDOA

point also marks the instant that the function will transition from positive to nega-

tive, or negative to positive, velocity as the target transitions from moving towards

to away from the sensor antenna.

3.1.4 Frequency Domain PDOA.   When the PDOA is analyzed in the fre-

quency domain it yields the distance from the target transmitter to the receive sensor.

We do this once again based on the phase found in Section 3.1.2 but we also must

find the phase of the captured signal at a different frequency. Based on the fc found

previously a frequency 1 MHz from the signal center frequency is selected and is rep-

resented by the variable $fc2$. The code snippet in Figure 3.3 implements Equation

2.12 from Chapter 2. The difference, $fc - fc2$, will remain constant at 1MHz this

combined with the fact that the equation relies on the same sample allows this tech-

nique to find the range to the target transmitter even if it is stationary. For a target

moving in a straight line perpendicular to the antenna array this value will have a

minimum value at the center crossing to the sensor antenna.

3.1.5 Spatial Domain PDOA.   To analyze the PDOA in the spatial domain,

a second antenna is added to the software defined radio. If the phase of the received

signal is inspected at each of the receive antennas, a bearing to the target transmitter

can be calculated. This bearing to the target transmitter is found using the following

the code seen in Figure 3.4. For this calculation, a second capture is taken from

```
theta_found = arcsin(-(3e10/(2*pi*fc))*((phase_x1_fc(sample)-phase_y1_fc(sample))/a));
```

Figure 3.4:   Code for SD-PDOA

the USRPś second daughter card. The antenna for this capture is positioned a set

distance from the first antenna. In the code, this distance is represented by a and is

given in centimeters. The phase for the second capture is calculated using the same

function as Section 3.1.2 and the samples are aligned in time. The phase of the second

sample is stored in the array phase $\_y1\_fc$. The SD-PDOA equation assumes that the

tag is at a distance greater than one wavelength. The experiment is configured so that

the tag is never closer than 86.0 cm – more than double the 37.5 cm wavelength of a

915 MHz signal. The result of this function, $theta\_found$, is the bearing to the target

tag from receive Antenna #1. Negative values distinguish that a target transmitter

is on the far side of Antenna #2 relative to Antenna #1. Positive values represent a

target transmitter that is on the same side of the Antenna #1 as Antenna #2.

3.2   System boundaries

The system under test (SUT) consists of a small scale test bed. This test bed

consists of a commercial RFID tag reader, a software defined radio, a track for the

tag to move along, and a controller for tag movement. A block diagram of the SUT

is shown in Figure 3.5 Each section is described in the following subsections.

3.2.1   RFID Reader.   The commercial RFID tag reader is an Alien 9800, and

it is used to energize the tag so that the interaction can be captured. It is controlled

by a Windows based PC via Ethernet. The reader is operated in Global Scroll mode.
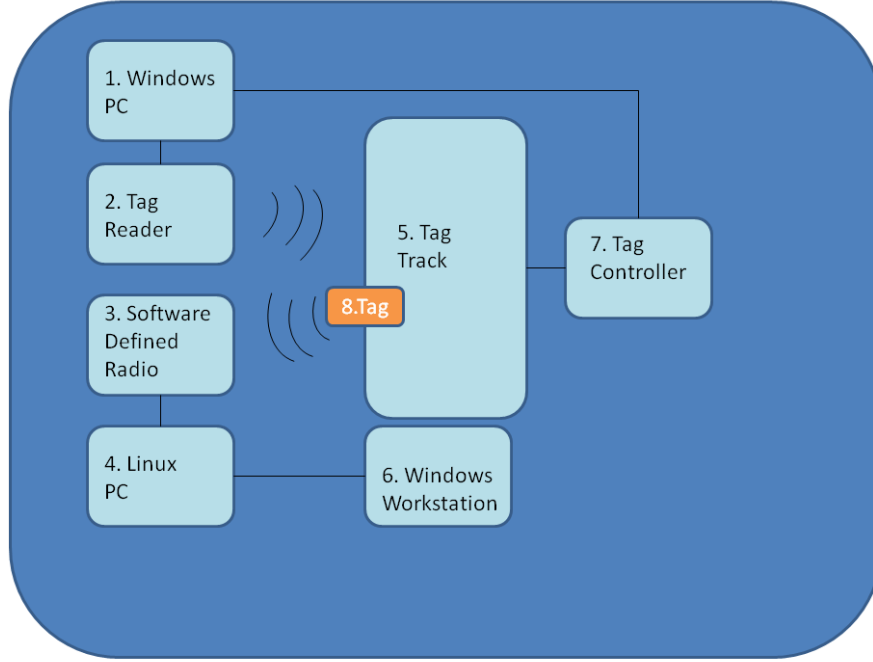
Figure 3.5:   System Under Test Block Diagram

This mode allows for faster reads, as it simplifies the query process by removing the time slots that allow a reader to interact with multiple tags. In order to remove the possibility of errant reads the lab is kept clear of other RFID tags that operate in the 900MHz band.

3.2.2 Windows PC.   The Windows PC is a Dell Laptop running Windows XP. The laptop directly controls the tag movement through the USB to serial port adapter. It also interfaces to the Alien 9800 reader over the Ethernet connection.

3.2.3 Software Defined Radio.   The receive sensor is a software defined radio; a USRP 1 was selected for its low cost, flexibility and the ability to hold two daughter cards. The two daughter cards, both which operate in the 900 MHz

Figure 3.6:   SDR RFID Reader

band, are required in order to accomplish the spatial domain PDOA. The radio is

configured to capture a 2.5 MHz band of the spectrum centered at 915 MHz with

a sample rate of 1.35 megasamples per second. The initial vision of the SUT had

the SDR acting as the RFID tag reader, capturing the interaction. To this end, the

RFID Gen2 reader developed by Buettner et al. was installed on the USRP 1 and

configured using the Linux workstation. This configuration can be seen in Figure 3.6

and consists of a Macbook running Ubuntu 10.10 and GNU Radio, a USRP1 SDR

with a Flex 900 daughter card and two Alien 9611-CR antennas. The GNU Radio

installation has been modified to enable the faster response times required by RFID

tags. Initial experiments focused on the use of a newer USRP 2 model, but due to

a requirement to use its proprietary UHD drivers, we reverted to the USRP1 which

uses the open-source drivers included in GNU Radio. As each tag response is received by the reader, a '0u' pattern is output to the terminal as can be seen in Figure 3.6. We are able to match the read distances of commercial readers. While the EPC Generation 2 specification is 3 m, this is largely dependant on line-of-sight and can be reduced quickly by interference of metallic objects in the lab. This verification was completed by mounting the two antennas along one lab wall and walking away from it with various tags. The edge of the read range was defined as the distance when the successful read rate dropped below 75%. The location of this cutoff was then marked on the floor. Without moving the tape, and with the SDR configured at the same power level and query rate the range to the read rate failure was verified for all tags tested. While the SDR was capable of reading the tags, limitations in either the USB interface or the age of the Macbook prevented the capture of all of the required signal information. It was decided that moving the burden of the tag query off of the Linux PC and onto the commercial reader would reduce this bottleneck.

The SDR is now configured with two Flex 900 daughter cards and twin whip style antennas. The SDR with Antenna #1 is positioned between the Rx and Tx antennas of the commercial reader as seen in Figure 3.7. This position allows for the strongest signal reception for the TD-PDOA and FD-PDOA. Antenna #2 is mounted to the test bench outside the Rx/Tx pair and alternate left and right for different test runs. This new configuration was then tested to verify the ability to capture the data required for the testing. Figure 3.8 shows an early capture of the interaction. The query/response can be clearly seen in this segment with the reader sending out the

Figure 3.7:   SDR RFID Reader

higher signal in the left portion of the wave and the tag's modulated response to the right.

3.2.4 Linux PC.   The radio is controlled by a Ubuntu 10.04 computer running GNU radio and the GNU Radio companion. The start and stop signal for the the capture is received over Ethernet from the PC controlling the reader and tag track. Each capture is saved to a different file for offline analysis on a workstation class computer.

3.2.5 Tag Track.   The tag tack is actually not a metal track, but a course of rope suspended twelve inches above the test table on wooden rods with nylon pulleys. The actual path of the tag can be changed by moving the wooden rods to other sets
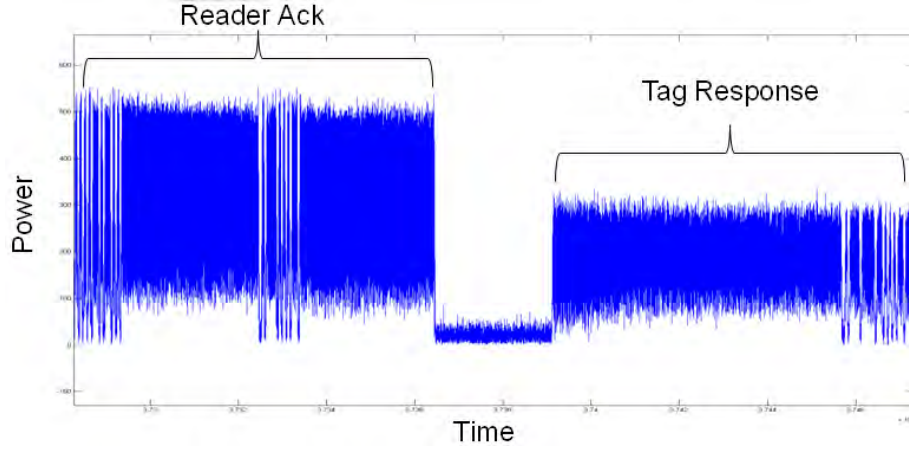
Figure 3.8:   SDR RFID Reader

Table 3.1:   Speed Verification Test Results

Desired Speed (cm/s)	Run 1 (cm/s)	Run 2 (cm/s)	Run 3 (cm/s)	Run 4 (cm/s)	Run 5 (cm/s)	Run 6 (cm/s)	Avg Time (s)	Observed Speed (cm/s)	Diff. (cm/s)
10	10.59	10.53	10.69	10.56	10.60	10.66	10.60	9.42	0.57
15	7.09	7.06	7.13	7.12	7.19	7.12	7.12	14.04	0.95
20	5.18	5.25	5.25	5.34	5.28	5.21	5.25	19.04	0.96
25	4.00	4.09	4.06	4.13	4.13	4.13	4.09	24.44	0.55
30	3.35	3.29	3.38	3.59	3.49	3.50	3.43	29.12	0.87
35	3.00	2.97	2.90	2.97	2.88	2.90	2.94	34.05	0.95
40	2.62	2.62	2.54	2.50	2.56	2.53	2.56	39.04	0.96
45	2.19	2.25	2.25	2.22	2.22	2.18	2.22	45.08	-0.08

of holes on the pegboard table. Four track configurations are tested, and these can

be seen in Figure 3.9. The speed of the tag was verified by placing two posts one

meter apart on the test table. A red marker was placed on the rope track. The time

to transverse the distance was measured, and six trials at each speed were conducted.

The results from those trials can be seen in Table 3.1

3.2.6   Windows Workstation.   The windows workstation is used to do the

offline processing of the collected data. It is a Dell Precision T7500 with 12 GB of
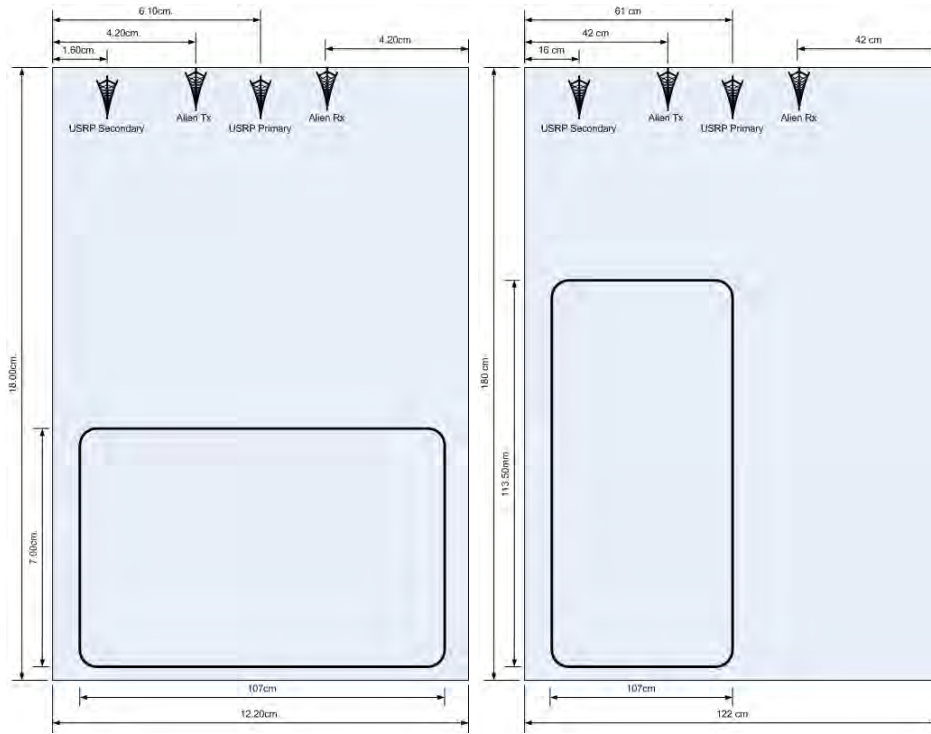
(a) Configuration 1

(b) Configuration 2
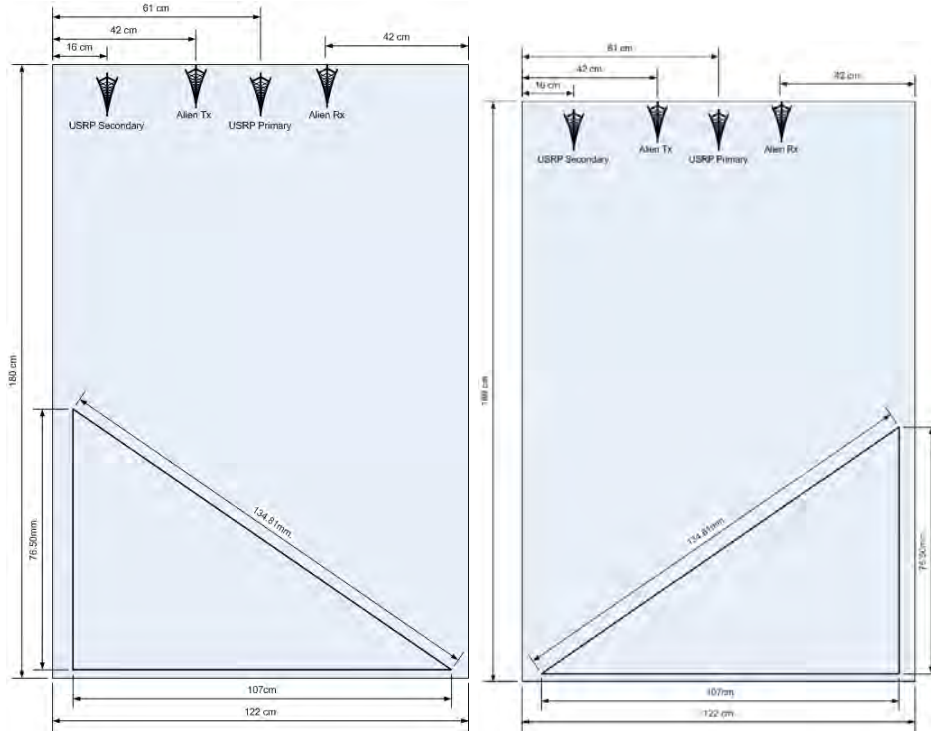
(c) Configuration 3

(d) Configuration 4

Figure 3.9:   Track Configurations

65
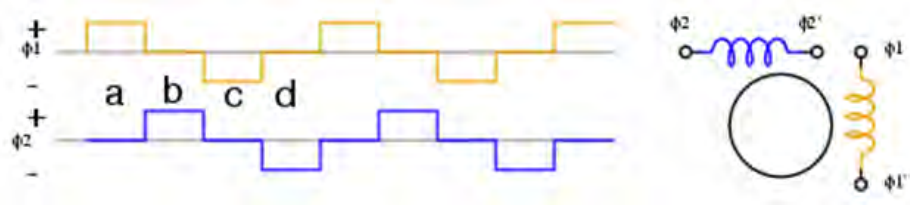
Figure 3.10:   Stepper Motor Drive Wave

RAM and 2TB of hard drive storage. It is running Windows 7 with MATLAB r2010b. The processing of the tag's spatial identification was moved to this system because of the large size of the capture files. This system implements the code from Sections 3.1.3 – 3.1.5.

3.2.7 Tag Controller.   The velocity and direction of travel of the tag is directed by the same PC as the Alien reader by serial port. A connection from the serial port to a ML507 Virtex board provides a timed pulse wave to a 12V stepper motor via an H-bridge to protect the electronics on the ML507. A stepper motor was chosen over a conventional motor due to the precise control it provides. Given a set pulse wave from the control board, the motor will always spin at the same velocity regardless of fluctuations in the supply voltage. The stepper motor is a bipolar 1.8 degree per step motor. The motor has four wires which connect to two different coils. In order to drive the motor, the coils must be activated in the sequence shown in Figure 3.10 Each progression in the waveform, called a "step," drives the motor 1/200th of a revolution, or 1.8 degrees. To reverse the direction of the motor, the coil activation sequence is simply reversed. A commercially H-bridge kit is inserted inline between the ML507 and the stepper motor. This H-bridge converts the 3.3V

66
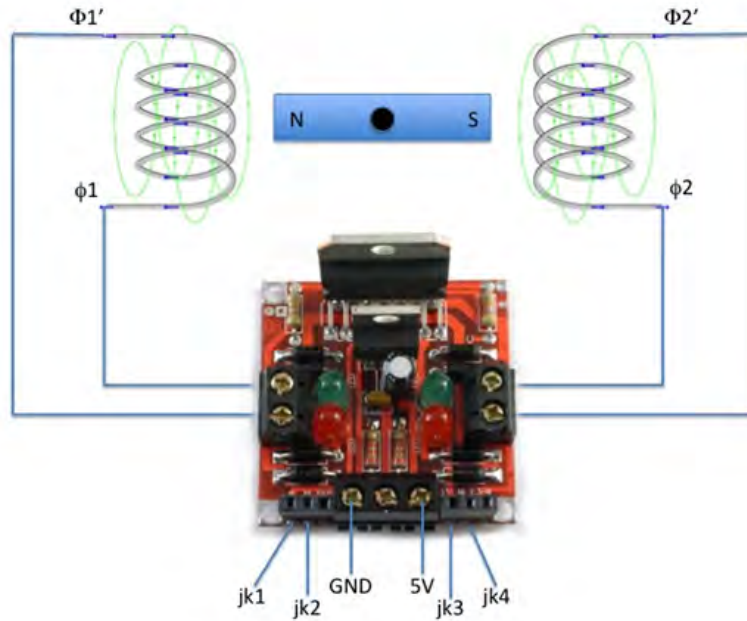
Figure 3.11:   Motor Hardware Circuit

TTL level logic from the output pins of the ML507 to the 12V required to drive the motor. Diodes on the bridge also prevent feedback from the inductive motor from flowing back to the ML507 and damaging the lower voltage components. Figure 3.11 depicts the motor controller's hardware circuit. Pins $\Phi1$ and $\Phi1'$ are driven by $jk1$ and $jk2$, while pins $\Phi2$ and $\Phi2'$ are driven by $jk3$ and $jk4$. The GND and 12V inputs are driven by an external computer power supply. This power supply was also used to power the ML507 so that a common ground was present from the two systems. The VHDL module developed functions as a finite state machine and produces the required waveform from the diagram in Figure 3.10. When the direction input is set to '0,' the module drives through a state table containing the coil activation sequences in the proper order. When the direction input is set to 1 the module iterates the state

table in the reverse order. At line 166 the *std_logic_vector* speed pulled from the bus in line 152 is converted to an unsigned integer using the *conv_integer* command. By multiplying this value by 20000 we cause the FSM to wait for 30 microseconds times the value of *speed*. For example if speed equaled 60 cycles each step would be spaced 180 microseconds apart. Early versions of this code simply accepted the speed from the bus and attempted to drive the motor at that speed. It was observed if that the speed was changed too quickly the motor would lock up. In order to prevent that a ramping function was added, lines 169-173, to the code so that the speed the motor received is increased, or decreased, by one each step it takes.

3.2.8   Tag.   Different tags are tested to observe differences in the response due to antenna shape. All tags are EPC generation two tags and respond to queries in the 915 MHz band. Four examples of the different antenna patterns under test are shown in Figure 3.12. The large silver shape in each tag is the antenna; the actual logic circuit for each tag is contained within the small black dot at the center of the antenna.

3.3   System Parameters

The workload parameters of the system are set to provide proof-of-concept for the use of PDOA as a spatial identification technique in regards to passive RFID tags. These parameters include the number of tags, distance to reader, and velocity of tag.

Figure 3.12:   Sample RFID Tag Antenna

3.3.1   Number of Tags.   The number of tags under test is limited to one in this research. While the reader is able to query multiple tags, only one is visible at a time. The reason for this is so that the reader can stay in Global Scroll mode for more rapid reads. While only one tag is visible at a time, several different tag antenna configurations are tested to compare accuracy.

3.3.2   Distance to Reader.   As shown above in Figure 3.9, the tag will not move more than two meters from the tag reader and sensor receiver. This is well within the specification of the EPC Gen 2 tags. The specification is for read distances of up to three meters and extended reads demonstrated at ranges of approximately six meters. The tags are kept within this range in order to ensure consistent, rapid, reads of the tags. If the test was to extend to the edge of the RFID tag's range there

69

would be additional noise as well as erroneous reads which could negatively affect the accuracy of the system.

3.3.3 Velocity of Tags. Tag velocity represents the final variable in the system under test. The velocity is set at 10, 20, 30 and 40 cm/s. These boundaries represent the equivalent of a slow crawl to the speed of a person walking. Given the small scale of the system, faster speeds are not able to provide enough captures of the tag moving in any one direction to produce an accurate characterization of the tag's spatial identification.

3.3.4 RFID Reader Configuration. As stated above the commercial reader is operated in Global Scroll mode. This mode was selected for the rapid read rates of a single visible tag. If the test was expanded to track multiple tags the reader would require reconfiguration.

3.3.5 SDR Configuration. The configuration of the SDR remains constant throughout the testing. Location and wiring of the antennas themselves remains constant throughout testing.

3.3.6 Tag track. The tag track is reconfigurable on the test bed. Paths along the track were chosen to vary the movement of the tag with respect to the receive antenna. By having the tag move in different directions relative to the antenna, it could be observed if the system is more proficient at detecting targets moving in different orientations. The tracks tested are illustrated in Figures 3.9

3.3.7 Tag type. Different RFID tags used different styles of antennas as shown in Figure 3.12. Runs of the same velocity and target track are repeated with different tags to observe any variation in accuracy of the different tags.

3.4 Performance Metrics

The metrics of the SID PDOA system measure the system performance. They are generally effective when comparing the system to the simulations and to judge the feasibility of the overall system. For this experiment the metric is the accuracy of the computed SID. The difference of the observed SID and the baseline will be found, and the variance of the observed SIDS will be calculated.

3.5 Evaluation Technique

The evaluation technique used to determine the performance of the PDOA algorithm is the analysis of an actual system. All three elements of the PDOA algorithm have been shown to be effective in simulation. What makes this research unique is the capture of real world data with the use of a SDR. The query of the tag is provided by an Alien 9800 RFID reader and two attached ALR-9611-CR antennas. The EPC Generation 2 RFID tags under test are shown in Figure 3.12. A python script running on the PC laptop controls the direction and velocity of the tag. Each capture started by the script is saved to the hard drive with a date and time stamp. Offline analysis of these captures occurs on a Dell T7500 workstation class PC using MATLAB 2010b.

3.5.1 Selection of Data Samples.   The initial captures of reader and tag interaction showed a large variance in several variables which made automatic processing of the data difficult. The first of these is the timing of the interactions. The Alien 9800, due largely to the robust design, reads at random times and spacing depending on the environment. This results in inventory rounds that are not evenly spaced in the time domain. Second is the highly variable power level of the response. If the tag is able to harvest a large portion of the reader's power the response can be relatively strong, 50-75% of reader's power. More often than not, the power level of the tags response is less than 50% of the reader's power level. For these reasons, analysis of the interactions was done manually.

The first analysis step is to plot the entire capture in the time domain as seen in Figure 3.13. This particular capture is from Configuration #2 with the tag moving at 10 centimeters per second towards the reader. After enlarging one interaction group, as shown in Figure 3.14, the sample numbers for the start of each reader message and tag response is logged in an Excel spreadsheet. The iteration in Figure 3.14 is the first group seen in Figure 3.13 and shows ten queries of the one tag within range. From this interaction two tag reads and their corresponding responses are selected for analysis. The phase of the response of the tag, ϕ_{tag1} and ϕ_{tag2}, is based on the signal it receives from the reader. This signal has its own phase, $\phi_{reader1}$ and $\phi_{reader2}$. If the reader is coherent between messages, than this will cancel out. If not, the final phases used in the SID metric calculation is the phase of the response minus the phase of the reader message, $\phi_{tag1} - \phi_{reader1}$ and $\phi_{tag2} - \phi_{reader2}$. I am using the first and last

72
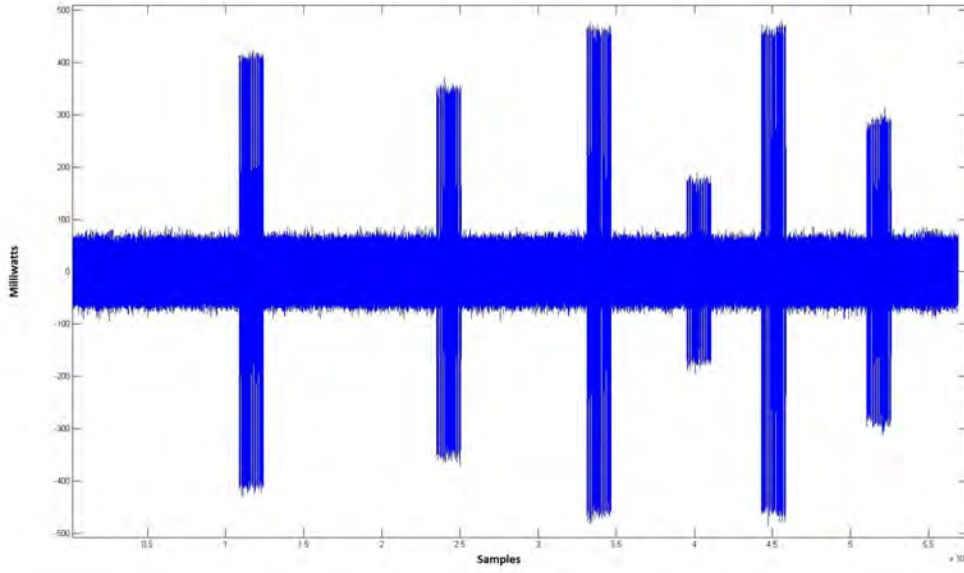
Figure 3.13:   Reader and tag interaction.

reader/tag pairs. These two pairs were chosen because of their separation in time. Given the known velocity of the tag, it had traveled about 11 centimeters between the first tag response and the last, and it should offer the best chance to see a phase difference due to movement. The starting sample numbers and the corresponding time are shown in Table 3.2. The time epoch was determined by taking the sampling rate, 1.35 megasamples per second after decimation, and multiplying by the sample number. The first 2048 samples after the time epoch are then copied into a new vector. The number of samples to analyze was chosen to be the largest power of two that will not exceed the tag's initial response. This sample size is large enough to include the preamble wave form, the SOF and 32 bits of data. The analysis of these vectors is discussed in the next section.

73
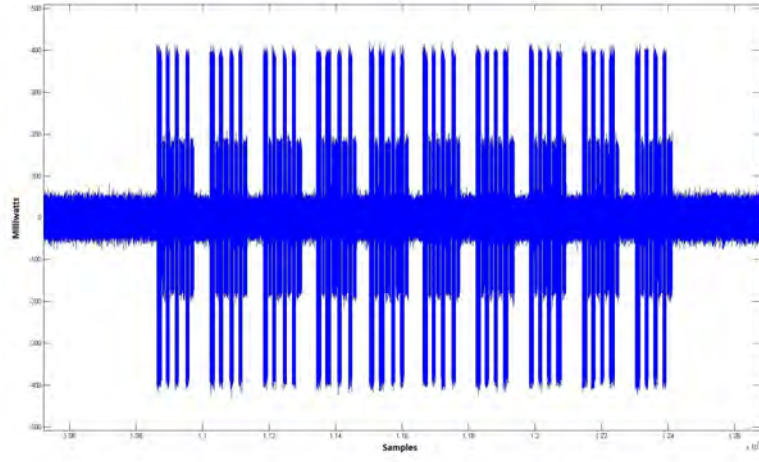
Figure 3.14:   Single group of reader and tag interactions.

Table 3.2:   Sample Vector Epochs

Vector	Sample Number	Time Epoch
Tx-1	10861525	8.045131
Rx-1	10878579	8.057763
Tx-2	12383164	9.172210
RX-2	12396643	9.182193

| [C,index] = abs(fftshift(fft(data_complex))/data_complex_len) |

Figure 3.15:   Code to Calculate Sample Vector Center Frequency

Table 3.3:   Vector Phases

Vector	Frequency	Observed Phase
Tx-1	914.8 MHz	-2.09953 radians
Rx-1	914.8 MHz	2.97874 radians
Tx-2	914.8 MHz	-2.13302 radians
RX-2	914.8 MHz	-3.11687 radians

3.5.2   Finding the Vector's Phase.   To find the phase of each of the selected vectors we first need to find the Fast Fourier Transform (FFT). MATLAB implements the FFT using FFTW, an adaptive software package that chooses the Cooley-Tukey algorithm or a modified form, depending on the data being processed. Either way the FFT is an N-point Discrete Fourier Transform (DFT), and in the case of this research, N = 2048. The first step in finding the sample vector's phase is to plot the magnitude of the FFT of the sample vector, this is shown in Figure 3.16 for the first reader transmission. Using the MATLAB *max* command, the center frequency of the sample vector is found. In this case it is just above 915 MHz. The index of this value is noted and the value at that index for the argument of the sample vector is found. As shown in Figure 3.17, the value is -2.00954 radians for the first reader transmission. This process is then repeated for each of the sample vectors identified. The phases found for the example sample can be seen in Table 3.3. The phase found for all other samples are then stored in the same Excel spreadsheet, as well as the vector time epochs for computation via the SID metric algorithms.

75
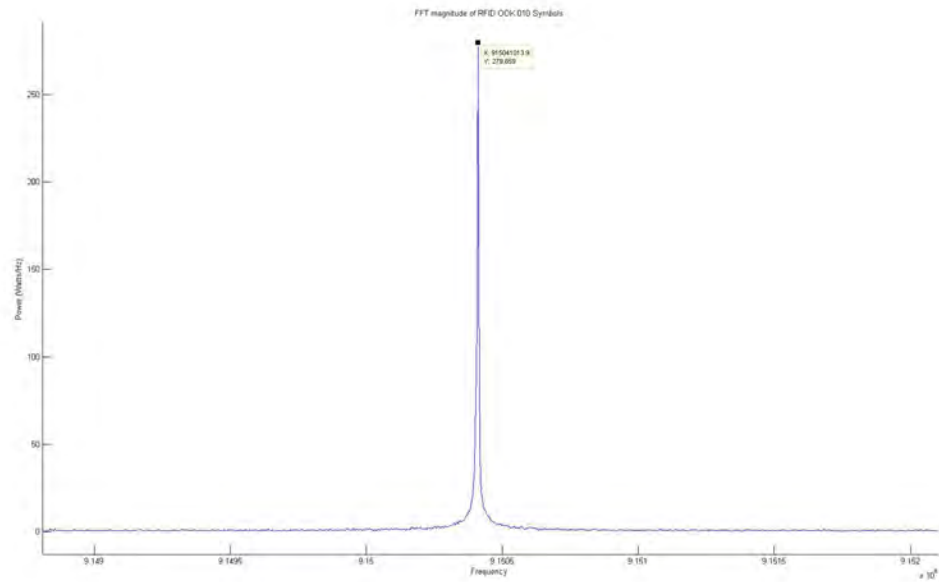
Figure 3.16:   Magnitude of FFT of reader transmission.
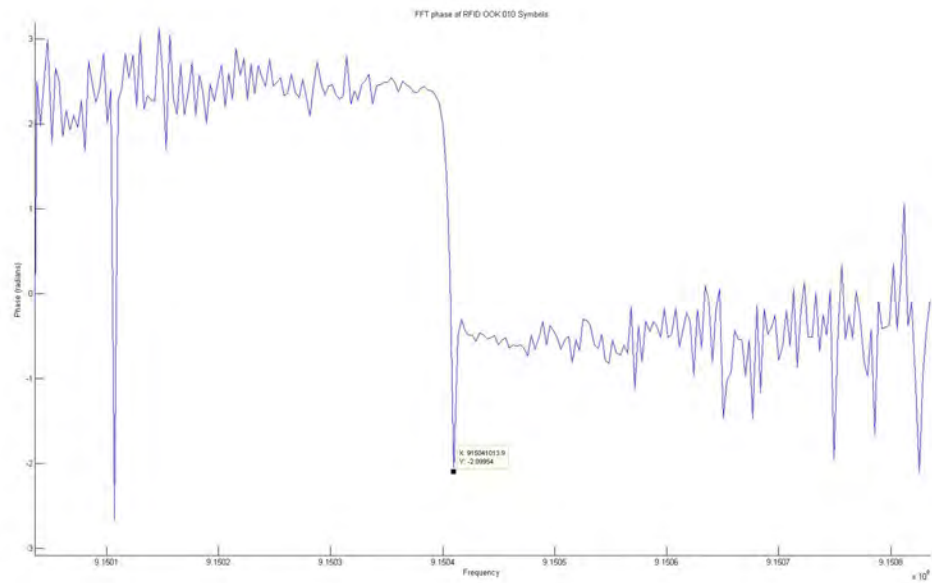
Figure 3.17:   Phase of FFT of reader transmission.

Table 3.4:   Experiment Configurations

Configuration	Speed (cm/s)	Tag	Number of Runs
Config 1	10	1	5
Config 1	20	1	5
Config 1	30	1	5
Config 1	40	1	5
Config 2	10	1	5
Config 2	20	1	5
Config 2	30	1	5
Config 2	40	1	5
Config 3	10	1	5
Config 3	20	1	5
Config 3	30	1	5
Config 3	40	1	5
Config 4	10	1	5
Config 4	20	1	5
Config 4	30	1	5
Config 4	40	1	5
Config 2	20	1	5
Config 2	20	2	5
Config 2	20	3	5
Config 2	20	4	5

3.6 Experimental Design

Table 3.4 shows the different configurations of the experiment and the number of runs for each configuration. The configurations referenced are shown in Figure 3.9.

3.7 Methodology Summary

This research is performed in two parts. First, a simulation models the physical test bed as shown in Figure 3.9. All of the plan tests in Table 3.4 are run in simulation

to provide a baseline of the system and provide expected values. Second the described

runs are performed on the physical test bed with their data stored for offline analysis.

IV. Results

4.1 Introduction

This chapter provides a discussion of the simulations used as the baseline, the data collected from the testbed, as well as the outcome of the analysis of that data. Due to the nature of the results arrived at in this research, there will also be analysis of the resolution required in the data for phas-based spatial identification to be successful, and how this resolution compares to the capabilities of the USRP software defined radio.

4.2 Simulation of RFID Tag Movement

The simulation described in Chapter 3 was tailored to fit the real world dimensions of the testbed and are listed in Table 4.1. The level of Additive Gaussian White noise used was based on the noise floor of the laboratory the research was conducted in. This noise floor was measured on a Sunday morning with only one person in the lab and all extraneous transmitters (cell phones, RFID reader, computer WiFi, etc.) turned off. These simulations represent what would amount to an ideal situation for the tag to be tracked. A constant tone is available and only the phase offset due

Testbed Feature	Variable	Value
Sampling Frequency	fs	500 MHz
Center Frequency	fc	915 MHz
Secondary Frequency	fc2	914MHz
Height of reader from tabletop	zReader	20cm
Tag vertical offset from reader	z	10 cm
3dB angle of sensor antenna	theat3db	0.698 radians

Table 4.1:   Simulation Enviromental Elements

to the propagation channel is measured. This constant response is mixed with the AGWN and a multipath response that simulates the multipath due to reflection off of the wooden tabletop. Due to the short range of the RFID tags and the distance to other reflectors in the laboratory, multipath from other objects was not considered. The error introduced due to multipath was minimal as can be seen in Figure 4.1 – Figure 4.16.

In all figures the dark line represents the one ray model with no multipath, the lighter shaded area is the two-ray model simulating the reflection from the tabletop. Only in Configuration #2 when the tag is traveling directly at the reader, is the noise from the multipath evident. In reality, the multipath level in this configuration is no higher than the other configurations, but due to the relative speed remaining constant over the course of the run. Only when the graph is zoomed in to seven significant figures to the right of the decimal point, does the noise becomes evident.

4.3   Capture of Real RFID Tag Interaction

The test runs described in Chapter 3 were run on the testbed and all data recorded into separate files. These captures took place on Sunday, 11 December in the morning, with extraneous emitters turned off to minimize the noise floor in the lab, in an effort to recreate the environment represented in the simulation. Despite the optimal configuration of the Alien 9800 reader and USRP, several problems with the captures emerged. First, the Alien is not configurable to perform continuous reads. As can be seen in Figure 4.17, there is not a steady series of queries and responses as
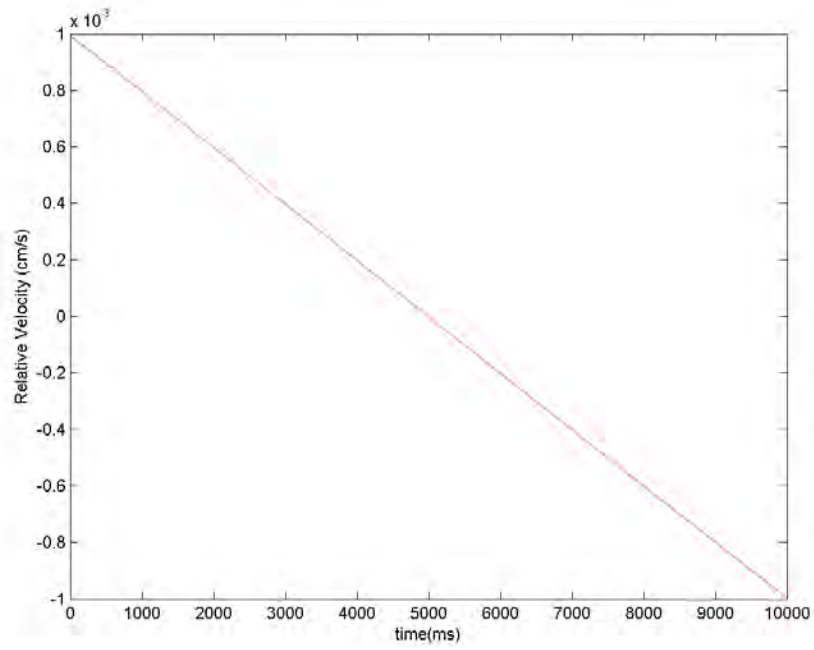
Figure 4.1:   Configuration #1: 10 cm/s Relatvie Velocity
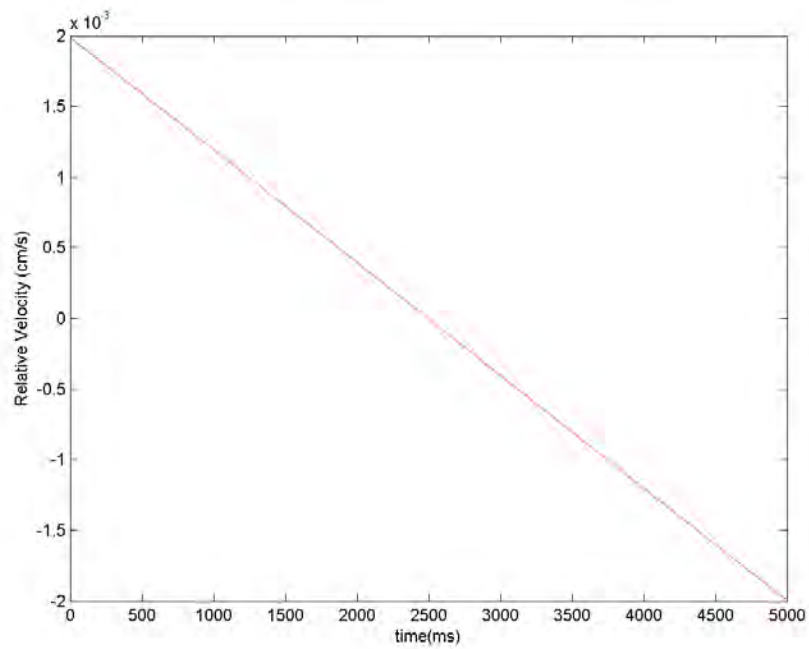
Figure 4.2:   Configuration #1: 20 cm/s Relatvie Velocity

81
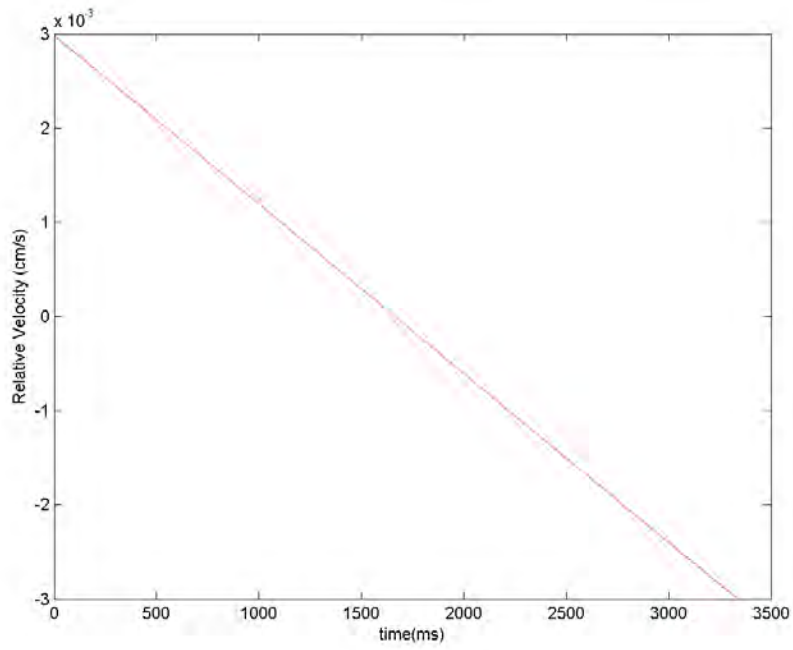
Figure 4.3:　　Configuration #1: 30 cm/s Relatvie Velocity
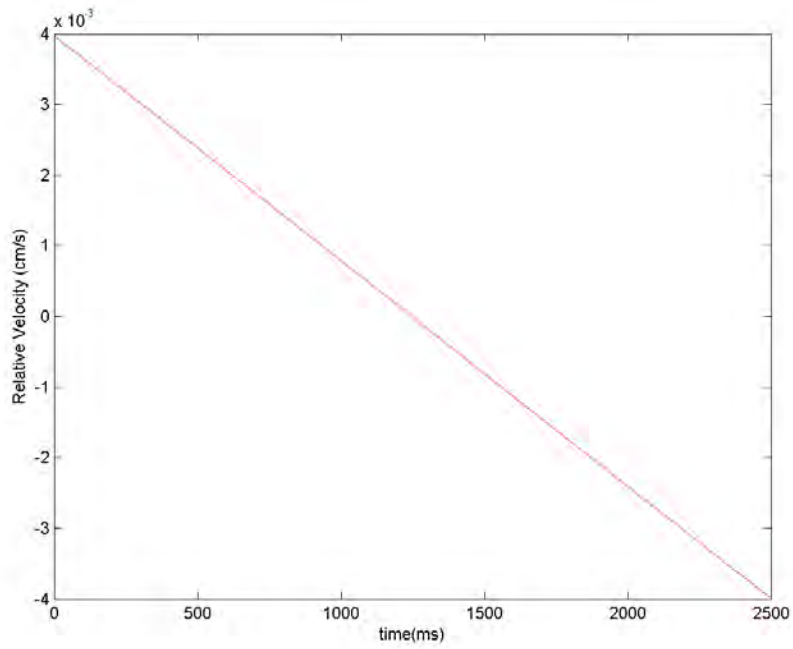
Figure 4.4:　　Configuration #1: 40 cm/s Relatvie Velocity
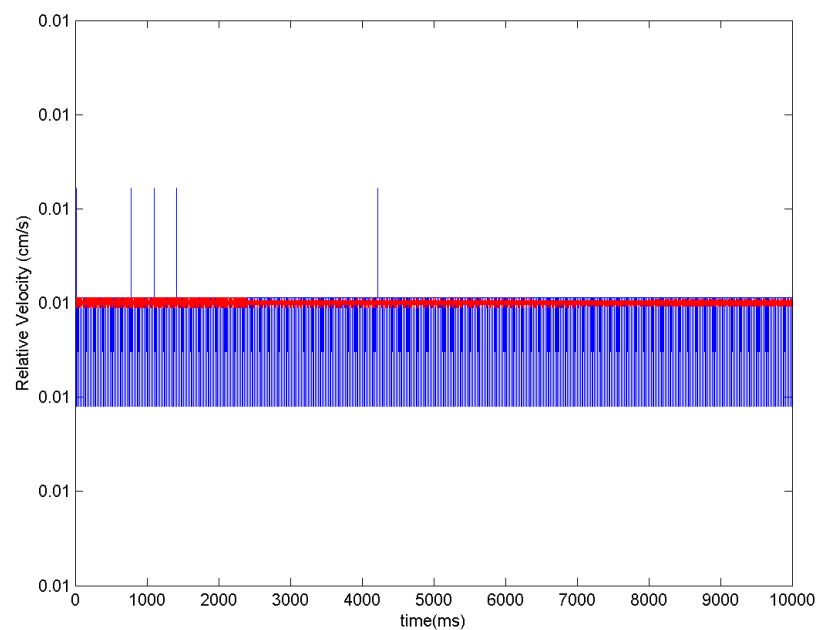
Figure 4.5:   Configuration #2: 10 cm/s Relatvie Velocity
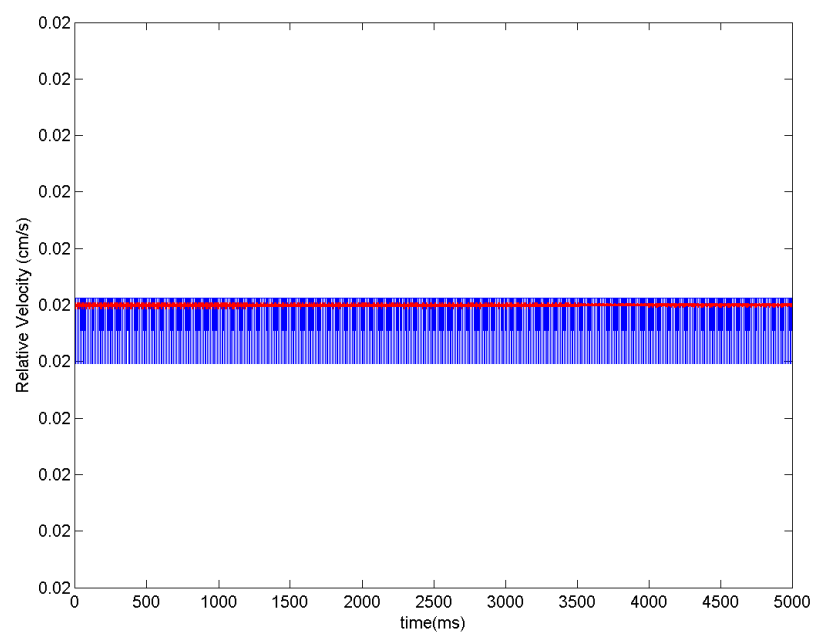
Figure 4.6:   Configuration #2: 20 cm/s Relatvie Velocity
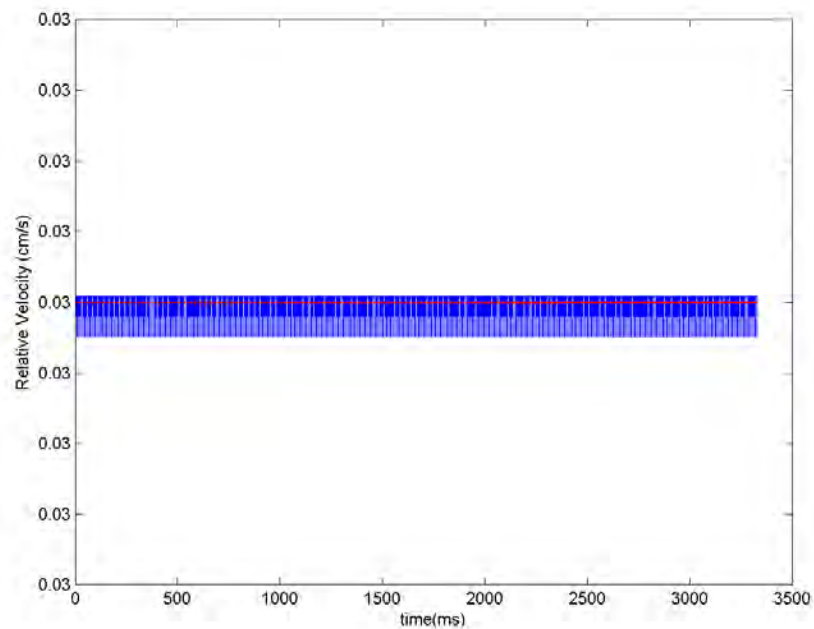
Figure 4.7:   Configuration #2: 30 cm/s Relatvie Velocity
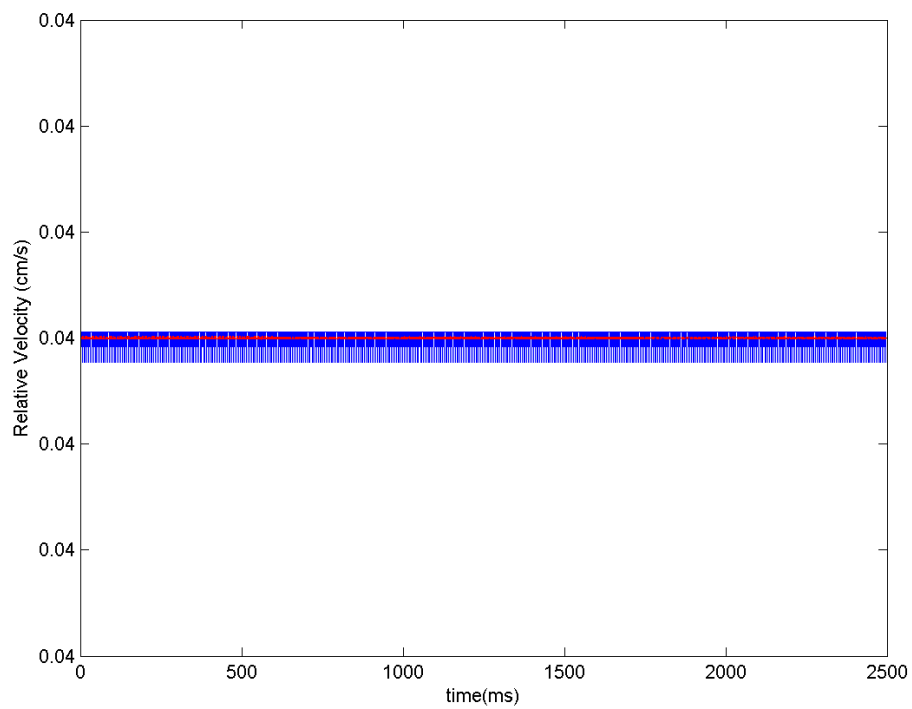
Figure 4.8:   Configuration #2: 40 cm/s Relatvie Velocity
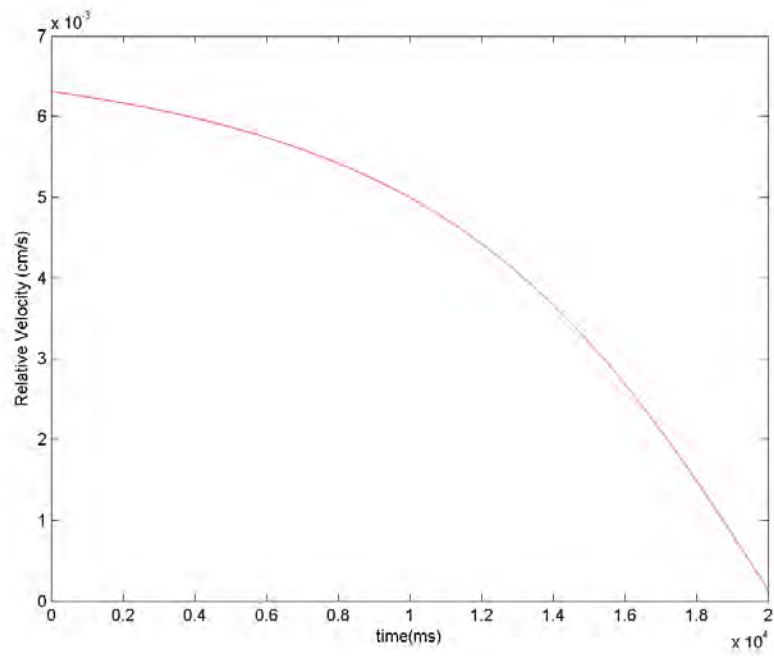
Figure 4.9:   Configuration #3: 10 cm/s Relative Velocity
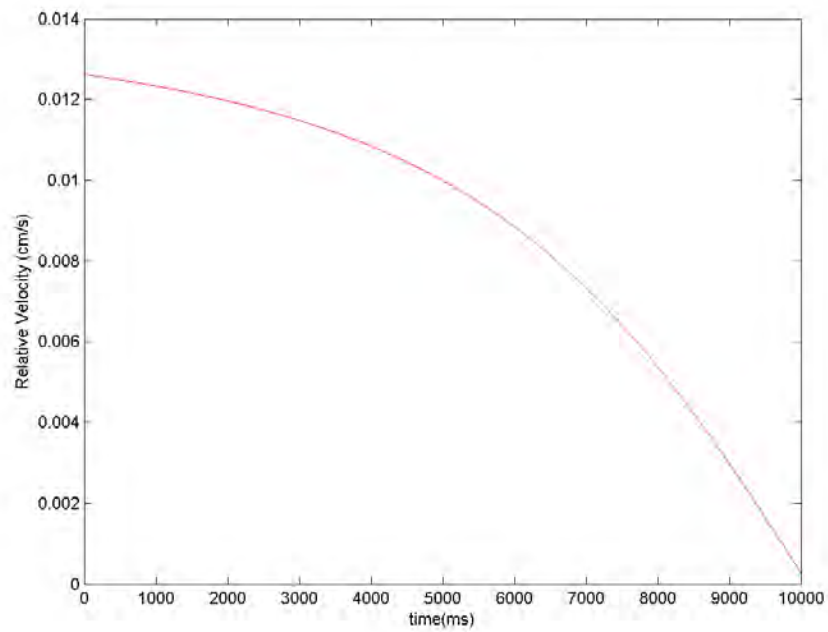
Figure 4.10:   Configuration #3: 20 cm/s Relative Velocity

85
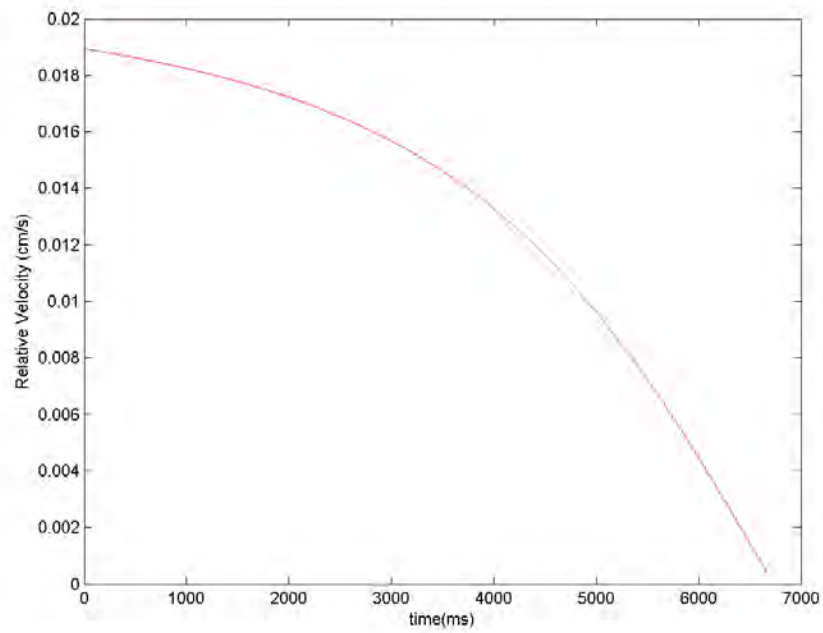
Figure 4.11:   Configuration #3: 30 cm/s Relative Velocity
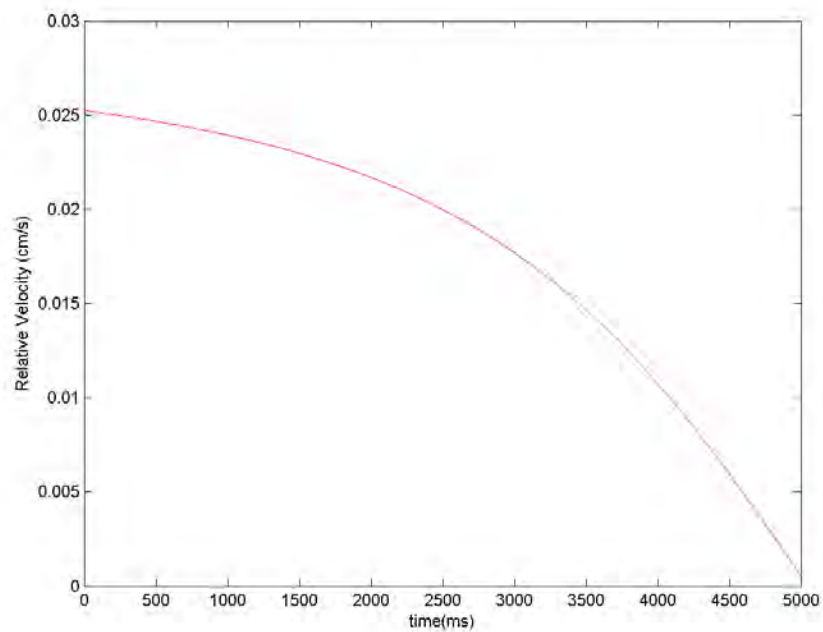
Figure 4.12:   Configuration #3: 40 cm/s Relative Velocity

86
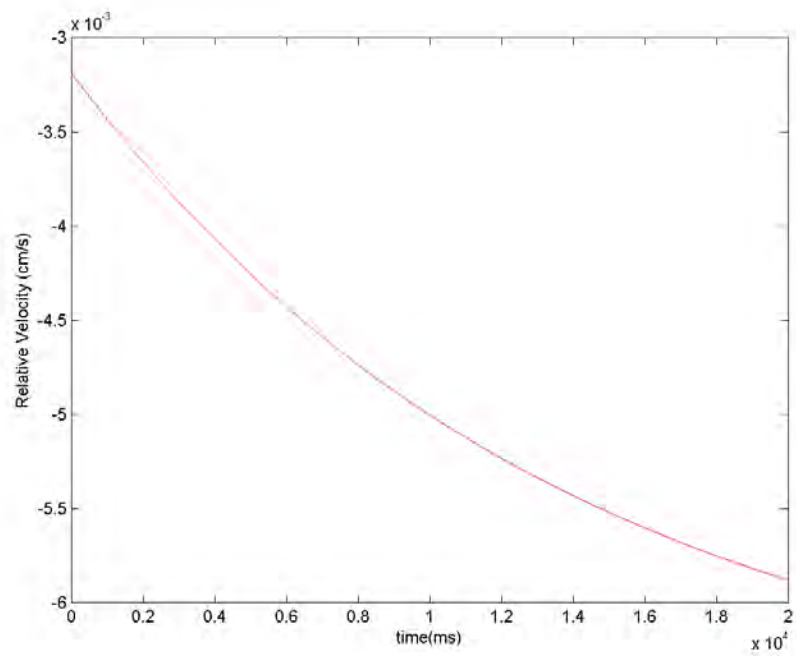
Figure 4.13:   Configuration #4: 10 cm/s Relative Velocity
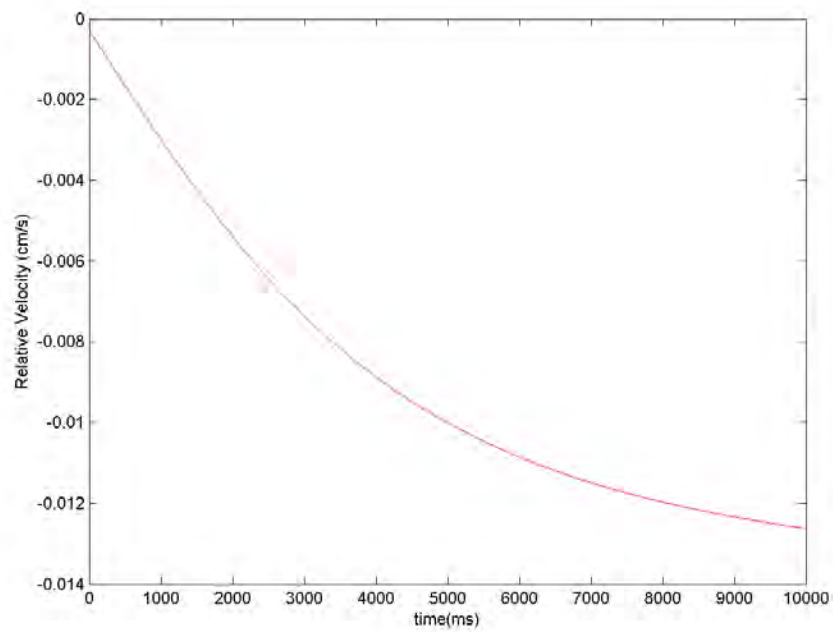
Figure 4.14:   Configuration #4: 20 cm/s Relative Velocity

87
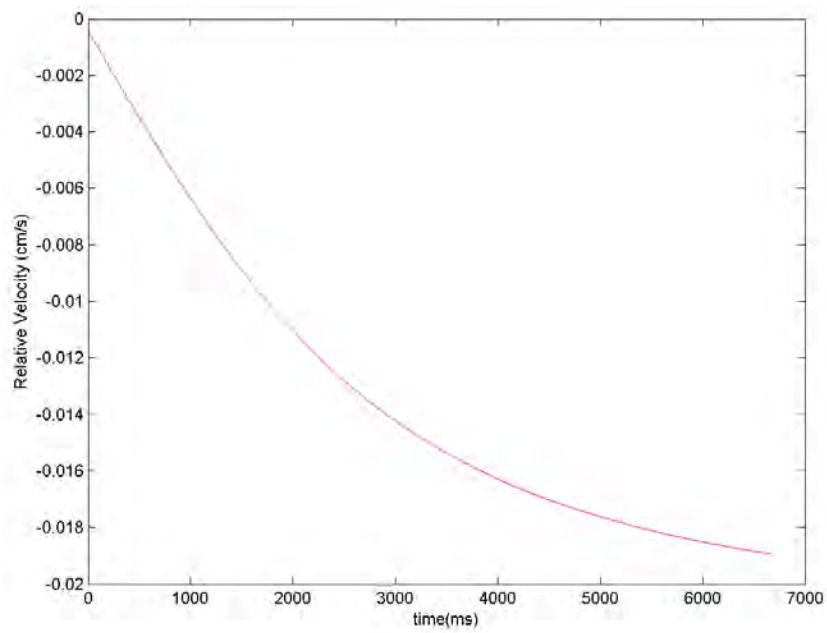
Figure 4.15:   Configuration #4: 30 cm/s Relative Velocity
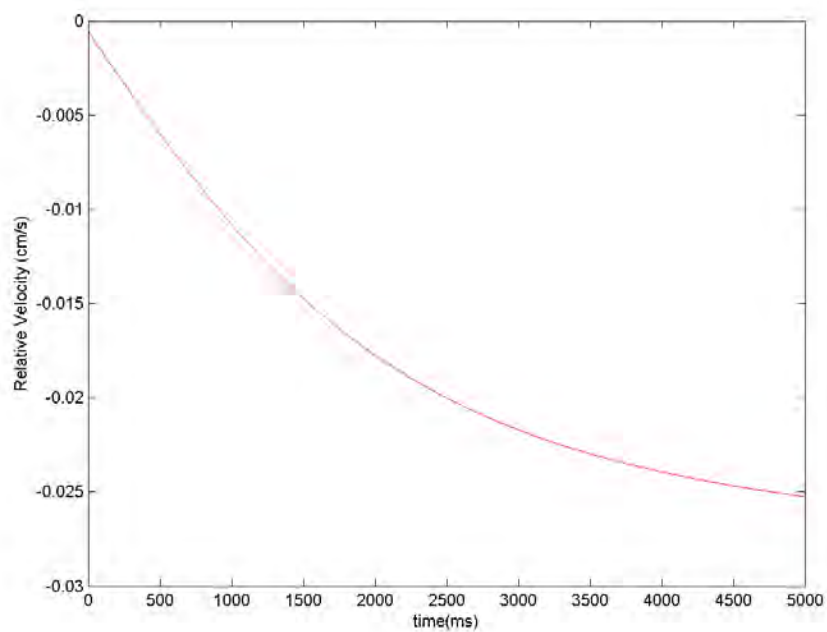
Figure 4.16:   Configuration #4: 40 cm/s Relative Velocity

88
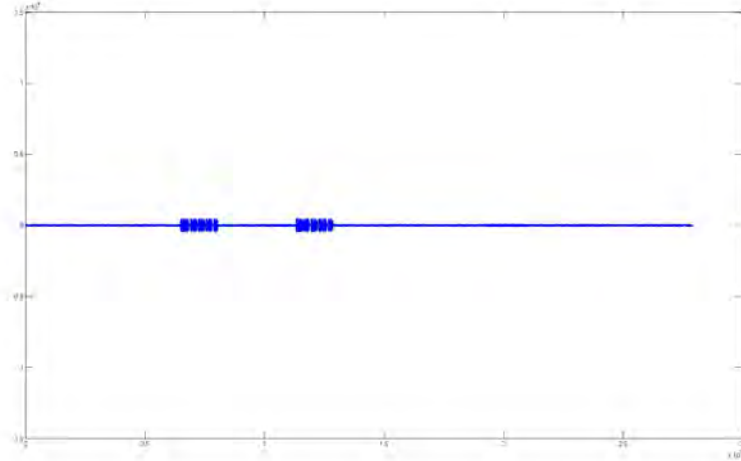
Figure 4.17:   Entire Capture

anticipated. Two distinct sets of reads can been seen starting at about $0.6x10^7$ and $1.3x10^7$ samples. In addition to the fact that there is not a constant query/response interaction from the reader, the two sets of reads are at different frequencies within the specification, 924.9MHz and 908 MHz, respectively. While this difference in frequency would complicate phase-based spatial identification it could be accounted for. It does become a problem when we look at spatial identification as a doppler problem. This is discussed in Section 4.4.2

The good news is that the query from the reader and the tag's response are easy to distinguish when you enlarge a set of reads as seen in Figure 4.18. The clusters with the larger amplitudes are the queries from the reader, with the clusters with smaller amplitudes being the responses from the tag. Zooming further into one of the tag responses, it is possible to visually decode the response of the on-off keying used in the EPC Gen 2 Type A tags, as seen in Figure 4.19. As described in the specification [1],

89
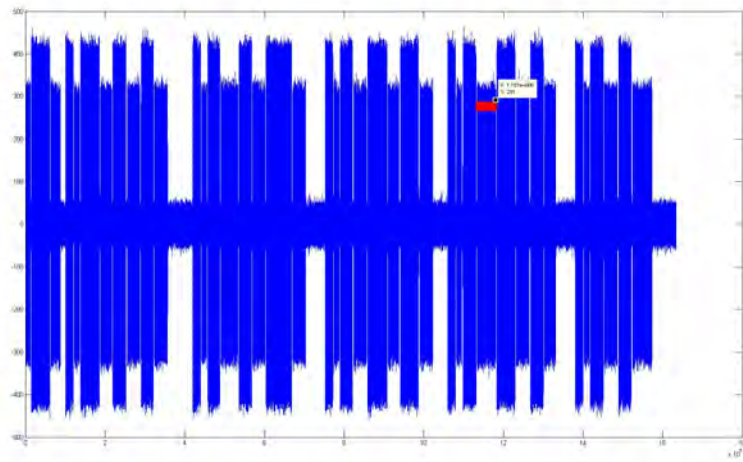
Figure 4.18:   Reader/Tag Conversation
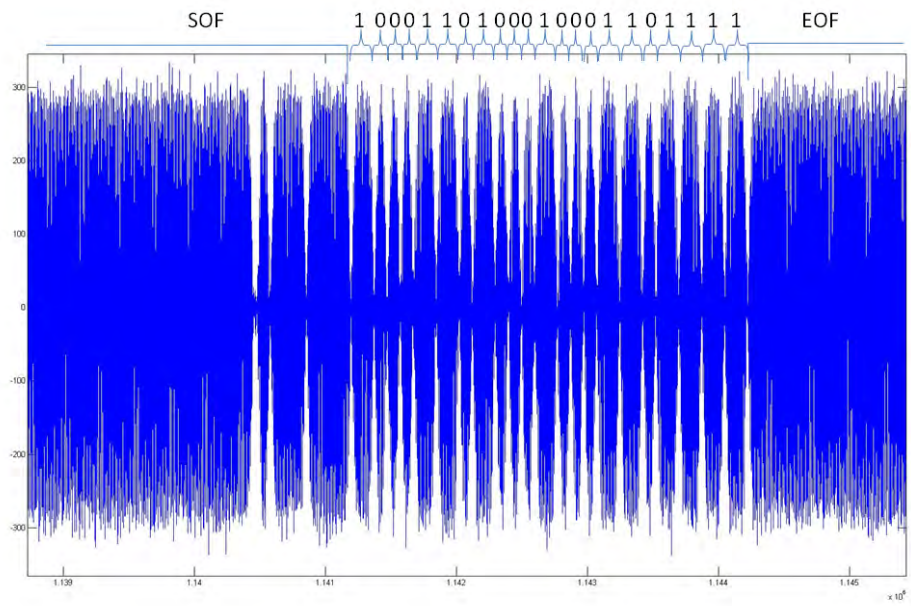
Figure 4.19:   Decoded Tag Response

90

a frame starts with the SOF (Start of Frame) symbol, followed by the data, and closes with a EOF (End of Frame). Each bit of data is encoded as a function of the Tari. One Tari equals roughly 20 microseconds, as defined in the standard. A zero is encoded as off for one half a Tari then high for the second half. A one is encoded as off for one half a Tari and then on for one and a half Taris. In this way we can simply read the ones and zeros of the data portion by the width of the on portions of the signal. It should be noted that with this method of encoding the frame size in time is determined by the payload. This introduces another complicating factor, in that tag responses do not contain the same number of samples from one frame to another. Simply put, ignoring the SOF and EOF, a frame consisting of sixteen bits of zeros would provide roughly half of the samples of a frame consisting of all ones. In the phase-based analysis this would not matter, but once again, it is problematic when approaching the issue from a frequency/doppler standpoint.

4.4   *Analysis of Data for Spatial Identification*

The data for the first run of Configuration #2 at 10 cm/s, (sample run) is analyzed in detail to show how the results were computed. Results for all other runs were analyzed in the same way but only a summary of the results for those runs is presented. The rest of this section is divided into two parts. The first subsection describes analysis of the captured data using the phase-base algorithms. The second subsection describes the requirements that would be needed if we tried to apply doppler radar principles to the captures.

4.4.1 Analysis by Phase Based Spatial Identification.   When the real portion
of the entire run was plotted in Figure 4.20, one can see that there were six groups of
interactions between the tag and reader. The fifth group was examined but the signal
to noise ratio in this group is to low to pick out the clear starts of the reader and the
tag responses, so it was ignored. As described in Chapter 3, Methodology, the starting
epochs of each of the reader and tag transmissions was entered into a spreadsheet.
These spreadsheets can be found in Appendix A. Each table is labeled with the
configuration, velocity and run number. Each grouping has 40 pairs of reader/tag
interaction, resulting in 200 epoch pairs for the entire run. The phases were calculated
as described in Chapter 3. The phases found were then put into Equation 2.1 and
the relative velocities were calculated. The results showed significant variation, so
the signal to noise ratio (SNR) for both the Alien reader and the tag's response were
also found for analysis. The results for the sample run can be seen in Table 4.2. One
can see that as the SNR increases the error, in general, decreases. While one run at
one speed allows us to only draw preliminary conclusions, it does provide clues on
how the rest of the data could be sorted and analyzed. To this end, the summary
of the remaining results are grouped by both the SNR of the reader and the SNR of
the tag. Calculated velocities are grouped according to Reader SNR in the following
three categories: ≤ 5, $5.01-6$, and > 6. In a similar fashion, the calculated velocities
are sorted by the tag's response SNR in the following three categories: ≤ 2.5, $2.51 -$
3.5, and > 3.5. Each of these is described in Table 4.3 as Low SNR, Medium SNR,
and High SNR. Each tag/reader group will then be placed in one of nine squares on
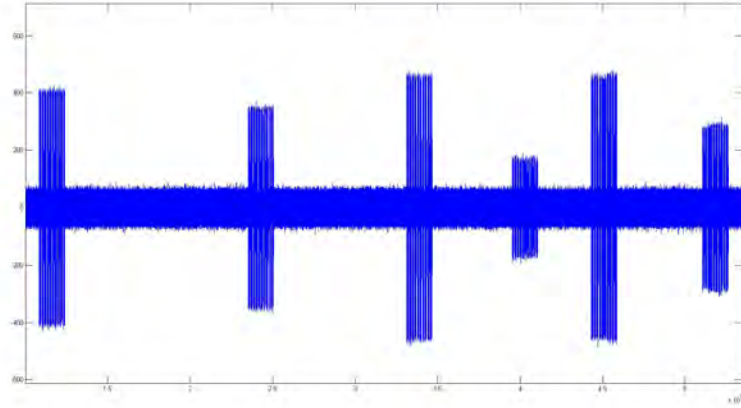
Figure 4.20:   Configuration 2, 10 cm/s, Run 1

Table 4.2:   Sample Run TD-PDOA Results

Group	Relative Velocity (cm/s)	Error (cm/s)	Reader SNR	Tag SNR
1	47	37	5.68	2.70
2	-9.0	19	4.90	2.31
3	37	27	6.50	3.38
4	11	1	6.50	3.55
5	-18	28	3.86	2.30

the chart with low reader SNR and low tag SNR being in the upper left hand corner
and high/high SNR in the lower right hand corner. When one considers that the tag's
actual velocity was ±2 cm/s when programmed for 10 cm/s the results in Table 4.3
for those groups with a high reader SNR, 40% of observed groups, are within 11 cm/s
of the actual velocity. The low variance of the Medium tag/high reader SNR block is
shows how tightly these are grouped.

4.4.2 Requirements for Doppler Spatial Identification.   Given the issues
with determining the relative velocity of the tag based on the phase of the response
an attempt to look at the doppler shift of the response frequency was made. The

93

Table 4.3:   Configuration 2, 10 cm/s TD-PDOA Results

	Tag SNR Low	Tag SNR Medium	Tag SNR High
Reader SNR Low	Groups: 14 Average Velocity: -5.8 Variance: 0.46	Groups: 4 Average Velocity: 17.6 Variance: 0.16	Groups: None Observed
Reader SNR Medium	Groups: 1 Velocity: 47 Variance: N/A	Groups: 3 Average Velocity: Variance: .11	Groups:1 32.1Velocity: 5.3 Variance: N/A
Reader SNR High	Groups: 6 Average Velocity: 26.1 Variance: 0.11	Groups: 7 Average Velocity: 21.2 Variance: 0.04	Groups:4 Velocity:14.5 Variance:0.06

Table 4.4:   Configuration 2, 20 cm/s TD-PDOA Results

	Tag SNR Low	Tag SNR Medium	Tag SNR High
Reader SNR Low	Groups: 5 Average Velocity: -13.0 Variance: 0.58	Groups: 1 Average Velocity: 6.7 Variance: N/A	Groups:None Observed
Reader SNR Medium	Groups: 1 Velocity: 9.3 Variance: N/A	Groups: 7 Average Velocity: 41.8 Variance: 0.24	Groups:None Observed
Reader SNR High	Groups: TBD Average Velocity: TBD Variance: TBD5	Groups: 3 Average Velocity: 23.5 Variance: 0.04	Groups:1 Velocity:11 Variance:TBD

Table 4.5:   Configuration 2, 30 cm/s TD-PDOA Results

	Tag SNR Low	Tag SNR Medium	Tag SNR High
Reader SNR Low	Groups: 7 Average Velocity: 16 Variance: 0.36	Groups: 1 Average Velocity: 60.8 Variance: N/A	Groups:None Observed
Reader SNR Medium	Groups: 2 Velocity: 52.7 Variance: 0.13	Groups: 3 Average Velocity: 41.8 Variance: .24	Groups:None Observed
Reader SNR High	Groups: 4 Average Velocity: 15.5 Variance: 0.03	Groups: 2 Average Velocity: 28.1 Variance: 0.11	Groups:1 Average Velocity:45.3 Variance:N/A

Table 4.6:   Configuration 2, 40 cm/s TD-PDOA Results

	Tag SNR Low	Tag SNR Medium	Tag SNR High
Reader SNR Low	Groups: 7 Average Velocity: -22.7 Variance: 0.61	Groups: None Observed	Groups:None Observed
Reader SNR Medium	Groups: 4 Velocity: 26.1 Variance: 0.95	Groups: 1 Average Velocity: 78.3 Variance: N/A	Groups:None Observed
Reader SNR High	Groups: 6 Average Velocity: 66.8 Variance: 0.81	Groups: None Observed	Groups:2 Average Velocity:32.7 Variance:0.43

calculations below were made assuming a tag moving in Configuration #2. This configuration is the easiest for analysis, due to the fact that the motion of the tag generates a velocity vector that is one hundred percent in the direction of the sensor. In line with Richards [21], the Doppler frequency is the difference between the tx (reader) and rx(tag) frequencies. Equation 4.1 is used to calculate the value of this frequency given the velocity of the target relative to the sensor, v_r, the speed of light, c, and the carrier frequency, $f_{carrier}$. When the parameters of the system under test are entered into Equation 4.1, we arrive at $f_d = 2.44Hz$, as seen in Equation 4.2. This means that when we analyze the captured interaction, we would have to separate the responses into FFT bins of size 2.44 Hz or less. This proves problematic due to the bursty nature of the communications between the reader and tags. With the short bursts of response the smallest bin size that I was able to achieve in this research was 330 Hz, much larger than the 2.44 Hz that would be required to accurately estimate the velocity of the tag.

$$f_d = \frac{2v_r}{c} f_{carrier} \qquad (4.1)$$

$$f_d = \frac{2(.4m/s)}{3x10^8 m/s} 915x10^6 Hz = 2.44Hz \tag{4.2}$$

V. Conclusions

5.1   Completed Objectives

The objectives of this research were attained as follows.

5.1.1   Validation of PDOA by Simulation.   The simulations developed as a part of this researched showed that, given a strong signal, the PDOA metrics described in Chapter 2 will provide an accurate characterization of a moving target signal. This model included multipath from the table top and AGWN to simulate the lab environment.

5.1.2   Generate SID of RFID Tag in Physical Space.   The results presented in Chapter 4 show a notable level of success in this area. While the SNR of both the captured tag reader and tag return impact the accuracy of the results greatly when the SNR is above certain thresholds, the calculated SIDs are within reasonable limits. Improvements to the SNR, expanded on in the future works section, would only serve to enhance the accuracy of this method.

5.2   Summary of Research Thrusts

This research's goal of successful SID measurement of a moving passive RFID tag is reliant on a foundation of four research thrusts. These thrusts are: algorithm theory, quality hardware, algorithm theory, and a reliable testbed.

5.2.1 Algorithm Theory. While the formulas for this research have been published previously [7], the publications did not provide any details to validate the correctness of the formulas. To this end, I started from basic princeples, and I solved for and derived in the literature. In this, an added level of confidence could be assigned to the accuracy of the formulas. In addition, the digital signal processing (DSP) theory for the USRP 1 was verified by construction of detailed block diagrams of the mainboard and the Flex 900 daughter card. Once the block diagram was created and the logical flow of the signal was mapped, the signal was modeled at each stage of the system. This analysis of the signal as it flowed through the system served to give the reader an understanding of the mixing of the signal from an analog RF signal to the digital baseband signal. That none of the specfic details required for the SID solution were omitted in any way.

5.2.2 Quality Hardware. The second thrust, quality hardware, showed issues with both the commercial tag reader and the USRP 1. Several assumptions were made in the early stages of the research that had to be adjusted as the research moved forward. First was control of the read patterns of the commercial Alien RFID reader. It was assumed that the reader would produce a rapid series of reads with little time gaps between queries when operating in Global Scroll mode. The reality was that the reads contained a series of large gaps in between them, a few as large as a second. This lack of control over the Alien 9800 read times created captures with an inconsistent number of reads per experiment. The lack of documentation also required

additional inital assumptions to be modified during the research. First among these was a lack of clear documenation for both the hardware and the supporting GNU Radio software. Installing the software and communicating with the radio is not a trival task. Following the installation documentation with the software, more often than not, resulted in a cryptic error message. This most often occured during the process of unpacking the software, compilation, and installation of the software on the system. Often collaboration with other students using the same system or searching online help forums was the only way to decipher the process. The other main concern with the USRP, was the sampling rate that was attainable for the research. The documented 64 megasample a second data rate is not achievable in reality on the hardware. As shown in the hardware description in Chapter 2 the ADC is capable of a raw 64 MSPS rate, but half of this is for the I portion and half being the Q portion. A large decimation rate is required to prevent overloading the USB interface. A sampling rate of 1.35 megasamples a second was the best achieved in practice by this research. The low sampling rate, after decimation, of the USRP 1 resulted in loss of fidelity in the data.

5.2.3 Algorithm Validation. A simulation of the testbed was created to validate the SID algorithms based on the assumption of a clear measurement of the target signal's phase. These simulations provided a verification that, given a accurate extraction of the phase of a signal, the PDOA metrics can be calculated from the captured data. The velocity of the target signal's source, reflection off of the table's

surface, and the path traveled in space were all modeled in MATLAB. Additive Gaussian White Noise was also added to the simulated signal based on the observed noise floor of the laboratory in use. These simulations support the results in Chapter 4, and show that the velocity and distance to the tag can be calculated within a reasonable margin of error given a sufficently high SNR.

5.2.4 Reliable Testbed. The testbed was able to reliably produce consistent speeds over a set track for data capture. The flexability of the pegboard surface allowed the four track configurations to be created and data recorded. There was some apparent stretching of the track's rope towards the end of data collection, so additional tension was later added but the velocity remained within 1 cm/s of the target velocity. The only possible issue with the testbed would be the noise floor of the lab. The reconfiguration of large metal shelving units and desks between data collection periods could have changed the RF fingerprint of the lab, while the research was ongoing.

5.3 Contributions

Several contributions to SID and SDR community resulted from this research.

5.3.1 USRP 1 Documentation. When this research started, the documentation of the USRP 1 and Flex 900 daughter cards was either spread across several sources or minimal. In the process of determining the shortfalls of the gathered data, extensive research was completed on the hardware platform itself. In one instance,

the system schematic called out a crystal oscillator that was not on the board, the functionality had been moved to a synthesized oscillator. In another case, packaged integrated circuits were swapped for updated versions. While this is normally a form, fit, and function, the newer chips had different operating characteristics that were not documented. In both cases assumptions on the operation of the equipment needed to be adjusted to fit the hardware that was actually implemented.

5.3.2 Identified Capability Gaps in SDR. The USRP 1 is a very capable platform but has significant capability gaps in regards to spatial identification and navigation applications. In particular the sampling rate rates that are attainable do not support either TDOA or dopler ranging of targets as described in Chapter 4.

5.3.3 Validated Feasibility of Velocity Estimation using TD-PDOA. The ability to calculate an estimate of relative velocity of a target signal was demonstrated. While it is largely dependant on the SNR of the reader and tag, velocity was calculated within an order of magnitude for all observed SNR values.

5.4 Future Work

This research raised additional questions and opportunities for continued research.

5.4.1 Improved Simulation. One possible improvement to the modeling and simulation portion of this research would be to better model the reader/tag interaction. The current simulation models a continuous wave in the 915 MHz band.

A more complete model would modulate this wave with data, model the delay between reader Tx and tag Rx, attenuate the powers realistically. This could also represent the bursty nature of the RFID communication link with varying start and stop times of the data.

5.4.2   Develop Method to Increase SNR for RFID.   With the robust OOK data encoding method, the primary focus of RFID tag antenna design is size to harvest enough power to reply. Additional effort and optimization of the antennas to improve the SNR would give the added benefit of improved SID accuracy. Increasing the SNR would also increase the read range and increase the number of situations in which the tags could be used.

5.4.3   Implement Reader on USRP N210.   Transistioning the tag reader to the USRP N210 would give a researcher more control over the read cycles and enable more reads of the tag as it transits through the range of the reader. Compatibility issues would still have to taken into consideration so as to not violate the rules of the unlicensed spectrum band in which the tags operate in.

5.5   Summary

This research's goal of successful SID measurement of a moving passive RFID tag is reliant on a foundation of four research thrusts. These thrusts are: algorithm theory, quality hardware, algorithm validation and a reliable testbed. First, the algorithm theory was validated through signal analysis of the theoretical waveform as

it transition through the SDR and through the derivation of the PDOA metrics. Second thrust, quality hardware, did show some potential issues. The inability to precisely control the read sequence of the Alien 9800 and the limited sampling rate of the USRP 1 hampered the success of this area. The lack of control over the Alien 9800 read times created captures with an inconsistent number of reads per trip. The low sampling rate, after decimation, of the USRP 1 resulted in loss of fidelity in the data. Third, validation of the algorithm with the simulation adequately supported this research, but could befurther improved as mentioned in the future work section. Fourth, the testbed was able to reliably produce consistent speeds over a set track for data capture. The only possible issue with the testbed would be the noise floor of the lab. In summary, this research established a solid, four focused research foundation for continued investigation into SID with SDR.

Appendix A. Raw Data

The following tables contain the raw data for the first three runs in configuration 2 at 10 cm/s.

Table A.1:   Configuration 2 10 cm/s Run 1

Zoom start point	Reader Epoch	Entire Capture Epoch	Time:	Phase Read	Tag Epoch	Entire Capture Epoch	Time:	Delta Time	Phase Response	Phase due to travel	Instant Velocity
10800000	61525	10861525	8.045	-2.0995	78579	10878579	8.058	0.01263	2.9787435	5.078279	10.44984
10800000	89577	10889577	8.066	-0.6303	102955	10902955	8.076	0.00991	-2.783440	-2.15315	-8.38029
10800000	116390	10916390	8.086	-1.2789	129883	10929883	8.096	0.00999	2.9743207	4.253265	5.635786
10800000	148824	10948824	8.110	-1.6221	162304	10962304	8.120	0.00998	-2.556050	-0.93393	-0.16304
10800000	221530	11021530	8.164	-2.3683	238534	11038534	8.176	0.01259	-2.949371	-0.58109	0.868145
10800000	249412	11049412	8.184	-1.6176	262841	11062841	8.194	0.00995	-2.797710	-1.18016	-5.48834
10800000	281175	11081175	8.208	-1.4276	294716	11094716	8.218	0.01003	2.3586412	3.786259	-0.16808
10800000	308104	11108104	8.228	-1.3041	321596	11121596	8.238	0.00999	2.6104310	3.914521	1.383694
10800000	381521	11181521	8.282	2.21781	398528	11198528	8.295	0.0126	3.1102997	0.892490	8.049314
10800000	409497	11209497	8.303	1.79103	422933	11222933	8.313	0.00995	-2.893336	-4.68437	-9.25181
10800000	441636	11241636	8.327	-0.8304	454962	11254962	8.337	0.00987	2.8976389	3.728074	6.779140
10800000	468496	11268496	8.347	-1.3499	481892	11281892	8.356	0.00992	-2.804587	-1.45471	-0.19796
10800000	541528	11341528	8.401	-2.0384	558531	11358531	8.413	0.01259	-3.062421	-1.02400	-5.91455
10800000	569410	11369410	8.421	-1.2906	587803	11387803	8.435	0.01362	2.6003854	3.891030	5.480277
10800000	606006	11406006	8.448	-1.7395	619420	11419420	8.458	0.00994	-2.767483	-1.02795	-0.09787
10800000	638228	11438228	8.472	-1.7879	651675	11451675	8.482	0.00996	-2.726226	-0.93833	-3.10429
10800000	701510	11501510	8.519	-2.0134	718578	11518578	8.532	0.01264	2.9442863	4.957697	0.732851
10800000	729392	11529392	8.540	-1.2732	749108	11549108	8.554	0.0146	3.0492997	4.322520	10.11914
10800000	767536	11567536	8.568	1.91484	780970	11580970	8.578	0.00995	-2.915754	-4.83059	-0.03560
10800000	794398	11594398	8.588	2.02606	807899	11607899	8.598	0.01	-2.777317	-4.80338	-2.69866
10800000	861517	11661517	8.638	2.3333	878507	11678507	8.650	0.01258	2.9393849	0.606085	-1.24761
10800000	889443	11689443	8.658	1.62808	902846	11702846	8.668	0.00993	3.0962222	1.468139	2.901882
10800000	917350	11717350	8.679	-1.7498	930797	11730797	8.689	0.00996	-2.584344	-0.83452	-5.25501
10800000	949212	11749212	8.703	-1.5892	962852	11762852	8.713	0.0101	2.3584122	3.947612	-0.72886
10800000	1E+006	11821507	8.756	-2.5404	1E+006	11838609	8.769	0.01267	2.9747465	5.515160	9.767917
10800000	1E+006	11849406	8.777	-1.4816	1E+006	11862835	8.787	0.00995	-2.684394	-1.20277	-8.00987
10800000	1E+006	11876350	8.797	-1.8086	1E+006	11889762	8.807	0.00993	3.1116312	4.920246	6.658885
10800000	1E+006	11903329	8.817	-1.2913	1E+006	11921611	8.830	0.01354	-2.391757	-1.10049	-0.10717
10800000	1E+006	11981558	8.875	-1.6544	1E+006	11998545	8.887	0.01258	-2.520830	-0.86641	0.365167
10800000	1E+006	12009356	8.895	-1.6104	1E+006	12022818	8.905	0.00997	-2.728411	-1.11804	-0.64587
10800000	1E+006	12036283	8.915	-2.1400	1E+006	12050271	8.926	0.01036	-2.754627	-0.61467	-0.02276
10800000	1E+006	12063785	8.936	-2.2652	1E+006	12082101	8.949	0.01357	-2.859319	-0.59410	-0.02808
10800000	1E+006	12141507	8.993	-2.4388	1E+006	12158544	9.006	0.01262	-2.971918	-0.53316	-8.71111
10800000	1E+006	12169387	9.014	-2.4089	1E+006	12182932	9.024	0.01003	3.0891168	5.498015	1.057119

Table A.1: Configuration 2 10 cm/s Run 1

Zoom start point	Reader Epoch	Entire Capture Epoch	Time:	Phase Read	Tag Epoch	Entire Capture Epoch	Time:	Delta Time	Phase Response	Phase due to travel	Instant Velocity
10800000	1E+006	12196398	9.034	-2.2082	1E+006	12209859	9.044	0.00997	2.4817541	4.689918	-0.32624
10800000	1E+006	12223212	9.054	-2.2046	1E+006	12241559	9.067	0.01359	2.7789235	4.983511	-0.08515
10800000	2E+006	12301459	9.112	-2.2706	2E+006	12318478	9.124	0.01261	2.8988199	5.169441	8.306549
10800000	2E+006	12329405	9.132	-2.1271	2E+006	12342803	9.142	0.00992	-2.693895	-0.56678	2.216121
10800000	2E+006	12356370	9.152	-0.6989	2E+006	12369731	9.162	0.0099	-2.959818	-2.26092	-1.67155
10800000	2E+006	12383164	9.172	-2.1330	2E+006	12396643	9.182	0.00998	-3.116866	-0.98384	-0.00593
2.30E+07	511783	23511783	17.42	1.48801	528714	23528714	17.43	0.01254	2.3789842	0.890971	-0.30793
2.30E+07	539560	23539560	17.44	0.85039	553050	23553050	17.45	0.00999	1.9541020	1.103712	0.426082
2.30E+07	571346	23571346	17.46	1.58806	584854	23584854	17.47	0.01001	2.3070714	0.719008	-1.38454
2.30E+07	598293	23598293	17.48	0.93451	611828	23611828	17.49	0.01003	2.7137572	1.779248	0.497871
2.30E+07	671400	23671400	17.53	1.19560	688407	23688407	17.55	0.0126	1.8924730	0.696871	0.259281
2.30E+07	699312	23699312	17.55	1.3826	712803	23712803	17.56	0.00999	1.8998977	0.517298	0.259668
2.30E+07	732280	23732280	17.58	2.79728	746903	23746903	17.59	0.01083	3.0631997	0.265922	-0.91961
2.30E+07	760421	23760421	17.60	0.75412	773739	23773739	17.61	0.00986	1.7206449	0.966523	0.201159
2.30E+07	831369	23831369	17.65	1.74333	848439	23848439	17.66	0.01264	2.2832593	0.539932	-0.78203
2.30E+07	859330	23859330	17.67	1.10158	872804	23872804	17.68	0.00998	2.1824441	1.080863	0.133725
2.30E+07	886242	23886242	17.69	1.07354	899732	23899732	17.70	0.00999	2.0521763	0.978635	0.316592
2.30E+07	913233	23913233	17.71	0.74765	931412	23931412	17.73	0.01347	1.4415528	0.693902	-0.05014
2.30E+07	991417	23991417	17.77	1.58625	1E+006	24008408	17.78	0.01259	2.3897480	0.803494	-0.63257
2.30E+07	1E+006	24019253	17.79	0.88346	1E+006	24037493	17.80	0.01351	2.2092731	1.325809	-0.70565
2.30E+07	1E+006	24051042	17.81	0.40505	1E+006	24074126	17.83	0.0171	2.4647209	2.059674	0.548998
2.30E+07	1E+006	24087595	17.84	0.92734	1E+006	24101115	17.85	0.01001	2.5663723	1.639035	0.276639
2.30E+07	1E+006	24155387	17.89	1.49234	1E+006	24172456	17.90	0.01264	2.5710935	1.078756	-0.12577
2.30E+07	1E+006	24183223	17.91	0.92647	1E+006	24196728	17.92	0.01	2.0918927	1.165422	0.685749
2.30E+07	1E+006	24210166	17.93	0.93909	1E+006	24223610	17.94	0.00996	1.5811822	0.642088	-0.19875
2.30E+07	1E+006	24237078	17.95	0.90220	1E+006	24255461	17.97	0.01362	1.7240024	0.821801	0.098102
2.30E+07	1E+006	24311387	18.01	1.37629	1E+006	24328363	18.02	0.01257	1.9950587	0.618767	-0.64668
2.30E+07	1E+006	24339254	18.03	0.87465	1E+006	24352681	18.04	0.00995	1.9398616	1.065215	0.026768
2.30E+07	1E+006	24366166	18.05	0.78972	1E+006	24379609	18.06	0.00996	1.8344743	1.044751	-0.61152
2.30E+07	1E+006	24393077	18.07	1.17960	1E+006	24411348	18.08	0.01353	2.7753524	1.595754	0.296891
2.30E+07	1E+006	24471419	18.13	1.11693	1E+006	24488457	18.14	0.01262	2.0627770	0.945843	0.239065
2.30E+07	1E+006	24499286	18.15	0.63708	2E+006	24517450	18.16	0.01345	1.3861503	0.749072	-0.21702
2.30E+07	2E+006	24530932	18.17	1.03284	2E+006	24544344	18.18	0.00993	1.9476063	0.914764	0.136882
2.30E+07	2E+006	24562688	18.19	1.16778	2E+006	24581025	18.21	0.01358	1.9400059	0.772223	0.008244
2.30E+07	2E+006	24631388	18.24	1.29373	2E+006	24648364	18.26	0.01257	2.0501966	0.756464	-0.05243
2.30E+07	2E+006	24659208	18.27	0.87256	2E+006	24672667	18.28	0.00997	1.6652033	0.792640	-0.69494
2.30E+07	2E+006	24686167	18.29	0.76857	2E+006	24699625	18.30	0.00997	2.0930608	1.324486	0.543424
2.30E+07	2E+006	24713236	18.31	0.52206	2E+006	24726523	18.31	0.00984	1.4315862	0.909522	-0.05607
2.30E+07	2E+006	24791373	18.36	1.51850	2E+006	24808411	18.38	0.01262	2.5583655	1.039864	0.119496
2.30E+07	2E+006	24819256	18.38	0.96203	2E+006	24832699	18.39	0.00996	1.9194984	0.957470	-0.28046

Zoom start point	Reader Epoch	Entire Capture Epoch	Time:	Phase Read	Tag Epoch	Entire Capture Epoch	Time:	Delta Time	Phase Response	Phase due to travel	Instant Velocity
2.30E+07	2E+006	24846152	18.40	1.05035	2E+006	24864424	18.42	0.01353	2.2604187	1.210069	-0.59227
2.30E+07	2E+006	24877862	18.43	0.92354	2E+006	24891366	18.44	0.01	2.5866133	1.663070	0.524247
2.30E+07	2E+006	24951420	18.48	1.425	2E+006	24968381	18.49	0.01256	1.9418616	0.516862	-0.68357
2.30E+07	2E+006	24979257	18.50	0.41037	2E+006	24997514	18.52	0.01352	1.4925825	1.082214	-0.44025
2.30E+07	2E+006	25010981	18.53	0.82648	2E+006	25024517	18.54	0.01003	2.2461851	1.419706	0.151377
2.30E+07	2E+006	25037924	18.55	0.86507	2E+006	25051382	18.56	0.00997	2.1693273	1.304255	0.010313
3.30E+07	111259	33111259	24.53	-0.1761	128213	33128213	24.54	0.01256	-1.236608	-1.06055	1.849340
3.30E+07	139082	33139082	24.55	0.49794	152561	33152561	24.56	0.00998	-1.840907	-2.33885	0.381486
3.30E+07	166086	33166086	24.57	0.66892	179511	33179511	24.58	0.00994	-1.961796	-2.63072	-0.88498
3.30E+07	192944	33192944	24.59	0.16991	211273	33211273	24.6	0.01358	-1.662823	-1.83273	-0.09682
3.30E+07	271213	33271213	24.64	-0.3536	288257	33288257	24.66	0.01262	-1.974702	-1.62114	0.308017
3.30E+07	299088	33299088	24.66	-0.0960	317379	33317379	24.68	0.01355	-1.971796	-1.87579	0.132293
3.30E+07	330844	33330844	24.69	0.05693	344377	33344377	24.70	0.01002	-1.920258	-1.97719	-0.89252
3.30E+07	357772	33357772	24.71	-0.2095	371225	33371225	24.72	0.00996	-1.506429	-1.29692	0.216197
3.30E+07	431208	33431208	24.76	-0.4358	448268	33448268	24.78	0.01264	-2.205589	-1.76978	0.703661
3.30E+07	459164	33459164	24.78	0.30136	472616	33472616	24.79	0.00996	-1.954799	-2.25616	-0.50746
3.30E+07	486065	33486065	24.80	-0.0826	504469	33504469	24.82	0.01363	-1.879849	-1.79728	-0.04368
3.30E+07	517961	33517961	24.83	0.23980	532438	33532438	24.84	0.01072	-1.522795	-1.76260	1.611850
3.30E+07	591254	33591254	24.88	3.04007	608245	33608245	24.89	0.01259	-2.191379	-5.23145	-1.55782
3.30E+07	619128	33619128	24.90	2.74949	632545	33632545	24.91	0.00994	-1.407287	-4.15678	-0.21254
3.30E+07	646024	33646024	24.92	2.71930	664860	33664860	24.94	0.01395	-1.242505	-3.96180	0.227124
3.30E+07	678398	33678398	24.95	2.43701	691745	33691745	24.96	0.00989	-1.698146	-4.13515	-2.36257
3.30E+07	751260	33751260	25	-3.0880	768224	33768224	25.01	0.01257	-2.093590	0.994395	7.994864
3.30E+07	779080	33779080	25.02	2.66586	793676	33793676	25.03	0.01081	-2.116514	-4.78237	-4.32620
3.30E+07	807109	33807109	25.04	0.11399	821651	33821651	25.05	0.01077	-1.232576	-1.34657	3.675206
3.30E+07	835071	33835071	25.06	2.74980	848547	33848547	25.07	0.00998	-1.402987	-4.15278	-1.31952
3.30E+07	911204	33911204	25.12	-0.4955	928216	33928216	25.13	0.0126	-1.663833	-1.16837	0.76138
3.30E+07	939187	33939187	25.14	0.38339	953621	33953621	25.15	0.01069	-1.334106	-1.71750	2.621952
3.30E+07	967068	33967068	25.16	2.81961	980566	33980566	25.17	0.01	-0.903539	-3.72315	0.579102
3.30E+07	993980	33993980	25.18	2.55259	1E+006	34007456	25.19	0.00998	-1.612640	-4.16523	-2.63255
3.30E+07	1E+006	34071229	25.24	-2.9581	1E+006	34088269	25.25	0.01262	-1.083709	1.874405	8.835876
3.30E+07	1E+006	34099151	25.26	2.62679	1E+006	34112611	25.27	0.00997	-1.604820	-4.23161	0.992496
3.30E+07	1E+006	34126074	25.28	2.70403	1E+006	34140643	25.29	0.01079	-2.317410	-5.02144	-0.59434
3.30E+07	1E+006	34155153	25.30	2.79563	1E+006	34173381	25.31	0.0135	-1.673429	-4.46906	0.195967
3.30E+07	1E+006	34231251	25.36	3.00429	1E+006	34248210	25.37	0.01256	-1.881068	-4.88536	-0.78551
3.30E+07	1E+006	34259098	25.38	2.46819	1E+006	34272531	25.39	0.00995	-1.874815	-4.34300	0.034352
3.30E+07	1E+006	34286021	25.40	2.53278	1E+006	34299454	25.41	0.00995	-1.836478	-4.36926	-0.54023
3.30E+07	1E+006	34312901	25.42	2.51793	1E+006	34326388	25.43	0.00999	-1.438246	-3.95618	0.059779
3.30E+07	1E+006	34391386	25.47	2.49403	1E+006	34408292	25.49	0.01252	-1.601150	-4.09518	0.556347
3.30E+07	1E+006	34419169	25.49	2.46868	1E+006	34433733	25.51	0.01079	-2.028320	-4.49700	-1.63533

Zoom start point	Reader Epoch	Entire Capture Epoch	Time:	Phase Read	Tag Epoch	Entire Capture Epoch	Time:	Delta Time	Phase Response	Phase due to travel	Instant Velocity
3.30E+07	1E+006	34456939	25.52	-0.0873	1E+006	34470477	25.53	0.01003	-2.878418	-2.79113	-0.13161
3.30E+07	1E+006	34483884	25.54	0.22045	1E+006	34497352	25.55	0.00998	-2.470269	-2.69072	-0.64302
3.30E+07	2E+006	34551229	25.59	-0.4855	2E+006	34568214	25.60	0.01258	-1.882600	-1.39715	-0.31313
3.30E+07	2E+006	34579142	25.61	0.08890	2E+006	34593738	25.62	0.01081	-1.081352	-1.17025	3.077118
3.30E+07	2E+006	34611991	25.64	2.52466	2E+006	34625397	25.65	0.00993	-1.411219	-3.93588	-0.69725
3.30E+07	2E+006	34639408	25.66	2.39153	2E+006	34652815	25.67	0.00993	-1.001636	-3.39316	-0.01935
4.42E+07	99949	44299949	32.81	-1.4063	116997	44316997	32.83	0.01263	0.5094232	1.915766	-0.39720
4.42E+07	127926	44327926	32.83	-2.4883	141352	44341352	32.84	0.00994	-0.297935	2.190394	-0.09089
4.42E+07	159732	44359732	32.86	-2.4039	177968	44377968	32.87	0.01351	-0.119007	2.284871	-1.64318
4.42E+07	191425	44391425	32.88	-3.0233	209900	44409900	32.89	0.01368	0.7510971	3.774446	1.181410
4.42E+07	259945	44459945	32.93	-2.1126	276972	44476972	32.94	0.01261	-0.587667	1.524905	-1.71872
4.42E+07	287828	44487828	32.95	-2.9523	306097	44506097	32.97	0.01353	-0.006286	2.945998	0.657109
4.42E+07	319522	44519522	32.98	-2.6777	332974	44532974	32.99	0.00996	-0.233051	2.444614	-0.81560
4.42E+07	346502	44546502	33.00	-2.7767	359964	44559964	33.01	0.00997	0.2928391	3.069543	0.469322
4.42E+07	419980	44619980	33.05	-2.4545	436959	44636959	33.06	0.01258	-0.410784	2.043689	-0.31092
4.42E+07	447889	44647889	33.07	-2.7029	461370	44661370	33.08	0.00999	-0.443709	2.259160	0.135034
4.42E+07	479670	44679670	33.09	-2.3500	493112	44693112	33.10	0.00996	-0.212534	2.137476	-1.94769
4.42E+07	506611	44706611	33.11	-2.8954	520218	44720218	33.12	0.01008	0.7408885	3.636257	0.757808
4.42E+07	579938	44779938	33.17	-2.3131	597007	44797007	33.18	0.01264	-0.328878	1.984257	-1.64709
4.42E+07	607908	44807908	33.19	-2.7298	621457	44821457	33.20	0.01004	0.3977147	3.127523	1.194417
4.42E+07	639634	44839634	33.21	-2.6717	653044	44853044	33.22	0.00993	-0.615266	2.056456	-1.33198
4.42E+07	666511	44866511	33.23	-2.9049	680018	44880018	33.24	0.01	0.1715913	3.076445	0.390516
4.42E+07	739989	44939989	33.29	-2.5782	756952	44956952	33.3	0.01256	-0.354646	2.223523	-0.61998
4.42E+07	767927	44967927	33.31	-2.7409	786675	44986675	33.32	0.01389	0.0057913	2.746670	5.917805
4.42E+07	805167	45005167	33.34	2.78574	818491	45018491	33.35	0.00987	0.1872757	-2.59846	-5.83051
4.42E+07	841655	45041655	33.36	-2.9363	855204	45055204	33.37	0.01004	0.5420611	3.478392	0.872129
4.42E+07	899937	45099937	33.41	-2.1936	916977	45116977	33.42	0.01262	-0.244676	1.948955	-1.43845
4.42E+07	927788	45127788	33.43	-2.7638	941295	45141295	33.44	0.01	0.1782153	2.942011	0.605399
4.42E+07	954768	45154768	33.45	-2.8331	968204	45168204	33.46	0.00995	-0.353615	2.479533	-0.83931
4.42E+07	981642	45181642	33.47	-2.7214	995223	45195223	33.48	0.01006	0.4019354	3.123319	0.343473
4.42E+07	1E+006	45260036	33.52	-2.8088	1E+006	45276983	33.54	0.01255	-0.482682	2.326084	-0.31820
4.42E+07	1E+006	45287823	33.54	-2.7984	1E+006	45306053	33.56	0.0135	-0.209744	2.588685	6.43149
4.42E+07	1E+006	45320638	33.57	1.51790	1E+006	45334047	33.58	0.00993	-1.004684	-2.52258	0.195720
4.42E+07	1E+006	45347586	33.59	1.63190	1E+006	45360982	33.60	0.00992	-1.040338	-2.67224	-0.55511
4.42E+07	1E+006	45419944	33.64	1.02501	1E+006	45436974	33.66	0.01261	-0.449656	-1.47467	1.719017
4.42E+07	1E+006	45447815	33.66	1.27193	1E+006	45461391	33.67	0.01006	-1.394322	-2.66625	0.004017
4.42E+07	1E+006	45474750	33.68	1.38203	1E+006	45488310	33.69	0.01004	-1.287296	-2.66932	0.360904
4.42E+07	1E+006	45501727	33.70	1.77337	1E+006	45515155	33.71	0.00995	-1.170995	-2.94437	-0.36024
4.42E+07	1E+006	45579953	33.76	0.89948	1E+006	45597002	33.77	0.01263	-1.207848	-2.10733	-0.52593
4.42E+07	1E+006	45607837	33.78	1.43360	1E+006	45621288	33.79	0.00996	-0.311114	-1.74472	0.491856

Table A.1: Configuration 2 10 cm/s Run 1

Zoom start point	Reader Epoch	Entire Capture Epoch	Time:	Phase Read	Tag Epoch	Entire Capture Epoch	Time:	Delta Time	Phase Response	Phase due to travel	Instant Velocity
4.42E+07	1E+006	45634730	33.80	1.11277	1E+006	45648242	33.81	0.01001	-1.008320	-2.12109	0.839252
4.42E+07	1E+006	45661662	33.82	1.62244	1E+006	45675148	33.83	0.00999	-1.139698	-2.76214	-0.28753
4.42E+07	2E+006	45739943	33.88	1.24783	2E+006	45756992	33.89	0.01263	-0.846231	-2.09406	-0.46428
4.42E+07	2E+006	45767801	33.9	1.27291	2E+006	45781297	33.91	0.01	-0.500796	-1.77371	0.80976
4.42E+07	2E+006	45799665	33.92	1.35826	2E+006	45813164	33.93	0.01	-1.148017	-2.50628	2.135945
4.42E+07	2E+006	45826581	33.94	1.83948	2E+006	45840211	33.95	0.0101	-2.306860	-4.14634	-0.02998
5.10E+07	38904	51038904	37.80	-0.1493	55842	51055842	37.82	0.01255	0.1437535	0.293033	-1.31079
5.10E+07	66799	51066799	37.83	-0.0194	80195	51080195	37.84	0.00992	1.1798949	1.199262	1.102619
5.10E+07	93639	51093639	37.85	0.80887	107100	51107100	37.86	0.00997	1.1659389	0.357071	-0.27814
5.10E+07	120571	51120571	37.87	0.30673	134032	51134032	37.87	0.00997	0.8764564	0.569730	0.124704
5.10E+07	198821	51198821	37.92	0.68315	215780	51215780	37.94	0.01256	0.9634731	0.280323	-0.96449
5.10E+07	226680	51226680	37.94	0.07666	240093	51240093	37.95	0.00994	1.0227010	0.946040	0.835641
5.10E+07	258374	51258374	37.97	0.28016	271825	51271825	37.98	0.00996	0.4734181	0.193257	-1.23326
5.10E+07	285365	51285365	37.99	-0.2554	298757	51298757	38.00	0.00992	0.8807696	1.136175	0.934750
5.10E+07	358784	51358784	38.04	1.11236	375797	51375797	38.05	0.0126	0.2041416	-0.90822	-2.51534
5.10E+07	386824	51386824	38.06	-0.6410	400216	51400216	38.07	0.00992	0.1944754	0.835506	0.862382
5.10E+07	419567	51419567	38.09	1.20171	442697	51442697	38.10	0.01713	0.9971794	-0.20453	0.133493
5.10E+07	456097	51456097	38.11	1.49586	469852	51469852	38.12	0.01019	1.1884286	-0.30744	-0.75771
5.10E+07	518777	51518777	38.16	0.63439	535822	51535822	38.17	0.01263	1.7460082	1.111618	3.502249
5.10E+07	546740	51546740	38.18	1.91997	560120	51560120	38.19	0.00991	0.6157436	-1.30423	-0.76101
5.10E+07	573646	51573646	38.20	1.80043	587036	51587036	38.21	0.00992	1.0777038	-0.72272	-1.26366
5.10E+07	600494	51600494	38.22	1.19933	618756	51618756	38.23	0.01353	1.6145407	0.415207	0.215937
5.10E+07	678804	51678804	38.28	0.52287	695850	51695850	38.29	0.01263	0.4654764	-0.05740	-0.07321
5.10E+07	706672	51706672	38.30	1.36616	724892	51724892	38.31	0.0135	1.3691262	0.002964	1.171138
5.10E+07	738356	51738356	38.32	1.06414	751958	51751958	38.33	0.01008	0.1672258	-0.89692	-1.13229
5.10E+07	765812	51765812	38.34	1.33467	779265	51779265	38.35	0.00996	1.3155371	-0.01914	0.310161
5.10E+07	838862	51838862	38.40	1.29639	855829	51855829	38.41	0.01257	0.6030945	-0.69330	-0.49225
5.10E+07	866736	51866736	38.42	1.06978	880253	51880253	38.43	0.01001	0.7177923	-0.35198	1.010644
5.10E+07	893726	51893726	38.44	1.82047	907164	51907164	38.45	0.00995	0.6963781	-1.12410	-1.26622
5.10E+07	920574	51920574	38.46	1.27137	938995	51938995	38.47	0.01364	1.2914948	0.020129	0.802497
5.10E+07	998978	51998978	38.52	2.10818	1E+006	52015824	38.53	0.01248	0.3779752	-1.73020	0.155178
5.10E+07	1E+006	52026730	38.54	2.18180	1E+006	52045063	38.55	0.01358	0.3227910	-1.85901	-1.79816
5.10E+07	1E+006	52058451	38.56	1.75609	1E+006	52076719	38.57	0.01353	1.5130608	-0.24303	0.006820
5.10E+07	1E+006	52090204	38.58	1.18086	1E+006	52103636	38.59	0.00995	0.9326136	-0.24824	-0.18146
5.10E+07	1E+006	52158794	38.63	0.57626	1E+006	52175829	38.65	0.01262	0.6999234	0.123662	1.147198
5.10E+07	1E+006	52186683	38.65	1.37276	1E+006	52201212	38.67	0.01076	0.6697530	-0.70301	-2.71928
5.10E+07	1E+006	52214667	38.68	-0.1021	1E+006	52228207	38.69	0.01003	1.2788841	1.380951	-2.29174
5.10E+07	1E+006	52241575	38.70	-2.7454	1E+006	52255034	38.71	0.00997	0.3809093	3.126331	1.020028
5.10E+07	1E+006	52318812	38.75	0.72140	1E+006	52335887	38.77	0.01265	1.5064162	0.785013	-5.34108
5.10E+07	1E+006	52346742	38.77	-2.7845	1E+006	52360348	38.78	0.01008	1.7094532	4.493999	5.53851

108

Table A.1: Configuration 2 10 cm/s Run 1

Zoom start point	Reader Epoch	Entire Capture Epoch	Time:	Phase Read	Tag Epoch	Entire Capture Epoch	Time:	Delta Time	Phase Response	Phase due to travel	Instant Velocity
5.10E+07	1E+006	52373698	38.79	0.04046	1E+006	52387133	38.80	0.00995	0.3229584	0.282500	-0.96056
5.10E+07	1E+006	52400593	38.81	0.19353	1E+006	52415116	38.82	0.01076	1.2391131	1.045585	0.676566
5.10E+07	1E+006	52478803	38.87	0.83937	1E+006	52495955	38.88	0.0127	0.3322719	-0.50710	1.08533
5.10E+07	2E+006	52506871	38.89	2.85264	2E+006	52529690	38.91	0.0169	1.3061127	-1.54653	-0.31831
5.10E+07	2E+006	52543222	38.92	1.70546	2E+006	52562630	38.93	0.01438	0.4566020	-1.24886	-2.24628
5.10E+07	2E+006	52576111	38.94	0.04273	2E+006	52589551	38.95	0.00996	0.5106245	0.467891	
										Averages:	0.133129

Table A.2: Configuration 2 10 cm/s Run 2

Zoom start point	Reader Epoch	Entire Capture Epoch	Time:	Phase Read	Tag Epoch	Entire Capture Epoch	Time:	Delta Time	Phase Response	Phase due to travel	Instant Velocity
9.00E+06	369529	9369529	6.94001	3.0466	386559	9386559	6.9526	1.5298	-1.5168	-9.34792	
9.00E+06	397395	9397395	6.96065	-2.345	410860	9410860	6.9706	2.5876	4.93214	2.359182	
9.00E+06	424313	9424313	6.98059	-1.991	442542	9442542	6.9941	0.8188	2.81023	6.870658	
9.00E+06	456034	9456034	7.00408	1.6923	469513	9469513	7.0141	-0.758	-2.4505	-0.97464	
9.00E+06	529536	9529536	7.05853	1.2517	546632	9546632	7.0712	0.9350	-0.3167	-6.56246	
9.00E+06	557431	9557431	7.07919	-2.489	570841	9570841	7.0891	1.7045	4.1935	3.982295	
9.00E+06	584342	9584342	7.09912	-3.032	602548	9602548	7.1126	-2.424	0.6089	-0.60224	
9.00E+06	616017	9616017	7.12258	0.5103	629473	9629473	7.1326	1.5795	1.06924	0.981072	
9.00E+06	689535	9689535	7.17704	1.8829	706523	9706523	7.1896	0.8062	-1.0767	0.177562	
9.00E+06	717368	9717368	7.19765	2.714	730886	9730886	7.2077	1.5144	-1.1996	3.460556	
9.00E+06	749112	9749112	7.22117	2.8521	762572	9762572	7.2311	-1.460	-4.3125	-10.5018	
9.00E+06	776048	9776048	7.24112	-1.366	789504	9789504	7.2511	2.3505	3.71697	1.793129	
9.00E+06	849511	9849511	7.29553	-1.674	866547	9866547	7.3082	-1.879	-0.2049	-5.10947	
9.00E+06	877470	9877470	7.31624	-2.044	890965	9890965	7.3262	1.2929	3.33698	1.576837	
9.00E+06	904436	9904436	7.33622	0.3559	922743	9922743	7.3498	2.2704	1.91444	7.070518	
9.00E+06	937280	9937280	7.36054	1.2124	950758	9950758	7.3705	-2.496	-3.7089	-0.63838	
9.00E+06	1009589	10009589	7.4141	-0.335	1026558	10026558	7.4267	-2.670	-2.3352	-6.56955	
9.00E+06	1037397	10037397	7.4347	0.5191	1050900	10050900	7.4447	2.7238	2.20471	2.860114	
9.00E+06	1064315	10064315	7.45464	-1.253	1077754	10077754	7.4646	-1.228	0.02427	-2.42341	
9.00E+06	1092376	10092376	7.47542	-2.292	1105857	10105857	7.4854	-0.334	1.95771	1.154708	
9.00E+06	1169536	10169536	7.53258	-1.977	1186526	10186526	7.5452	-2.664	-0.6867	-5.09673	
9.00E+06	1197362	10197362	7.55319	-2.544	1211968	10211968	7.564	0.4506	2.99453	3.015732	
9.00E+06	1225426	10225426	7.57397	-2.563	1239933	10239933	7.5847	-1.963	0.60034	3.392044	
9.00E+06	1267797	10267797	7.60536	1.8214	1281326	10281326	7.6154	-1.564	-3.3857	-1.76398	
9.00E+06	1329539	10329539	7.65109	1.9906	1346566	10346566	7.6637	1.8720	-0.1186	-2.26267	
9.00E+06	1357521	10357521	7.67182	0.4786	1372090	10372090	7.6826	1.9995	1.52092	-2.16904	
9.00E+06	1386602	10386602	7.69336	-1.090	1410407	10410407	7.7110	2.7903	3.88038	4.401195	

109

Table A.2: Configuration 2 10 cm/s Run 2

Zoom start point	Reader Epoch	Entire Capture Epoch	Time:	Phase Read	Tag Epoch	Entire Capture Epoch	Time:	Delta Time	Phase Response	Phase due to travel	Instant Velocity
9.00E+06	1423770	10423770	7.72089	-0.700	1437203	10437203	7.7308	-0.168	0.53232	1.428516	
9.00E+06	1489540	10489540	7.7696	2.4306	1506521	10506521	7.7822	0.1518	-2.2788	-0.53341	
9.00E+06	1517382	10517382	7.79022	0.3492	1530923	10530923	7.8003	-1.560	-1.9093	0.237306	
9.00E+06	1544307	10544307	7.81017	-0.125	1558876	10558876	7.8210	-2.223	-2.0976	1.295356	
9.00E+06	1572293	10572293	7.8309	-0.046	1585826	10585826	7.8409	-3.135	-3.0887	-2.39571	
9.00E+06	1649556	10649556	7.88813	0.5396	1666525	10666525	7.9007	2.9395	2.39983	2.117432	
9.00E+06	1677364	10677364	7.90872	-3.026	1695945	10695945	7.9225	-2.394	0.63133	-2.75002	
9.00E+06	1709354	10709354	7.93242	-2.170	1722803	10722803	7.9424	0.5582	2.72815	4.809235	
9.00E+06	1736288	10736288	7.95237	0.3575	1749783	10749783	7.9624	-0.598	-0.9554	0.70135	
9.00E+06	1809517	10809517	8.00661	2.9143	1826576	10826576	8.0192	0.4299	-2.4844	-6.55530	
9.00E+06	1837593	10837593	8.02741	-2.584	1850962	10850962	8.0373	-0.531	2.05379	4.433737	
9.00E+06	1864394	10864394	8.04726	-0.442	1877873	10877873	8.0572	-1.776	-1.3335	-5.25711	
9.00E+06	1891312	10891312	8.06719	-0.216	1904768	10904768	8.0772	2.4648	2.68044	0.04016	
1.40E+07	169521	14169521	10.4954	-0.032	186480	14186480	10.508	-1.094	-1.0611	-6.63086	
1.40E+07	197430	14197430	10.516	-1.405	210856	14210856	10.526	2.1221	3.52756	3.297688	
1.40E+07	229018	14229018	10.5394	-2.236	242588	14242588	10.549	-1.679	0.55685	-6.70927	
1.40E+07	255945	14255945	10.5594	-2.759	269381	14269381	10.569	2.9012	5.66012	1.725057	
1.40E+07	329459	14329459	10.6138	-2.335	346507	14346507	10.626	-0.452	1.88304	-0.59641	
1.40E+07	357459	14357459	10.6346	-1.844	370968	14370968	10.645	0.4528	2.29721	2.435199	
1.40E+07	385431	14385431	10.6553	-2.196	398942	14398942	10.665	-1.833	0.36328	-4.72843	
1.40E+07	412487	14412487	10.6753	-2.608	430747	14430747	10.689	2.0247	4.63265	1.577771	
1.40E+07	489480	14489480	10.7324	1.2797	506497	14506497	10.745	2.5194	1.23969	-0.12860	
1.40E+07	517412	14517412	10.753	-2.423	530780	14530780	10.763	-1.094	1.32835	-2.38571	
1.40E+07	544294	14544294	10.773	-0.933	557815	14557815	10.783	2.2263	3.15938	9.417442	
1.40E+07	571736	14571736	10.7933	2.2982	585251	14585251	10.803	-1.878	-4.1757	-1.85659	
1.40E+07	649601	14649601	10.851	-2.376	666475	14666475	10.863	-2.271	0.10536	0.907091	
1.40E+07	677352	14677352	10.8715	0.1784	690806	14690806	10.881	-0.343	-0.5212	3.210221	
1.40E+07	704256	14704256	10.8914	0.3810	717739	14717739	10.901	-2.595	-2.9757	-4.55402	
1.40E+07	731192	14731192	10.9114	-3.101	744646	14744646	10.921	-2.599	0.50291	1.236896	
1.40E+07	809554	14809554	10.9694	0.1892	826495	14826495	10.982	-2.182	-2.3712	-3.12689	
1.40E+07	837305	14837305	10.99	2.8856	850794	14850794	11	2.6714	-0.2142	2.142733	
1.40E+07	869060	14869060	11.0135	-0.139	882545	14882545	11.024	-2.285	-2.1456	-2.52543	
1.40E+07	896100	14896100	11.0335	-0.203	909430	14909430	11.043	-0.421	-0.2181	-0.06263	
1.40E+07	969599	14969599	11.088	0.6302	986486	14986486	11.100	0.5491	-0.0810	-0.26281	
1.40E+07	997452	14997452	11.1086	3.0023	1011002	15011002	11.119	3.1042	0.10187	-1.54237	
1.40E+07	1024426	15024426	11.1286	-1.473	1037826	15037826	11.139	-0.196	1.2764	-1.56420	
1.40E+07	1056044	15056044	11.152	-2.385	1069539	15069539	11.162	0.2998	2.68466	1.380256	
1.40E+07	1129495	15129495	11.2064	-2.667	1146477	15146477	11.219	-2.997	-0.3301	-0.69803	
1.40E+07	1157354	15157354	11.2271	-2.694	1170805	15170805	11.237	-2.542	0.152	1.55813	
1.40E+07	1189144	15189144	11.2506	2.9922	1202540	15202540	11.261	1.7404	-1.2518	-0.55955	

Table A.2: Configuration 2 10 cm/s Run 2

Zoom start point	Reader Epoch	Entire Capture Epoch	Time:	Phase Read	Tag Epoch	Entire Capture Epoch	Time:	Delta Time	Phase Response	Phase due to travel	Instant Velocity
1.40E+07	1222018	15222018	11.2749	-1.250	1240324	15240324	11.289	-1.901	-0.6516	2.518828	
1.40E+07	1289450	15289450	11.3249	2.7363	1306517	15306517	11.338	-2.649	-5.3848	-12.7344	
1.40E+07	1317329	15317329	11.3455	-2.855	1330851	15330851	11.356	0.5575	3.41232	2.200557	
1.40E+07	1344284	15344284	11.3655	-2.706	1357714	15357714	11.375	-0.972	1.73414	1.314284	
1.40E+07	1371169	15371169	11.3854	2.4726	1389424	15389424	11.399	3.0236	0.55099	-1.37833	
1.40E+07	1449486	15449486	11.4434	-2.867	1466486	15466486	11.456	0.6999	3.56639	11.17503	
1.40E+07	1477333	15477333	11.4641	2.5849	1490804	15490804	11.474	-1.564	-4.1485	-6.19241	
1.40E+07	1509208	15509208	11.4877	0.4604	1522619	15522619	11.498	1.9049	1.44451	6.784865	
1.40E+07	1536052	15536052	11.5076	1.8169	1549539	15549539	11.518	-1.924	-3.7407	0.747278	
1.40E+07	1609487	15609487	11.5619	2.4224	1626528	15626528	11.575	-2.952	-5.3740	-9.03954	
1.40E+07	1637385	15637385	11.5826	-2.484	1650926	15650926	11.593	-1.597	0.88712	-0.16781	
1.40E+07	1664356	15664356	11.6026	-2.013	1682617	15682617	11.616	-0.975	1.03809	2.935017	
1.40E+07	1700935	15700935	11.6297	0.9392	1714352	15714352	11.640	-0.667	-1.6062	-0.00312	
3.45E+07	469177	34969177	25.9017	0.7637	486192	34986192	25.914	0.8640	0.10025	-7.64728	
3.45E+07	497131	34997131	25.9224	-2.807	510967	35010967	25.933	2.6715	5.47889	5.799531	
3.45E+07	529222	35029222	25.9461	-3.049	542627	35042627	25.956	-2.783	0.26627	1.513445	
3.45E+07	556091	35056091	25.966	-1.216	569564	35069564	25.976	-2.107	-0.8911	-2.58570	
3.45E+07	629249	35129249	26.0202	-2.727	646213	35146213	26.033	2.0088	4.7354	12.0264	
3.45E+07	657265	35157265	26.041	1.5517	671101	35171101	26.051	-2.210	-3.7618	-8.37023	
3.45E+07	689385	35189385	26.0648	-2.335	703025	35203025	26.075	1.4890	3.82406	-0.19418	
3.45E+07	716322	35216322	26.0847	-3.021	729778	35229778	26.095	0.9506	3.97154	1.553374	
3.45E+07	789168	35289168	26.1387	-1.594	806196	35306196	26.151	-0.993	0.60159	1.473622	
3.45E+07	817152	35317152	26.1594	-2.077	830575	35330575	26.169	-2.495	-0.4183	3.109202	
3.45E+07	844073	35344073	26.1794	1.1748	857546	35357546	26.189	-1.624	-2.7990	-3.85878	
3.45E+07	875994	35375994	26.203	0.5184	889353	35389353	26.213	1.2038	0.68541	-2.11025	
3.45E+07	949200	35449200	26.2572	-2.865	966179	35466179	26.270	2.4226	5.2879	1.876193	
3.45E+07	977037	35477037	26.2778	-2.637	990511	35490511	26.288	1.3548	3.99189	2.721384	
3.45E+07	1004498	35504498	26.2982	-1.715	1022791	35522791	26.312	-0.217	1.49801	-1.19158	
3.45E+07	1036256	35536256	26.3217	-0.420	1049713	35549713	26.332	1.9889	2.40873	-0.42807	
3.45E+07	1109281	35609281	26.3758	-2.958	1126228	35626228	26.388	0.3808	3.33858	9.09682	
3.45E+07	1137069	35637069	26.3964	2.1113	1150493	35650493	26.406	-0.817	-2.9279	-3.58262	
3.45E+07	1163989	35663989	26.4163	-0.632	1177430	35677430	26.426	-0.820	-0.1882	3.155586	
3.45E+07	1195766	35695766	26.4399	-0.018	1209251	35709251	26.450	-3.057	-3.0388	1.439347	
3.45E+07	1269167	35769167	26.4942	3.1310	1286262	35786262	26.507	-3.055	-6.1857	-13.9151	
3.45E+07	1297036	35797036	26.5149	-2.779	1310492	35810492	26.525	0.6069	3.38611	2.171855	
3.45E+07	1324021	35824021	26.5349	-2.873	1343240	35843240	26.549	-1.506	1.36697	-0.75281	
3.45E+07	1361627	35861627	26.5627	-2.245	1376203	35876203	26.574	-0.173	2.07144	-0.33900	
3.45E+07	1429166	35929166	26.6127	-1.071	1446178	35946178	26.625	1.6739	2.74486	0.949186	
3.45E+07	1457035	35957035	26.6334	-2.652	1470491	35970491	26.643	-0.562	2.08971	-0.12428	
3.45E+07	1483956	35983956	26.6533	0.1487	1498468	35998468	26.664	2.3372	2.18842	2.694628	

Table A.2: Configuration 2 10 cm/s Run 2

Zoom start point	Reader Epoch	Entire Capture Epoch	Time:	Phase Read	Tag Epoch	Entire Capture Epoch	Time:	Delta Time	Phase Response	Phase due to travel	Instant Velocity
3.45E+07	1512004	36012004	26.6741	3.0004	1525897	36025897	26.684	3.0906	0.09015	1.487572	
3.45E+07	1589157	36089157	26.7312	2.2884	1606167	36106167	26.744	-1.011	-3.2997	-7.75406	
3.45E+07	1617080	36117080	26.7519	-2.051	1635381	36135381	26.765	1.0797	3.13118	-0.02114	
3.45E+07	1648920	36148920	26.7755	-2.383	1662285	36162285	26.785	0.7645	3.14733	6.14904	
3.45E+07	1675773	36175773	26.7954	3.0145	1689762	36189762	26.806	1.3653	-1.6492	-1.95056	
3.45E+07	1749172	36249172	26.8498	-2.542	1766245	36266245	26.862	0.0436	2.58601	6.778392	
3.45E+07	1777079	36277079	26.8704	-0.262	1791018	36291018	26.881	-2.443	-2.1811	-4.90639	
3.45E+07	1804524	36304524	26.8908	-0.255	1817956	36317956	26.901	1.3164	1.57102	-1.12107	
3.45E+07	1831543	36331543	26.9108	-0.493	1844942	36344942	26.921	1.9364	2.42988	2.31764	
3.45E+07	1913338	36413338	26.9714	1.7705	1930391	36430391	26.984	-1.422	-3.1923	-8.84278	
3.45E+07	1941045	36441045	26.9919	-2.388	1959284	36459284	27.005	1.6725	4.06096	-0.18994	
3.45E+07	1972802	36472802	27.0154	-3.004	1986412	36486412	27.025	1.2033	4.20724	3.780139	
3.45E+07	2004574	36504574	27.0389	-3.108	2022861	36522861	27.052	-2.812	0.29572	0.00407	
4.75E+07	369001	47869001	35.4566	-0.564	286011	47786011	35.395	-1.570	-1.0056	-4.09005	
4.75E+07	296952	47796952	35.4032	-1.472	315242	47815242	35.417	0.9160	2.38845	6.002641	
4.75E+07	328731	47828731	35.4267	-0.321	342130	47842130	35.437	-2.515	-2.1935	1.010692	
4.75E+07	355619	47855619	35.4467	-0.074	369049	47869049	35.457	-3.040	-2.9659	-1.19983	
4.75E+07	429095	47929095	35.5011	0.7901	446023	47946023	35.514	0.4461	-0.344	2.069522	
4.75E+07	456949	47956949	35.5217	-0.551	470459	47970459	35.532	-2.331	-1.7797	-4.84115	
4.75E+07	483884	47983884	35.5417	0.6378	497344	47997344	35.552	2.5532	1.91531	2.852769	
4.75E+07	515710	48015710	35.5652	0.4902	529153	48029153	35.575	-0.171	-0.6608	0.020309	
4.75E+07	589028	48089028	35.6195	1.9728	606049	48106049	35.632	1.2676	-0.7052	-3.55249	
4.75E+07	616866	48116866	35.6402	-0.052	630343	48130343	35.650	1.6928	1.74494	2.40303	
4.75E+07	643816	48143816	35.6601	2.1606	657277	48157277	35.670	2.0681	-0.0925	2.90306	
4.75E+07	670765	48170765	35.6801	0.3065	688944	48188944	35.694	-2.396	-2.7023	-1.26798	
4.75E+07	749007	48249007	35.738	-2.521	766044	48266044	35.751	-2.448	0.07301	-5.47875	
4.75E+07	776876	48276876	35.7587	-2.839	795148	48295148	35.772	1.7607	4.59976	12.80662	
4.75E+07	808545	48308545	35.7821	2.7953	822052	48322052	35.792	-2.386	-5.1817	-7.62831	
4.75E+07	835557	48335557	35.8021	-0.132	849002	48349002	35.812	0.5231	0.65462	-1.53970	
4.75E+07	913009	48413009	35.8595	-2.541	930104	48430104	35.872	1.6588	4.19965	11.19896	
4.75E+07	940977	48440977	35.8802	1.2868	954415	48454415	35.890	-2.243	-3.5295	-0.71756	
4.75E+07	967941	48467941	35.9002	1.0520	981365	48481365	35.910	-1.929	-2.9805	1.019854	
4.75E+07	999640	48499640	35.9237	2.7697	1013095	48513095	35.934	-1.129	-3.8992	-2.58964	
4.75E+07	1068989	48568989	35.9751	-0.861	1086190	48586190	35.988	0.6132	1.47457	9.074025	
4.75E+07	1096894	48596894	35.9957	2.2164	1110315	48610315	36.006	-2.524	-4.7401	-5.02751	
4.75E+07	1123765	48623765	36.0156	-2.890	1146891	48646891	36.033	-2.410	0.48025	3.207747	
4.75E+07	1160417	48660417	36.0428	2.3693	1173855	48673855	36.053	0.3940	-1.9752	-1.71606	
4.75E+07	1228999	48728999	36.0936	-1.855	1246048	48746048	36.106	-0.313	1.54183	4.436516	
4.75E+07	1256920	48756920	36.1143	1.8097	1275309	48775309	36.128	-0.334	-2.1436	-5.99946	
4.75E+07	1289717	48789717	36.1385	-2.703	1303177	48803177	36.149	-0.100	2.60291	4.278535	

Table A.2: Configuration 2 10 cm/s Run 2

Zoom start point	Reader Epoch	Entire Capture Epoch	Time:	Phase Read	Tag Epoch	Entire Capture Epoch	Time:	Delta Time	Phase Response	Phase due to travel	Instant Velocity
4.75E+07	1316604	48816604	36.1585	1.2584	1330130	48830130	36.168	0.5875	-0.6709	-0.98826	
4.75E+07	1389002	48889002	36.2121	-2.669	1405991	48905991	36.225	-1.212	1.45744	0.162724	
4.75E+07	1417026	48917026	36.2328	-2.234	1430395	48930395	36.243	-0.890	1.3447	6.472563	
4.75E+07	1443961	48943961	36.2528	1.1632	1457425	48957425	36.263	-2.459	-3.6221	-7.40490	
4.75E+07	1470787	48970787	36.2727	-1.233	1489092	48989092	36.286	1.8015	3.03492	1.599073	
4.75E+07	1548998	49048998	36.3306	-2.321	1566020	49066020	36.343	-2.778	-0.4573	-0.95571	
4.75E+07	1576898	49076898	36.3513	-2.008	1595125	49095125	36.365	-1.675	0.33234	1.845607	
4.75E+07	1608583	49108583	36.3747	0.2490	1622060	49122060	36.385	-0.830	-1.0789	3.084542	
4.75E+07	1635501	49135501	36.3947	0.5179	1649026	49149026	36.405	-2.922	-3.4403	0.120219	
4.75E+07	1708995	49208995	36.4491	2.1100	1726017	49226017	36.462	-1.593	-3.7030	-7.02334	
4.75E+07	1736959	49236959	36.4698	1.3937	1750420	49250420	36.480	2.5563	1.1626	3.682822	
4.75E+07	1768785	49268785	36.4934	0.7490	1787199	49287199	36.507	-1.934	-2.6827	-5.05904	
4.75E+07	1800608	49300608	36.517	-2.845	1814103	49314103	36.527	-1.664	1.18127		
									Averages=	-0.06827	

Table A.3: Configuration 2 10 cm/s Run 3

Zoom start point	Reader Epoch	Entire Capture Epoch	Time:	Phase Read	Tag Epoch	Entire Capture Epoch	Time:	Delta Time	Phase Response	Phase due to travel	Instant Velocity
9.00E+05	74993	974993	0.722177	0.0324	92059	992059	0.7348	1.5635	1.531140	-1.05249	
9.00E+05	102864	1002864	0.742821	-2.792	117449	1017449	0.7536	-0.502	2.289779	1.869244	
9.00E+05	130998	1030998	0.763660	-0.645	144362	1044362	0.7736	0.217	0.861608	1.071816	
9.00E+05	167534	1067534	0.790722	-0.592	180892	1080892	0.8006	-0.842	-0.24992	1.833265	
9.00E+05	234940	1134940	0.840650	1.7273	252002	1152002	0.8533	-2.224	-3.95083	0.257100	
9.00E+05	262793	1162793	0.861281	1.7058	281275	1181275	0.8750	-2.459	-4.16449	-0.38733	
9.00E+05	294560	1194560	0.884811	2.5108	308015	1208015	0.8948	-1.360	-3.87046	-4.14756	
9.00E+05	321478	1221478	0.904749	-1.872	339787	1239787	0.9183	-2.001	-0.12945	1.812149	
9.00E+05	394437	1294437	0.958789	2.5877	411934	1311934	0.9717	-1.253	-3.84107	-3.40718	
9.00E+05	422822	1322822	0.979814	1.1663	436239	1336239	0.9898	-0.324	-1.49012	-6.56696	
9.00E+05	449708	1349708	0.999729	-1.588	463162	1363162	1.0097	1.941	3.529140	2.248486	
9.00E+05	481539	1381539	1.023306	-2.678	494956	1394956	1.0332	-1.179	1.499647	0.581115	
9.00E+05	554939	1454939	1.077673	-1.499	571979	1471979	1.0903	-1.270	0.228972	1.660946	
9.00E+05	582872	1482872	1.098363	2.9602	597345	1497345	1.1091	1.9931	-0.96711	2.597576	
9.00E+05	616213	1516213	1.123059	1.0809	629660	1529660	1.1330	-2.269	-3.35011	0.175407	
9.00E+05	643201	1543201	1.143049	1.4526	656562	1556562	1.1529	-2.031	-3.48407	-1.58742	
9.00E+05	714917	1614917	1.196169	-1.269	731977	1631977	1.2088	-1.354	-0.08546	-0.39028	
9.00E+05	742900	1642900	1.216896	-1.554	757523	1657523	1.2277	-1.356	0.197584	7.205332	
9.00E+05	770905	1670905	1.237639	2.8842	784376	1684376	1.2476	-2.411	-5.29528	-2.51561	
9.00E+05	797914	1697914	1.257645	2.7548	811272	1711272	1.2675	-0.620	-3.37448	-1.11069	

Zoom start point	Reader Epoch	Entire Capture Epoch	Time:	Phase Read	Tag Epoch	Entire Capture Epoch	Time:	Delta Time	Phase Response	Phase due to travel	Instant Velocity
9.00E+05	874975	1774975	1.314724	3.0316	891924	1791924	1.3273	2.2002	-0.83140	3.912011	
9.00E+05	902887	1802887	1.335398	2.2106	916369	1816369	1.3454	-1.336	-3.54622	-4.62692	
9.00E+05	929794	1829794	1.355328	-2.825	948039	1848039	1.3688	-2.212	0.613766	-7.22978	
9.00E+05	961475	1861475	1.378795	-3.140	974908	1874908	1.3887	2.9888	6.12855	2.806304	
9.00E+05	1035036	1935036	1.433281	1.1426	1051947	1951947	1.4458	1.1336	-0.00903	4.395710	
9.00E+05	1062862	1962862	1.453892	1.3225	1076279	1976279	1.4638	-1.723	-3.04543	-3.11222	
9.00E+05	1089710	1989710	1.473778	-1.742	1103170	2003170	1.4837	-2.411	-0.66953	3.938660	
9.00E+05	1116644	2016644	1.493728	2.3321	1130212	2030212	1.5038	-1.361	-3.69323	-2.87502	
9.00E+05	1194920	2094920	1.551707	-0.573	1211955	2111955	1.5643	2.4058	2.978583	7.583311	
9.00E+05	12227788	13127788	9.723753	2.534	1241039	2141039	1.5859	-0.749	-3.28273	-10.9911	
9.00E+05	1255500	2155500	1.596579	-2.785	1268937	2168937	1.6065	2.637	5.422199	6.153907	
9.00E+05	1282402	2182402	1.616505	2.0023	1295887	2195887	1.6265	2.7163	0.713925	1.118339	
9.00E+05	1354930	2254930	1.670227	-1.247	1371926	2271926	1.6828	-2.947	-1.70021	5.176455	
9.00E+05	1382967	2282967	1.690994	2.1688	1396371	2296371	1.7009	-3.124	-5.29253	-6.04565	
9.00E+05	1414604	2314604	1.714427	-0.536	1428062	2328062	1.7244	-0.389	0.146617	-4.06517	
9.00E+05	1441598	2341598	1.734422	-2.936	1455007	2355007	1.7444	0.3206	3.256246	3.977141	
9.00E+05	1514921	2414921	1.788732	3.0876	1531949	2431949	1.8013	-2.343	-5.43109	-4.16226	
9.00E+05	1542985	2442985	1.809519	0.4753	1556351	2456351	1.8194	-2.072	-2.54768	-1.96883	
9.00E+05	1569784	2469784	1.829369	2.9096	1583258	2483258	1.8393	1.8659	-1.04375	-4.02860	
9.00E+05	1596734	2496734	1.849331	-2.599	1615036	2515036	1.8629	-0.009	2.590644	-0.00461	
7.20E+06	174906	7374906	5.462593	-2.759	191918	7391918	5.4752	0.4702	3.228902	8.865066	
7.20E+06	202739	7402739	5.483209	0.7331	216190	7416190	5.4932	-2.147	-2.87967	2.127821	
7.20E+06	230772	7430772	5.503973	3.0635	244226	7444226	5.5139	-1.510	-4.57324	-6.92212	
7.20E+06	257698	7457698	5.523917	-2.943	271188	7471188	5.5339	-2.217	0.725143	-0.28171	
7.20E+06	334901	7534901	5.581101	-2.493	351913	7551913	5.5937	-1.122	1.370751	5.090453	
7.20E+06	362843	7562843	5.601798	-0.150	376349	7576349	5.6118	-2.311	-2.16058	-1.02505	
7.20E+06	389721	7589721	5.621706	0.6147	408075	7608075	5.6353	-0.623	-1.23734	-0.36326	
7.20E+06	421510	7621510	5.645252	2.1431	435166	7635166	5.6554	1.1851	-0.95797	-0.64380	
7.20E+06	494847	7694847	5.699573	-1.934	511857	7711857	5.7122	-1.490	0.443714	0.352997	
7.20E+06	522739	7722739	5.720233	-0.563	536179	7736179	5.7302	-0.363	0.199977	-2.03450	
7.20E+06	549717	7749717	5.740215	-0.422	567998	7767998	5.7538	1.6153	2.037769	2.352563	
7.20E+06	581397	7781397	5.763681	-1.447	594878	7794878	5.7737	-1.204	0.242528	0.286248	
7.20E+06	654914	7854914	5.818135	-2.566	671876	7871876	5.8307	-2.949	-0.38318	-4.37491	
7.20E+06	628703	7828703	5.798720	-2.46	701041	7901041	5.8523	0.7791	3.239110	9.101404	
7.20E+06	715655	7915655	5.863126	3.1233	734012	7934012	5.8767	-2.157	-5.27997	-2.41275	
7.20E+06	747403	7947403	5.886641	1.2539	760867	7960867	5.8966	-2.187	-3.44051	-2.70374	
7.20E+06	814853	8014853	5.936602	-1.602	831911	8031911	5.9492	0.4106	2.012590	3.501556	
7.20E+06	842697	8042697	5.957226	-2.117	856176	8056176	5.9672	-2.516	-0.39950	-0.89548	
7.20E+06	874511	8074511	5.980790	-1.498	887954	8087954	5.9907	-1.090	0.408356	-0.28809	
7.20E+06	906239	8106239	6.004291	-1.814	919727	8119727	6.0143	-1.145	0.668217	0.310554	

Table A.3: Configuration 2 10 cm/s Run 3

Zoom start point	Reader Epoch	Entire Capture Epoch	Time:	Phase Read	Tag Epoch	Entire Capture Epoch	Time:	Delta Time	Phase Response	Phase due to travel	Instant Velocity
7.20E+06	978847	8178847	6.058072	-3.114	995864	8195864	6.0707	-3.117	-0.00303	-0.58151	
7.20E+06	1006755	8206755	6.078743	-2.429	1020186	8220186	6.0887	-2.031	0.398491	-1.18284	
7.20E+06	1033635	8233635	6.098653	-2.718	1052005	8252005	6.1123	-1.251	1.466965	-2.13011	
7.20E+06	1065486	8265486	6.122245	-0.749	1078942	8278942	6.1322	2.3464	3.095899	2.914894	
7.20E+06	1134841	8334841	6.173617	2.6925	1151869	8351869	6.1862	-0.246	-2.93891	-7.14789	
7.20E+06	1162742	8362742	6.194283	0.0011	1181032	8381032	6.2078	2.98	2.978918	-0.30286	
7.20E+06	1194490	8394490	6.217799	-2.156	1207953	8407953	6.2278	1.0542	3.210382	9.670078	
7.20E+06	1226286	8426286	6.24135	2.6697	1239724	8439724	6.2513	-2.842	-5.51155	-3.65363	
7.20E+06	1294838	8494838	6.292127	0.2933	1311844	8511844	6.3047	2.2623	1.968978	8.625103	
7.20E+06	1322711	8522711	6.312772	2.8187	1336173	8536173	6.3227	-1.169	-3.98820	-9.50393	
7.20E+06	1354498	8554498	6.336317	-2.638	1367903	8567903	6.3462	1.9346	4.572816	7.102472	
7.20E+06	1381351	8581351	6.356207	-1.533	1394815	8594815	6.3662	-2.386	-0.85353	-1.87658	
7.20E+06	1454950	8654950	6.410721	-2.166	1471840	8671840	6.4232	1.0836	3.249931	4.464893	
7.20E+06	1482780	8682780	6.431335	0.874	1496228	8696228	6.4413	1.0327	0.158644	-0.37593	
7.20E+06	1509733	8709733	6.451299	-1.765	1528024	8728024	6.4648	-1.267	0.497982	-0.25930	
7.20E+06	1541438	8741438	6.474783	0.2063	1554989	8754989	6.4848	0.9028	0.696481	-1.14986	
7.20E+06	1614864	8814864	6.529170	-0.452	1631861	8831861	6.5418	2.7543	3.205860	11.28869	
7.20E+06	1642703	8842703	6.549790	1.4676	1656151	8856151	6.5598	-3.111	-4.5785	-4.27411	
7.20E+06	1670157	8870157	6.570125	3.1181	1688473	8888473	6.5837	2.4615	-0.65661	0.049675	
7.20E+06	1706721	8906721	6.597208	-1.749	1720226	8920226	6.6072	-2.450	-0.70139	-0.00505	
1.20E+07	178812	12178812	9.020846	-2.182	195873	12195873	9.0335	-2.414	-0.23202	-4.42513	
1.20E+07	206653	12206653	9.041468	-0.849	220145	12220145	9.0515	1.9678	2.817159	2.867211	
1.20E+07	233694	12233694	9.061497	2.5913	248156	12248156	9.0722	3.1285	0.537130	4.190459	
1.20E+07	266638	12266638	9.085899	1.3373	285554	12285554	9.0999	-2.575	-3.91187	-1.78604	
1.20E+07	334792	12334792	9.136380	-1.792	351816	12351816	9.1490	-2.344	-0.55211	-1.28677	
1.20E+07	362659	12362659	9.157022	0.7398	376098	12376098	9.1670	1.0747	0.334921	6.715029	
1.20E+07	389575	12389575	9.176958	2.0743	403056	12403056	9.1869	-2.730	-4.80419	-3.27831	
1.20E+07	416494	12416494	9.196897	0.1989	429978	12429978	9.2069	-2.100	-2.29860	-1.66312	
1.20E+07	494808	12494808	9.254904	-2.463	511829	12511829	9.2675	-0.897	1.565965	6.009792	
1.20E+07	522643	12522643	9.275522	3.0037	536137	12536137	9.2855	0.4224	-2.58129	1.183840	
1.20E+07	549591	12549591	9.295482	2.6138	563056	12563056	9.3055	-0.872	-3.48599	-4.20705	
1.20E+07	576510	12576510	9.315421	2.4368	590004	12590004	9.3254	2.1693	-0.26747	-0.66450	
1.20E+07	654869	12654869	9.373461	-0.932	671832	12671832	9.3860	0.3438	1.276171	6.092085	
1.20E+07	682669	12682669	9.394053	2.9876	696221	12696221	9.4041	0.0458	-2.94188	-9.22942	
1.20E+07	709665	12709665	9.414049	-1.924	723098	12723098	9.424	2.1764	4.100304	0.126893	
1.20E+07	736494	12736494	9.433921	-1.422	749962	12749962	9.4439	2.5812	4.003530	1.425410	
1.20E+07	814776	12814776	9.491905	-1.067	831829	12831829	9.5045	-0.376	0.690687	-3.95581	
1.20E+07	842730	12842730	9.512610	-2.403	856173	12856173	9.5226	1.0211	3.424564	0.332799	
1.20E+07	874601	12874601	9.536217	-2.673	888095	12888095	9.5462	0.4499	3.122968	3.556132	
1.20E+07	901478	12901478	9.556125	-1.620	914943	12914943	9.5661	-1.208	0.412516	1.489885	

Table A.3: Configuration 2 10 cm/s Run 3

Zoom start point	Reader Epoch	Entire Capture Epoch	Time:	Phase Read	Tag Epoch	Entire Capture Epoch	Time:	Delta Time	Phase Response	Phase due to travel	Instant Velocity
1.20E+07	974773	12974773	9.610414	0.3129	991794	12991794	9.6230	-2.525	-2.83802	-0.51699	
1.20E+07	1002724	13002724	9.631118	0.2097	1020999	13020999	9.6447	-2.200	-2.40938	-4.46541	
1.20E+07	1034479	13034479	9.654639	0.9278	1047973	13047973	9.6646	1.9379	1.010088	6.166887	
1.20E+07	1061459	13061459	9.674623	2.1064	1074863	13074863	9.6846	-1.591	-3.69761	-0.79614	
1.20E+07	1134793	13134793	9.728941	2.9115	1151788	13151788	9.7415	0.9525	-1.95897	3.728345	
1.20E+07	1162715	13162715	9.749623	2.5187	1176257	13176257	9.7597	-2.030	-4.54888	-11.9963	
1.20E+07	1189785	13189785	9.769674	-1.534	1203112	13203112	9.7795	3.0632	4.596992	11.34611	
1.20E+07	1216582	13216582	9.789522	2.9927	1234873	13234873	9.8031	-2.641	-5.63342	-0.46438	
1.20E+07	1294771	13294771	9.847437	1.8932	1311779	13311779	9.8600	-2.726	-4.61955	-4.27656	
1.20E+07	1322664	13322664	9.868097	0.4339	1336103	13336103	9.8781	-1.233	-1.66642	-7.35487	
1.20E+07	1349657	13349657	9.888091	-1.882	1363048	13363048	9.8980	2.0772	3.959646	2.031626	
1.20E+07	1376528	13376528	9.907994	-2.904	1390006	13390006	9.9180	-0.499	2.404814	3.177332	
1.20E+07	1454778	13454778	9.965954	2.1788	1471786	13471786	9.9786	-2.793	-4.97188	-12.3091	
1.20E+07	1482700	13482700	9.986636	-2.677	1496317	13496317	9.9967	0.9229	3.600369	4.461013	
1.20E+07	1514320	13514320	10.01006	-1.034	1527817	13527817	10.020	-1.423	-0.38893	-0.61277	
1.20E+07	1541239	13541239	10.03000	-2.761	1554704	13554704	10.04	-2.682	0.078801	-0.45968	
1.20E+07	1614804	13614804	10.08449	-1.848	1631867	13631867	10.097	-0.762	1.085782	-1.85402	
1.20E+07	1642710	13642710	10.10516	0.1644	1656191	13656191	10.115	2.5304	2.366052	7.006134	
1.20E+07	1674420	13674420	10.12864	1.4012	1689513	13689513	10.140	-2.860	-4.26163	-5.34169	
1.20E+07	1707820	13707820	10.15338	1.1356	1721236	13721236	10.163	1.6846	0.549040	0.004382	
1.88E+07	133843	18933843	14.02430	-0.676	150866	18950866	14.037	-0.777	-0.10147	-3.13020	
1.88E+07	161699	18961699	14.04493	-0.232	180762	18980762	14.059	2.3232	2.555196	-1.31833	
1.88E+07	192256	18992256	14.06756	-2.657	207738	19007738	14.079	0.9076	3.564808	4.789902	
1.88E+07	226085	19026085	14.09262	-1.724	239550	19039550	14.103	-2.485	-0.76102	0.429026	
1.88E+07	289848	19089848	14.13985	1.1912	306836	19106836	14.152	-0.389	-1.58055	-0.66230	
1.88E+07	317702	19117702	14.16048	1.7033	331135	19131135	14.170	0.5796	-1.12368	-1.67440	
1.88E+07	344636	19144636	14.18043	-2.553	358058	19158058	14.190	-2.397	0.156101	-2.00498	
1.88E+07	372579	19172579	14.20113	-0.806	386031	19186031	14.211	0.9419	1.748310	1.259309	
1.88E+07	449856	19249856	14.25837	0.766	466837	19266837	14.271	-0.375	-1.14056	3.269545	
1.88E+07	477690	19277690	14.27898	2.211	495941	19295941	14.293	-1.631	-3.84198	-3.94423	
1.88E+07	509397	19309397	14.30247	3.0436	522922	19322922	14.312	2.2228	-0.82083	-0.74713	
1.88E+07	541257	19341257	14.32607	2.5566	554777	19354777	14.336	2.4114	-0.14518	-1.06119	
1.88E+07	609888	19409888	14.37690	0.9368	626864	19426864	14.389	2.9633	2.026534	4.028048	
1.88E+07	637738	19437738	14.39753	-2.093	651168	19451168	14.407	-2.846	-0.75270	-1.34420	
1.88E+07	664693	19464693	14.41750	-3.000	678081	19478081	14.427	-2.725	0.274320	-5.48932	
1.88E+07	691553	19491553	14.43739	-2.643	705036	19505036	14.447	1.8314	4.474910	3.385222	
1.88E+07	769851	19569851	14.49539	3.0046	786875	19586875	14.508	-0.386	-3.39010	-4.76591	
1.88E+07	797738	19597738	14.51604	2.6658	811158	19611158	14.526	2.5612	-0.10461	1.932020	
1.88E+07	824816	19624816	14.53610	0.1711	847818	19647818	14.553	-1.944	-2.11535	1.836753	
1.88E+07	861332	19661332	14.56315	2.0189	874820	19674820	14.573	-1.504	-3.52334	-2.11632	

116

Table A.3: Configuration 2 10 cm/s Run 3

Zoom start point	Reader Epoch	Entire Capture Epoch	Time:	Phase Read	Tag Epoch	Entire Capture Epoch	Time:	Delta Time	Phase Response	Phase due to travel	Instant Velocity
1.88E+07	929878	19729878	14.61392	-1.280	946870	19746870	14.627	-0.474	0.805455	1.509517	
1.88E+07	957723	19757723	14.63455	2.6334	971169	19771169	14.645	2.3975	-0.23585	1.594245	
1.88E+07	985133	19785133	14.65485	-0.977	998653	19798653	14.665	-2.457	-1.47976	3.200908	
1.88E+07	1012570	19812570	14.67517	1.2127	1026011	19826011	14.685	-2.753	-3.96580	-1.81836	
1.88E+07	1089831	19889831	14.73240	-1.497	1106839	19906839	14.745	-1.290	0.206661	1.380855	
1.88E+07	1117697	19917697	14.75304	0.9249	1131133	19931133	14.763	0.1792	-0.74569	-5.93430	
1.88E+07	1145776	19945776	14.77384	-2.505	1159235	19959235	14.784	1.4837	3.988637	7.611767	
1.88E+07	1172678	19972678	14.79376	1.0491	1186153	19986153	14.804	-0.779	-1.82811	1.215011	
1.88E+07	1249871	20049871	14.85094	3.0373	1266849	20066849	14.864	-1.574	-4.61157	-12.2314	
1.88E+07	1277794	20077794	14.87162	-1.138	1291243	20091243	14.882	2.7207	3.858985	-0.68776	
1.88E+07	1304728	20104728	14.89157	-2.194	1318278	20118278	14.902	2.193	4.386844	3.053101	
1.88E+07	1336541	20136541	14.91514	0.0894	1349910	20149910	14.925	1.7345	1.645145	1.547141	
1.88E+07	1409950	20209950	14.96951	-0.622	1426860	20226860	14.982	-2.357	-1.73465	-2.19721	
1.88E+07	1437599	20237599	14.98999	-0.131	1451148	20251148	15	-0.350	-0.21964	0.632078	
1.88E+07	1464633	20264633	15.01001	-1.458	1482828	20282828	15.023	-2.247	-0.78811	-3.27324	
1.88E+07	1496266	20296266	15.03344	-1.721	1519868	20319868	15.051	0.9325	2.653811	-0.89042	
1.88E+07	1569819	20369819	15.08792	-1.593	1586833	20386833	15.101	2.754	4.346571	4.512828	
1.88E+07	1597741	20397741	15.10861	-2.176	1612245	20412245	15.119	-1.085	1.090907	0.889721	
1.88E+07	1625738	20425738	15.12934	-2.227	1643857	20443857	15.143	-1.934	0.292438	1.108112	
1.88E+07	1657371	20457371	15.15277	-0.234	1670796	20470796	15.163	-0.789	-0.55502	0.005860	
3.15E+07	229694	31729694	23.50218	2.1358	246706	31746706	23.515	-0.295	-2.43097	-2.91835	
3.15E+07	257634	31757634	23.52288	-0.919	271127	31771127	23.533	-1.326	-0.40770	-3.38730	
3.15E+07	289318	31789318	23.54635	-2.506	302793	31802793	23.556	0.1318	2.637385	2.701855	
3.15E+07	316278	31816278	23.56632	-2.463	334514	31834514	23.580	-2.259	0.204280	0.518232	
3.15E+07	389685	31889685	23.62069	-1.595	406685	31906685	23.633	-2.452	-0.85751	0.598152	
3.15E+07	417576	31917576	23.64135	1.3933	431028	31931028	23.651	0.1224	-1.27088	-2.22638	
3.15E+07	444476	31944476	23.66127	-1.847	457928	31957928	23.671	-1.418	0.429336	-5.69872	
3.15E+07	471390	31971390	23.68121	-2.229	484851	31984851	23.691	2.5558	4.784986	3.784189	
3.15E+07	549698	32049698	23.73921	2.56	566675	32066675	23.752	-1.445	-4.00535	-8.24521	
3.15E+07	577527	32077527	23.75982	-2.747	590995	32090995	23.770	-1.060	1.687338	2.918989	
3.15E+07	609305	32109305	23.78336	0.1968	622835	32122835	23.793	-0.754	-0.95117	-4.20861	
3.15E+07	636212	32136212	23.80329	-2.133	649774	32149774	23.813	0.1342	2.267476	2.873154	
3.15E+07	709681	32209681	23.85771	2.1583	725588	32225588	23.869	-1.758	-3.91639	-0.09381	
3.15E+07	737618	32237618	23.87840	2.4626	751072	32251072	23.888	-1.386	-3.84852	-7.80989	
3.15E+07	764589	32264589	23.89838	-1.209	778495	32278495	23.909	1.0228	2.231591	0.540956	
3.15E+07	801704	32301704	23.92587	-0.934	819931	32319931	23.939	0.6617	1.595247	2.619384	
3.15E+07	869680	32369680	23.97622	0.4782	886703	32386703	23.989	-2.892	-3.37005	-5.24520	
3.15E+07	897617	32397617	23.99691	-2.834	915823	32415823	24.010	-1.868	0.966109	4.354651	
3.15E+07	938986	32438986	24.02756	1.506	952459	32452459	24.038	-2.057	-3.56301	-10.2585	
3.15E+07	970785	32470785	24.05111	-3.098	984253	32484253	24.061	2.5984	5.696370	1.685166	

117

Zoom start point	Reader Epoch	Entire Capture Epoch	Time:	Phase Read	Tag Epoch	Entire Capture Epoch	Time:	Delta Time	Phase Response	Phase due to travel	Instant Velocity
3.15E+07	1029688	32529688	24.09474	-1.987	1046743	32546743	24.107	0.7202	2.706823	3.789003	
3.15E+07	1057609	32557609	24.11542	-1.766	1075822	32575822	24.129	-2.187	-0.42110	-0.09992	
3.15E+07	1089268	32589268	24.13887	2.3948	1102713	32602713	24.149	2.05	-0.34483	-2.46437	
3.15E+07	1116184	32616184	24.15881	-0.502	1129645	32629645	24.169	1.037	1.539376	-1.33046	
3.15E+07	1189662	32689662	24.21323	-2.178	1206646	32706646	24.226	2.2701	4.447747	7.646785	
3.15E+07	1217608	32717608	24.23393	1.4684	1235890	32735890	24.247	-0.432	-1.90070	2.518200	
3.15E+07	1249386	32749386	24.25747	2.3974	1262884	32762884	24.267	-1.433	-3.83049	-4.98013	
3.15E+07	1276293	32776293	24.2774	-2.075	1289761	32789761	24.287	-2.106	-0.03058	0.914760	
3.15E+07	1349661	32849661	24.33174	1.9177	1366659	32866659	24.344	-0.110	-2.02756	-3.91368	
3.15E+07	1377637	32877637	24.35247	-2.504	1391107	32891107	24.362	-1.815	0.688757	3.090238	
3.15E+07	1404514	32904514	24.37237	2.184	1418039	32918039	24.382	0.5101	-1.67396	-3.04149	
3.15E+07	1431453	32931453	24.39233	1.9944	1449735	32949735	24.406	3.0572	1.062839	0.263609	
3.15E+07	1509644	33009644	24.45024	-2.610	1526667	33026667	24.463	-2.122	0.487107	1.626755	
3.15E+07	1537503	33037503	24.47088	-0.720	1550971	33050971	24.481	-1.355	-0.63530	-1.66899	
3.15E+07	1569336	33069336	24.49446	-2.979	1582772	33082772	24.504	-2.107	0.871463	-5.62646	
3.15E+07	1596211	33096211	24.51436	-3.057	1609750	33109750	24.524	2.1238	5.180664	1.818700	
3.15E+07	1669673	33169673	24.56878	-2.520	1686712	33186712	24.581	-1.313	1.207014	2.141827	
3.15E+07	1697571	33197571	24.58944	-0.112	1716378	33216378	24.603	-0.709	-0.59681	-0.77787	
3.15E+07	1729824	33229824	24.61333	0.6774	1743349	33243349	24.623	0.6762	-0.00121	-0.76836	
3.15E+07	1761524	33261524	24.63681	-1.313	1774953	33274953	24.647	-0.625	0.688171	0.022258	
3.65E+07	29594	36529594	27.05747	-1.078	46652	36546652	27.070	-2.457	-1.37917	-2.87117	
3.65E+07	57479	36557479	27.07812	-2.701	80511	36580511	27.095	-1.320	1.380679	3.688543	
3.65E+07	94084	36594084	27.10524	0.6881	112221	36612221	27.119	-1.252	-1.93982	-4.75579	
3.65E+07	125695	36625695	27.12865	0.4847	139156	36639156	27.139	2.1815	1.696749	0.586544	
3.65E+07	189678	36689678	27.17604	-2.766	206659	36706659	27.189	-2.193	0.572724	2.752329	
3.65E+07	211727	36711727	27.19238	2.6758	232088	36732088	27.207	1.2616	-1.41420	4.805869	
3.65E+07	245452	36745452	27.21736	3.1309	258934	36758934	27.227	-1.946	-5.07692	-4.09171	
3.65E+07	277254	36777254	27.24091	-0.243	290711	36790711	27.251	-1.629	-1.38571	-1.90669	
3.65E+07	349640	36849640	27.29453	-2.522	366652	36866652	27.307	0.2028	2.724923	-0.56505	
3.65E+07	377533	36877533	27.31519	-0.248	390960	36890960	27.325	2.8664	3.114856	5.335304	
3.65E+07	404497	36904497	27.33516	-1.315	422707	36922707	27.349	-3.009	-1.69369	-5.47908	
3.65E+07	441010	36941010	27.36221	-2.929	454462	36954462	27.372	0.3168	3.245678	2.326785	
3.65E+07	509665	37009665	27.41306	0.818	526617	37026617	27.426	-0.703	-1.52055	-2.27921	
3.65E+07	537495	37037495	27.43367	1.4726	555750	37055750	27.447	1.8371	0.364492	-1.02528	
3.65E+07	569179	37069179	27.45714	-3.078	582593	37082593	27.467	-1.932	1.145809	0.912559	
3.65E+07	600886	37100886	27.48063	-1.264	614366	37114366	27.491	-0.942	0.322673	-1.90296	
3.65E+07	669668	37169668	27.53157	-2.456	686649	37186649	27.544	1.7721	4.227641	10.91506	
3.65E+07	697501	37197501	27.55219	0.7039	710931	37210931	27.562	-2.593	-3.29660	-1.08709	
3.65E+07	724449	37224449	27.57215	0.5949	737914	37237914	27.582	-1.869	-2.46386	-1.63864	
3.65E+07	756067	37256067	27.59557	1.6679	769560	37269560	27.606	0.6762	-0.99170	-2.15345	

Table A.3: Configuration 2 10 cm/s Run 3

Zoom start point	Reader Epoch	Entire Capture Epoch	Time:	Phase Read	Tag Epoch	Entire Capture Epoch	Time:	Delta Time	Phase Response	Phase due to travel	Instant Velocity
3.65E+07	829614	37329614	27.65005	-2.706	846623	37346623	27.663	1.0135	3.719511	7.511571	
3.65E+07	857517	37357517	27.67071	-1.420	870953	37370953	27.681	-2.889	-1.46879	-4.31003	
3.65E+07	884452	37384452	27.69066	-1.153	898953	37398953	27.701	0.8038	1.957239	1.839316	
3.65E+07	912390	37412390	27.71136	-1.630	925907	37425907	27.721	-1.08	0.549793	0.217784	
3.65E+07	989593	37489593	27.76854	-2.507	1006627	37506627	27.781	-2.456	0.050727	2.237358	
3.65E+07	1017446	37517446	27.78917	-0.370	1030906	37530906	27.799	-1.862	-1.49139	-1.33862	
3.65E+07	1045545	37545545	27.80999	-1.135	1058984	37558984	27.820	-1.560	-0.42436	4.726212	
3.65E+07	1072445	37572445	27.82991	1.2339	1085967	37585967	27.840	-2.811	-4.04475	-3.57495	
3.65E+07	1149593	37649593	27.88705	-1.790	1166617	37666617	27.900	2.3506	4.140396	12.12872	
3.65E+07	1177462	37677462	27.90770	1.9706	1190947	37690947	27.918	-2.266	-4.23700	-5.68964	
3.65E+07	1204439	37704439	27.92768	-2.623	1217835	37717835	27.938	-2.517	0.106052	4.456310	
3.65E+07	1231323	37731323	27.94759	0.9572	1244824	37744824	27.958	-2.351	-3.30835	-0.00793	
3.65E+07	1309590	37809590	28.00556	2.8128	1326595	37826595	28.018	-0.477	-3.28995	-2.45785	
3.65E+07	1337462	37837462	28.02621	-0.903	1350941	37850941	28.036	-2.494	-1.59118	-7.42908	
3.65E+07	1369168	37869168	28.04969	-2.890	1382622	37882622	28.060	2.2004	5.090508	5.204102	
3.65E+07	1396107	37896107	28.06965	1.1079	1409589	37909589	28.080	2.2143	1.106406	0.374751	
3.65E+07	1469606	37969606	28.12409	-1.960	1486589	37986589	28.137	-1.672	0.287213	4.111272	
3.65E+07	1497606	37997606	28.14483	1	1511021	38011021	28.155	-1.564	-2.56438	-2.15943	
3.65E+07	1529357	38029357	28.16834	-0.277	1547654	38047654	28.182	-0.596	-0.31861	-5.15898	
3.65E+07	1561012	38061012	28.19179	-2.784	1574459	38074459	28.202	0.8227	3.607220		
								Averages=		-0.08121	

Bibliography

1. ISO/ISE, "ISO. Information Technology – Radio frequency identification for item management – part 6," 2010.

2. P. V. Nikitin, "Theory and measurement of backscattering from RFID tags," *Antennas and Propagation Magazine, IEEE*, 2006.

3. D. M. Dobkin, "The RF in RFID: Passive UHF RFID in Practice," 2008.

4. Analog Devices Inc., "Mixed-signal Front End Processor for Broadband Communications," 2002.

5. ——, "0.8 GHz to 2.7 GHz Direct Conversion Quadrature Demodulator," 2005.

6. ——, "Integrated Synthesizer and VCO," 2004.

7. P. V. Nikitin, R. Martinez, S. Ramamurthy, H. Leland, G. Spiess, and K. S. Rao, "Phase based spatial identification of UHF RFID tags," *IEEE International Conference on RFID*, 2010.

8. "Title 47, Part 18 United States Code of Federal Regulations," 1985. [Online]. Available: http://ecfr.gpoaccess.gov/cgi/t/text/text-idx?c=ecfr&sid=cea99fa06a0ed0eebf524dcca2d73cad&rgn=div5&view=text&node=47:1.0.1.1.16&idno=47

9. Aerospace Corporation, "How GPS Works," 2003. [Online]. Available: http://www.aero.org/education/primers/gps/howgpsworks.html

10. R. K. Martin, C. Anderson, R. W. Thomas, and A. S. King, "Modelling and Analysis of Radio Tomography," *Proc. The Fourth International Workshop on Computational Advances in Multi-Sensor Adaptive Processing (CAMSAP)*, December 2011.

11. L. M. Ni, Y. Liu, Y. C. Lau, and A. P. Patil, "LANDMARC : Indoor Location Sensing Using Active RFID," *Science And Technology*, 2003.

12. EPCglobal, "EPC Radio-Frequncy Identity Protocols," 2005.

13. N. Abramson, "The ALOHA System - Another Alternative for Computer Communications," *Proc. 1970 Fall Joint Computer Conf. AFIPS Press*, vol. 37, 1970.

14. M. Buettner and D. Wetherall, "A Software Radio-based UHF RFID Reader for PHY/MAC Experimentation," 2010. [Online]. Available: http://www.cs.washington.edu/homes/buettner/docs/buettner_gen2_reader.pdf

15. C. Paget, "Extreme-range RFID Tracking," *DEFCON, Las Vegas, NV, 18*, September 2010. [Online]. Available: http://www.tombom.co.uk/extreme_rfid.pdf

16. M. Buettner, "A Flexible Software Radio Transceiver for UHF RFID Experimentation," 2010. [Online]. Available: http://www.cs.washington.edu/homes/buettner/docs/UW-CSE-09-10-02.PDF

17. ——, "A Gen 2 RFID Monitor Based on the USRP," *Computer Communication Review*, vol. 40(3), 2010.

18. M. Buettner and D. Wetheral, "Dewdrop : An Energy-Aware Runtime for Computational RFID," 2010.

19. Altera Corporation, "Cyclone Family Data Sheet," 2008.

20. Cypress Semiconductor Corporation, "CYC68013 EZ-USB FX2 USB Microcontroller High-Speed USB Peripheral Controller," 2002.

21. M. A. Richards, J. A. Scheer, and W. A. Holm, *Principles of Modern Radar*, 2010.

REPORT DOCUMENTATION PAGE

1. REPORT DATE (DD-MM-YYYY) 22-03-2012	2. REPORT TYPE **Master's Thesis**	3. DATES COVERED (From – To) 09-2010 – 03-2012

4. TITLE AND SUBTITLE **Spatial Identification of Passive Radio Frequency Identification Tags Using Software Defined Radios**	5a. CONTRACT NUMBER
	5b. GRANT NUMBER
	5c. PROGRAM ELEMENT NUMBER
6. AUTHOR(S) Cornn, Paul A. Capt USAF	5d. PROJECT NUMBER 11G182
	5e. TASK NUMBER
	5f. WORK UNIT NUMBER

7. PERFORMING ORGANIZATION NAMES(S) AND ADDRESS(S) Air Force Institute of Technology Graduate School of Engineering and Management (AFIT/EN) 2950 Hobson Way Wright-Patterson AFB OH 45433-7765	8. PERFORMING ORGANIZATION REPORT NUMBER **AFIT/GCE/ENG/12-04**
9. SPONSORING/MONITORING AGENCY NAME(S) AND ADDRESS(ES) Air Force Research Labroatory Sensors Directorate Dr. Vasu Chakravarthy 2241 Avionic Circle WPAFB OH, 45433 (937) 255-8269 vasu.chakravarthy@wpafb.us.mil	10. SPONSOR/MONITOR'S ACRONYM(S) **AFRL/RYWE**
	11. SPONSOR/MONITOR'S REPORT NUMBER(S)

12. DISTRIBUTION/AVAILABILITY STATEMENT
 Approved for Public Release; Distribution Unlimited

13. SUPPLEMENTARY NOTES
This material is declared a work of the U.S. Government and is not subject to copyright protection in the United States.

14. ABSTRACT

This research seeks to utilize a software defined radio for the detection and spatial identification of radio frequency identification tags. A software defined radio (SDR) is a hardware platform that provides the ability to broadcast and receive across multiple bands of the radio frequency (RF) spectrum, depending on the RF frontend and software profile loaded on it. The focus of this research will be on the spatial identification (SID) of passive radio frequency identification tags (RFID). This research is applicable to many areas of day-to-day operation both within the DoD and industry. Flight line safety tracking of equipment and personnel, as well as perimeter defense, are two areas that may benefit from this technology. One dual-purpose, civilian and military, application would be the tracking and locating of inventory within a warehouse. This research developed and implemented a SID process, and proved its suitability to quickly identify and locate target tags within range. A profile of the system's capabilities and limitations in the lab environment was developed including the range, sensitivity and accuracy.

15. SUBJECT TERMS
^ Localization, Software Defined Radios, Phase Difference of Arrival, RFID

16. SECURITY CLASSIFICATION OF:			17. LIMITATION OF ABSTRACT	18. NUMBER OF PAGES	19a. NAME OF RESPONSIBLE PERSON **Maj Mark D. Silvius**
REPORT **U**	**ABSTRACT** **U**	**c. THIS PAGE** **U**	**UU**	136	19b. TELEPHONE NUMBER (Include area code) (937) 255-3636 x 4684 mark.silvius@afit.edu